8-26-2022

BAG3 Mutation Interferes Myofibril Integrity of hiPSC-derived Cardiomyocytes on a Dynamic Substrate

Xiangjun Wu
Syracuse University

Abstract

BAG3 gene mutation is one of the major reasons for dilated cardiomyopathy, which is a leading cause of sudden heart failure. Previous studies have investigated the impairment of α-actinin assembly and force generation capacity by the BAG3 gene mutation. In this work, shape memory polymers have been implemented to create a dynamic environment to study the disturbance of sarcomere structure and function caused by the BAG3 gene mutation. The integrity and function of the sarcomere Z-line, M-band, and the thin filament have been studied in a dynamic environment by analyzing the change in sarcomere parameters.

Keywords: Dilated cardiomyopathy, BAG3, Shape memory polymer, Myofibril formation, Dynamic Substrate.

BAG3 Mutation Interferes Myofibril Integrity of hiPSC-derived Cardiomyocytes on a Dynamic Substrate

By

Xiangjun Wu

B.S., South China University of Technology, 2019

Thesis

Submitted in partial fulfillment of the requirements for the degree of

Master of Sciences (M.S.) in *Bioengineering*

Syracuse University

August 2022

Contents

Table of Figures

1 Introduction

1.1 Human Induced Pluripotent Stem Cell (hiPSC) and Cardiomyocyte

1.1.1 Human Induced Pluripotent Stem Cell

Induced pluripotent stem cells (iPSCs) are a type of pluripotent stem cell introduced by Dr. Shinya Yamanaka in 2006. iPSCs can be converted from somatic cells by programming with the Yamanaka factors **(Figure 1)**[1,2]. Compared to embryonic stem cells, iPSCs can be derived from adult tissues without the destruction of the early stage embryo[3]. This unique advantage makes iPSCs an ideal source for regenerative drug research, tissue repair, and organ regeneration. One of the clinical applications of iPSC is to generate iPSC-derived cardiomyocytes. The iPSC-derived cardiomyocytes have the same beating ability compared to natural cardiomyocytes and can also reflect cardiac drug responses because they possess the same genetic background as the patients from whom the iPSCs are derived[4]. The characteristics of iPSC-derived cardiomyocytes make it possible to study various kinds of cardiovascular disease in vitro.

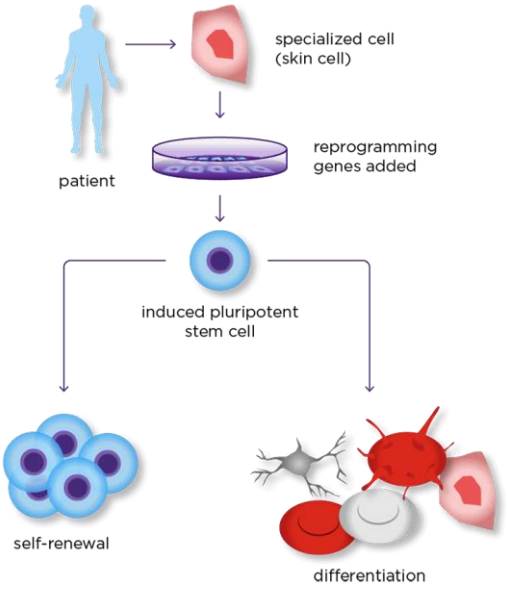

Figure 1 *The origin and the application of iPSCs*[2].

1.1.2 Cardiomyocytes

Smooth muscle, skeletal muscle, and cardiac muscle are three kinds of muscle that exist in the human body. Cardiac muscle is mostly composed of cardiomyocytes that only exist in hearts[5]. The shape of cardiomyocytes changes with the maturation process, from a round shape to a cylinder shape, with an average length of 100 μm[6]. Cardiomyocytes are connected to each other to form the contractile coordination of cardiac myofibrils. This structure allows the heart to pump blood. Cardiac myofibrils are contained in the cardiomyocytes and connected with intercalated discs to form long fibers[7]. Sarcomeres are the fundamental functional unit of myofibrils: about 50 sarcomeres form a myofibril fiber in matured cardiomyocytes. The resting length of sarcomere units is about 2μm, and it can increase up to 70% strain during contraction[8]. The structural unit of the sarcomere is called Z-line, which is composed of actinin, supports the sarcomere, and maintains the stability and integrity of the sarcomere. The sliding transverse filament system between the z-lines, which

are thin and thick filaments, enables sarcomere contraction. Actin and myosin are the major components of thin and thick filaments, respectively. Thin filaments are anchored to the z-line, while thick filaments are connected to titin and titin connects to the z-line. The other end of thin filaments is connected to the structure in the middle of the sarcomere unit, which is M-bands. An M-band is composed of myomesin, and this structure provides elasticity and plasticity to the sarcomere during contraction. The increased overlap caused by thin and thick filament sliding leads to myofibril contraction. The length of A-bands of thick filament and thin filaments are 1.6μm and 1.0μm in the human body **(Figure 2)**[6-9]**.**

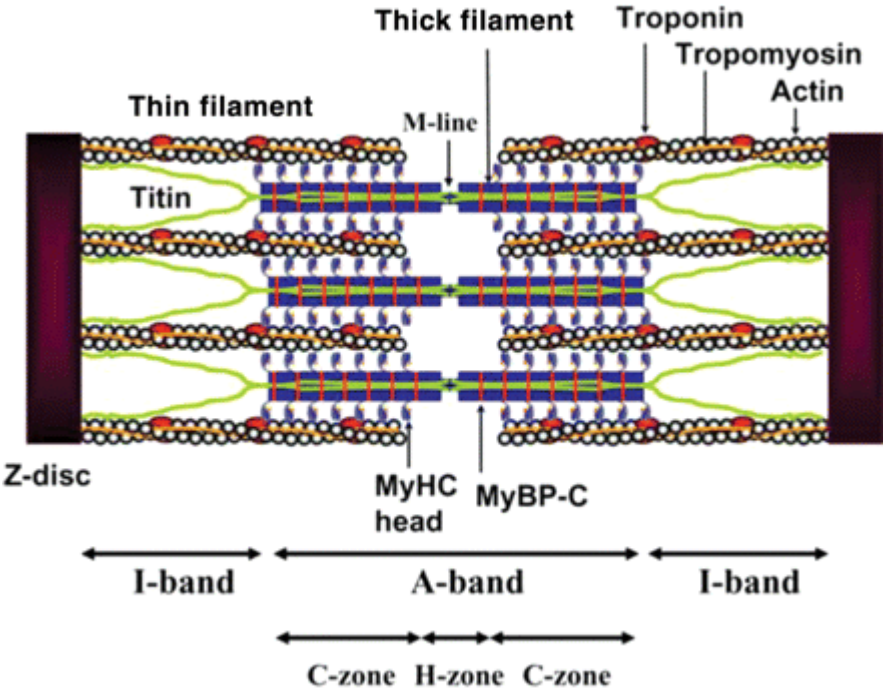

Figure 2 *Schematic image of sarcomere structure. Tropomyosin forms an a-helical coiled-coil double-strand lying along the grooves of actin double strands through head-to-tail polymerization. Myosin heavy chain (MyHC) has a globular head domain-containing actin-binding and ATP hydrolytic sites. Myosin-binding protein C (MyBP-C) is a thick filament-associated protein, which forms 7–9 transverse stripes at regular intervals of 43 nm in the*

C-zone of the sarcomere A-band. Titin is a giant protein constituting the third myofilament spanning the entire half of the sarcomere from Z-disc to M-line[9].

The maturation of sarcomere is divided into three stages: pre-myofibril, nascent myofibril, and mature myofibril **(Figure 3)**[10]. The sarcomere formation starts with pre-myofibril. Non-striated, continuous, non-muscle myosin II fibers that appear in the overlapping actin filaments near the cell membrane as the precursor of myofibrils[11]. The non-muscle myosin fibers function as templates or scaffolds for sarcomere proteins to assemble[12]. F-actin also forms the non-striated template and alpha-actinin then aligns and starts to connect to the template in the form of z-body filaments[13]. The non-striate pattern represents the stage of the nascent myofibril[14-15]. Muscle-specific myosin and non-muscle myosin both exist in the nascent myofibrils. Titin filaments are added to the nascent myofibril, and alpha-actinin becomes more aligned with the pattern in a beaded band shape[16]. As the mature myofibril forms, the beaded Z-bands become linear, and non-muscle myosin is replaced by muscle-specific myosin[17].

The formation of myofibril is impacted by the mutated sarcomere protein genes and results in a wide range of cardiomyopathies, including dilated cardiomyopathy (DCM).

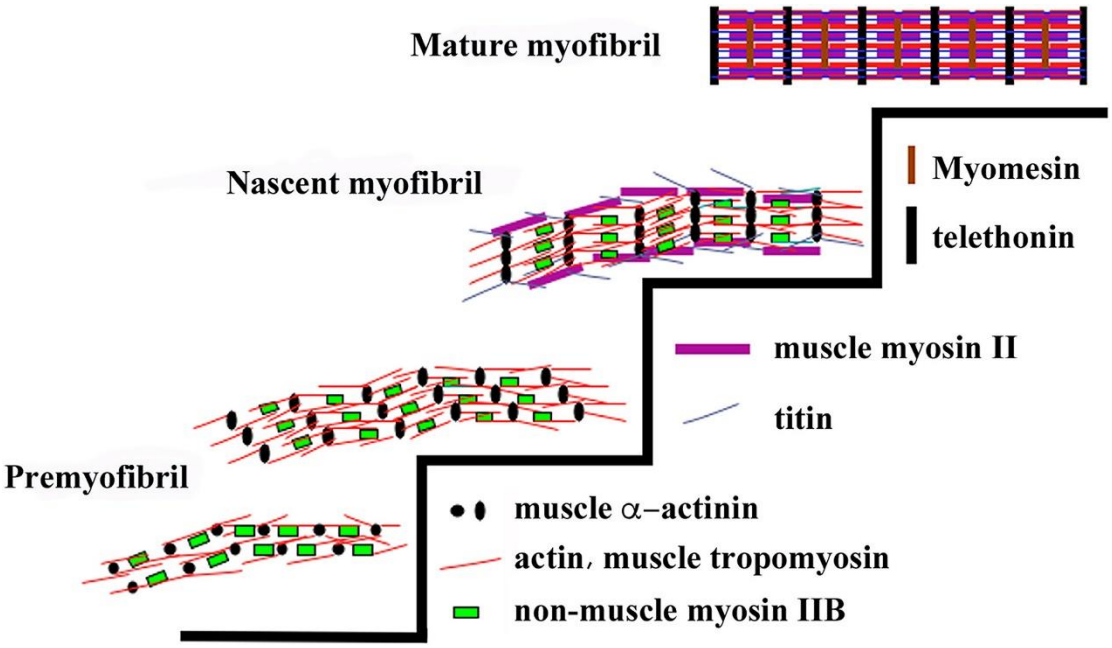

Figure 3 *The schematic description of the three stages of myofibril formation. Non-muscle myosin IIB is present in premyofibrils and in nascent myofibrils but is not present in mature myofibrils. Non-muscle myosin II is the only non-muscle protein in the premyofibril. Muscle myosin II appears in nascent myofibrils, in overlapping myosin II filaments that will then align to form the A-Bands of mature myofibrils. Titin makes its first appearance in the nascent myofibrils and may play a role in the alignment of the muscle myosin II thick filaments to form the A-Bands of the mature myofibrils*[10].

1.1.3 Gene mutation in Cardiac Myofibril Formation

Since the first discovery of β-myosin heavy chain gene mutation, which causes hypertrophic cardiomyopathy (HCM), over 400 gene mutations that cause HCM, DCM, and restrictive cardiomyopathy (RCM) has been discovered related to the sarcomere proteins of cardiac muscle[18]. However, it is still hard to predict the exact impact on cardiac functions based on the nature and position of the gene mutations. The study on

cardiomyopathy-related gene mutation has provided a wider view of cardiomyopathy studies.

Studies have discovered the mutation of genes in different sarcomere positions including thin filament, thin filament, titin, and Z-line. In thin filament, actin gene mutation has been discovered to be related to HCM and DCM. The α-Cardiac actin mutation impairs the formation of myofilaments by decreasing the thermal stability of the actin monomer in HCM[19-21]. It also suggested that the actomyosin interaction is impaired by the mutation such that the average sliding velocity is decreased and the affinity of actin for myosin is impaired[21]. In DCM, the affinity of actin for α-actinin slightly impairs force transmission. The α-Cardiac actin mutation also impairs the protein-folding pathway and filament formation, similar to the impact in HCM[19-20].

In thick filaments, the mutation in the myosin gene has been reported as an important cause of HCM and DCM. Mutations in the β-MyHC gene (MYH7) are the most common causes of HCM[22-23]. Mice with the MYH6 gene knocked out expressed delayed left ventricular relaxation, resulting in the diastolic dysfunction of the heart, which indicated the primary response to the mutation[24]. Other studies also demonstrated that myosin gene mutation impaired the ability to generate force by the heart[25]. The myosin gene mutation has been reported to impair heart contractility. The gene knock-out mouse model shows that this gene mutation impairs force-generating capacity and the velocity of actin filament sliding, which may trigger the cascade event that leads to DCM[26].

In the Z-line area, gene mutations of titin and α-actinin have been studied and reported. Titin plays an important role in muscle structure as a structural unit that determines muscle stiffness and acts as a biomechanical sensor, controlling gene expression. The affinity of titin for α-actinin is increased by HCM-causing gene mutations, and is decreased by DCM-causing gene mutations[27]. This phenomenon suggests that the mutations have distinct impacts on sarcomere structure and integrity. The actinin gene mutation has been reported to impair the interaction between α-actinin and muscle Lim protein (MLP), impairing muscle integrity. The above studies indicate that gene mutations have been involved in cardiac muscle formation and result in cardiomyopathies[28-29].

1.2 Dilated Cardiomyopathy and BAG3 Gene Mutation

1.2.1 Dilated Cardiomyopathy

Heart failure is characterized by low contractility and impaired cardiac output ability, and it is one of the biggest causes of morbidity and mortality. The left ventricle (LV) of a healthy human heart has a thick heart wall and a bullet-shaped chamber, while the right ventricle (RV) is thinner and has a crescent-shaped structure **(Figure 4)**. The force generation capacity in both the LV and the RV is impaired in heart failure cases. Heart failure results in the dysfunction of cells at the cellular level, including the impaired ability of calcium transportation, hormone imbalance, and sarcomere dysfunction. Increased calcium sensitivity and decreased contraction force generation capacity are reported in heart failure cases[30].

Dilated cardiomyocyte (DCM) is a heart disease in which the heart become same enlarged and cannot pump blood efficiently. The enlargement and dilation of one or both heart ventricles are characteristics of DCM, in which the left ventricular ejection fraction is less than 40%[31]. DCM can lead to sudden heart death and chronic heart failure, and 30-40% of all heart failure cases are caused by DCM. DCM is one of the major reasons for heart transplantation, the survival rate is poor for patients without heart transplantation[32]. Since 20-35% of DCM patients have family histories with DCM inheritance, gene mutations in DCM have been brought to attention. The cardiomyocytes collected from DCM patients have shown a decreased capacity to generate contraction force[33]. The cells also showed a decrease in the calcium concentration required to elicit half-maximal force (EC50), indicating an increase in calcium sensitivity[34]. One of the common features of heart failure is the impairment of the sarcomere protein quality control mechanism and the decreased ability to remove the misfolded and dysfunctional sarcomere proteins, resulting in a decrease in force generation capacity. By detecting the ubiquitin level, which serves as the indicator of misfolded sarcomere protein rate, the protein misfolding rate is significantly increased in DCM cells. The proteins which are detected as highly misfolded included myosin regulatory light chain-2, desmin, myozenin-2, α-actinin-2, and tropomyosin alpha-1. These proteins serve as important structural proteins of the Z-line, M-band, and thin filaments. This result may explain the decrease in the force-generating capacity, in that the misfolded proteins are not being removed from the contractile apparatus and are still being assembled into the sarcomere structure so they can be detected with the ubiquitin indicator[35].

DCM has also been reported to impair the sarcomere structure. Arimura et al has shown that the localization of Z-line proteins is impaired in DCM cells that the proteins are localized in the nuclei instead of the sarcomere[35]. On the M-band which is believed to act as structural linkers between the thick filaments, the expression of myomesin is downregulated. EH-Myomesin, a member of the myomesin family, is considered a signal of DCM when its expression is decreased[36].

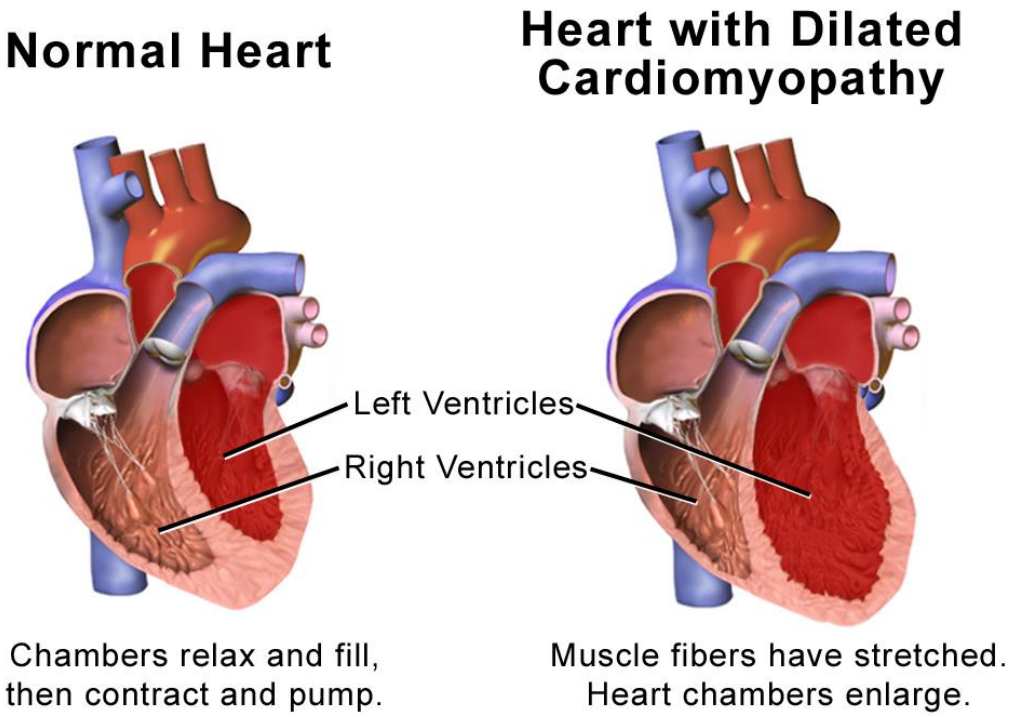

Figure 4 *The comparison between normal heart and DCM heart. DCM heart is characterized by the enlarged left ventricles31.*

1.2.2 BAG3 Gene Mutation

The DCM cardiomyocytes have shown a significant decrease in the BAG3 production level. The myofilament BAG3 expression level is shown to be correlated with the force-generating capacity, DCM cells which have lower force-generating also showed a

decreased BAG3 expression level. No association between the BAG3 level and calcium sensitivity has been discovered in DCM cells. This evidence supported that the BAG3 gene mutation is one of the mutations that cause DCM[34].

B-cell lymphoma 2 (Bcl-2)-associated anthanogene (BAG3) is a member of the antiapoptotic BAG protein family and a heat shock protein co-chaperone factor that binds heat shock protein 70 (Hsp70) within the C-terminal BAG domain and controls the chaperone activity of Hsp70[37]. BAG3 functions in protein quality control by mediating autophagic clearance of misfolded proteins. BAG3 plays an important role in maintaining myocardial homeostasis, in that myofibrillar disorganization occurs in cardiac-specific homozygous BAG3 knocked-out mice and leads to death in four weeks[38]. BAG3 mice with heterozygous BAG3 deletion express a substantial reduction in ventricular function[39]. BAG3 localizes to the Z-line in the sarcomere structure in adult myocytes, in contrast to the localization of BAG3 in the cytoplasm in neonatal myocytes. At the cell level, BAG3 knocked-out neonatal myocytes express rapid disruption of the myofibril structure under mechanical stretch, which indicates BAG3 plays an important role in excitation-contraction coupling[40].

BAG3 gene mutation is also one of the key factors in a wide range of cardiomyopathies. Around 15% of DCM cases are caused by BAG3 mutation[41]. The left ventricular tissue obtained from a DCM patient shows a reduced BAG3 level of less than 25% compared to the normal subject, resulting in the haploinsufficiency[42]. The BAG3 mutation in DCM impairs the localization of α-actinin and desmin to the sarcomere and enhanced the

localization within the nuclei. The interaction between BAG3 and Hsc70/Hsp70 is also disrupted in DCM cardiomyocytes, which suggests that the interaction is critical for BAG3 to stabilize heat shock proteins and maintain cardiomyocyte protein homeostasis[35].

1.3 Surface Microtopography and Cell-Material Interactions.

1.3.1 Cardiomyocyte Alignment Regulatory with Surface Topography

The extracellular matrix (ECM) is a supportive three-dimensional extracellular structure that contains a wide range of specific proteins and growth factors that regulate the morphology and functions of cells. The major protein components of ECM are proteoglycans and fibrous proteins that form the ECM structure, while the ECM in different tissues is also composed of unique proteins, indicating that the ECM in different tissues has unique properties. The ECM also regulates cell morphology and functions by applying mechanical signals to cells; mechanical signals can be transduced to biochemical forces in the cells to regulate cell behaviors. The morphology changes by applying external force can trigger protein production and gene expression in the cells.

In recent decades, new technologies have been introduced to study how morphology change impacts cells. Structural compartments, including cytomembrane and nuclei in cells, are interrelated and involved in the perception of mechanical signals. In the nuclei, the DNA is connected to the nuclei envelope, and the mechanical signals applied to the nuclear envelope also alternate DNA, which results in the functioning of gene expression regulation in cells. The cytomembrane is directly involved in receipt and transmission of

contractile force. Vinculin, talin, actin, titin, a-actinin desmin, and other proteins are assembled into a three-dimensional structure in the muscle cells to detect force and position the cell with adjacent muscle cells. The interaction between cytomembrane and nuclei, which transmit force signal, determines the position of nuclei in the cell and the position of nuclei is very important for protein production in the cell[43].

The topic of how cell morphological change by external force regulates cell functions has been brought into interest for decades and one of the most popular research topics is how mechanical cues regulate the behavior and cardiomyocytes functions[44]. Although the behavior of cardiomyocytes can also be regulated by cell-ECM adhesion, cell-cell contact, and ECM proteins, the nature that cardiomyocytes experienced lifelong wrinkling and squeezing makes the mechanical stimuli the most critical regulatory factor. External mechanical signals are believed to play an important role in cardiomyocyte maturation and morphogenesis, in that the cell elongates from a round shape to a cylinder shape. Bishop et al. transplanted an intact and functional neonatal rat heart into an external force-free chamber, and the result shows that insufficient external force leads to the failure of cardiomyocytes' elongation, while Olivetti et al. discovered that the increased load of force results in additional myofibril assembly[45,46].

Since ECM serves as an important factor in cardiomyocytes' development and functioning, developing biomaterials to mimic the topography of ECM and regulate cell behavior has been a popular research field in recent years. The development of microscale and nanoscale fabrication technology has enabled researchers to create substrates that mimic the natural

ECM, as well as the regulation on cells to empower in vitro studies on cell behaviors. Two-dimensional substrates with microscale topography are used to control the cell orientation, movement, differentiation, and proliferation. Surface topography features can be responded to by cells by the change in morphology, protein production, and gene expression[47,48].

To understand cell-ECM interactions, a wide range of substrate designs and technologies have been implemented in different research topics **(Figure5)**. One of the classic technologies is micropipette aspiration. This technique deforms a cell and elongates a part of the cell into the micropipette by a low magnitude, negative pressure to the cell[49].

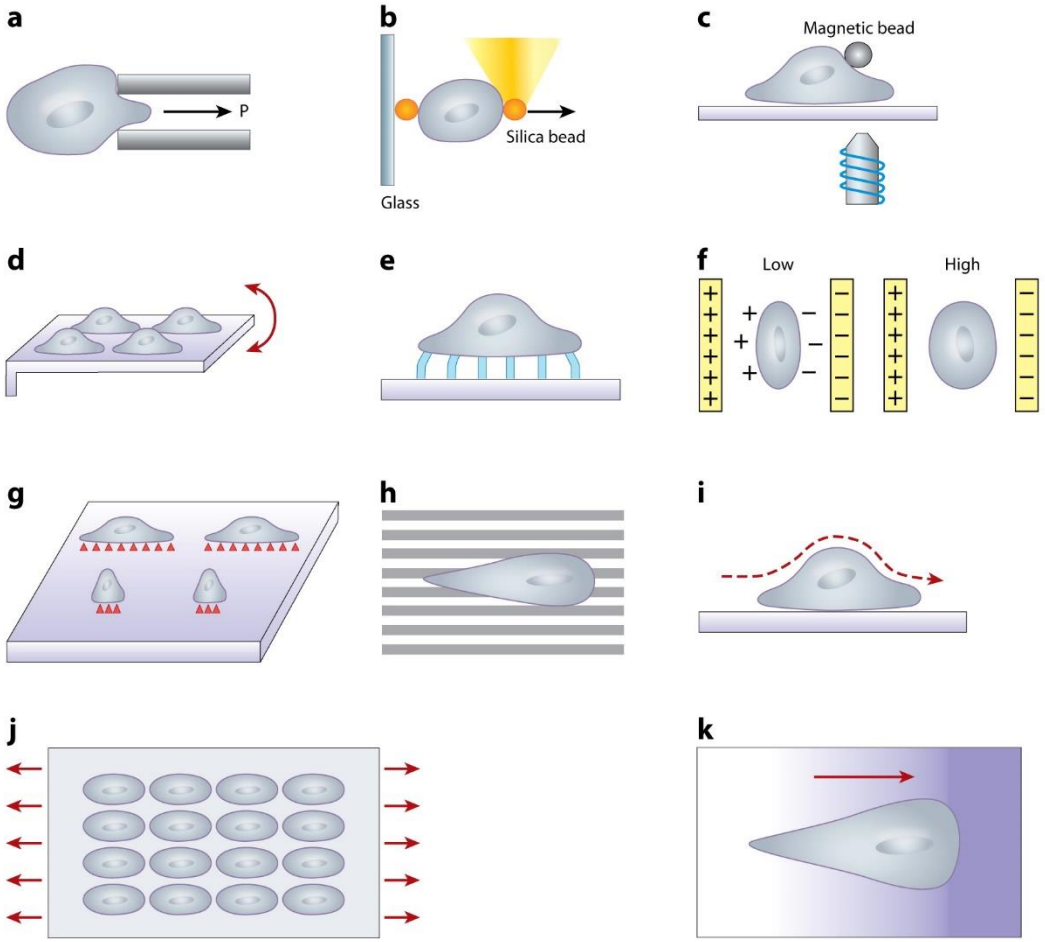

Figure 5 *Schematic illustrations of micro-engineered techniques for characterizing and*

stimulating single cells for cell mechanobiology. (a) Micropipette aspiration. (b) Laser trapping. (c) Magnetic bead measurement. (d) Microcantilever sensor. (e) Micro post sensor array. (f) Electrodeformation. (g) ECM micropatterning. (h) Micro- and nano-topographic substrate. (i) Microfluidic shear device. (j) Micromechanical cell stretching. (k) Substrate stiffness[48].

Hogan et al. used micropatterned coverslip and micropipette fabrication to study how constant rate aspiration detached cells and how detachment impacted cell behaviors **(Figure 6)**. The micropattern on coverslips was prepared by applying UV light through a photomask on the PLL-g-PEG surface solution and then incubating the coverslips in fibronectin solution. The micropipettes are fabricated by placing glass capillaries on a micropipette puller and cutting the capillaries with a micro forge to the desired diameter. This system can apply well-controlled aspiration force to a single cell adhering to a substrate, and the aspiration pressure and pipette section can be fixed to a constant rate to monitor the detachment of cells on the micropatterned substrate. The system works in two modes: the in-plane mode and the profile mode. The micropipette works directly with the cells cultured on the bottom of a petri dish, and the tip of the micropipette contacts perpendicular to the luminal surface to monitor the detachment of cells and measure the projected cell area. In the profile mode, cells are held by a second micropipette and aspired into another pipette parallelly. The profile mode enables the observation of cell detachment from a side view, although the parallel aspiration cannot show the cell projected area on the petri dish. The mode provides an opportunity to study the dynamics of cell detachment[50].

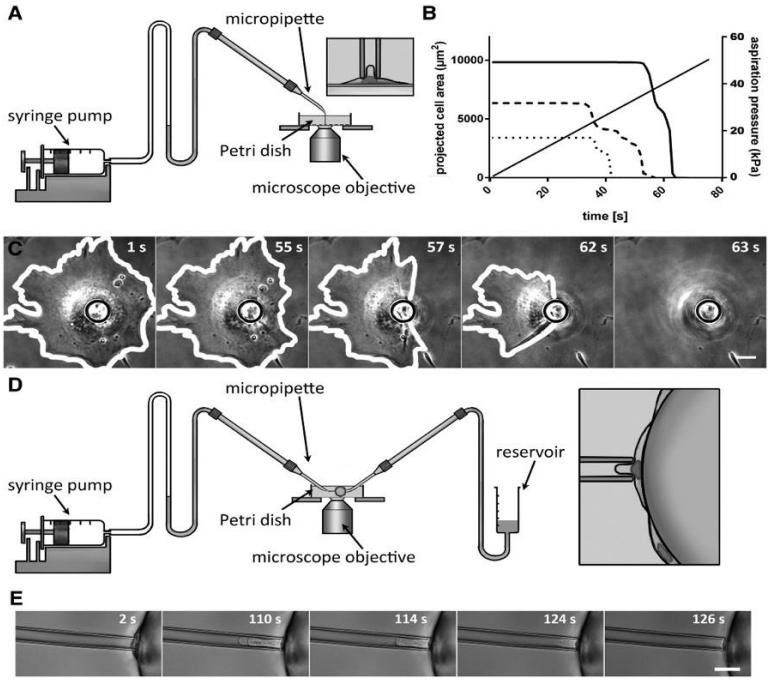

Figure 6 *(A) Experimental setup for in-plane aspiration experiments. The micropipette is positioned perpendicular to the surface of adherent endothelial cells cultured on the bottom of a petri dish. The syringe pump on the left creates a constant-rate aspiration pressure increase. (B) The plot of the projected cell area versus time for three different cells. (C) Time-lapse of a cell throughout a detachment assay. (D) Experimental setup for profile aspiration experiments. (E) Time-lapse of the detachment assay of an endothelial cell adhering to a Cytodex-3 bead*[50]*.*

The other popular substrate to study how morphology change affects cell behavior is micro post arrays. For the last 20 years, microfabricated elastomeric post arrays were implemented to measure the force generated by cells and manipulate the mechanical compliance of the substrate with the cells[51]. Tan et al. used a micro post array system with adjustable mechanical properties and surface chemistry to measure the force generated by cells at different adhesion sites **(Figure 7)**. Microfabricated post array substrates are

prepared by replica molding. The template for array fabrication is prepared by pouring polydimethylsiloxane (PDMS) over an array of SU-8 posts on a silicon wafer, which is prepared by photolithography. The microfabricated post array substrates are then fabricated by pouring PDMS prepolymers on the template, degassing under vacuum, fixed at 110 °C overnight, and then peeled off from the template. The substrate is then immersed into fibronectin and washed and sanitized for cell seeding. The tips of the micro-posts are fluorescently stained for fibronectin or coated with fluorescently labeled collagen IV for tacking and detecting the force generation. The controlling of substrate stiffness is achieved by controlling the height and dimension of micro-posts, and the different dimensions and heights of the posts ranged from 2 to 10 μm and 3 to 50 μm, respectively. The stiffness of micro-posts ranges from 2.7 to 1600 nN/μm. By changing the heights of specific posts in the array, the stiffness can be adjusted in designated target areas. The effective stiffness of posts can be adjusted by changing the heights of posts, decreasing the height of posts by half causing an 8-fold local change in stiffness. The effective stiffness can also be adjusted by changing the shape of the posts. The specific posts with an oval shape require 8 times more force to deflect along the long axis than along the short axis. This micro post system can be used to detect force generated by cells and determine the mechanisms of cell-ECM interaction. Smooth muscle cells with inhibited myosin generation capacity are seeded on the substrate and a decrease in post deflected is observe[51,52].

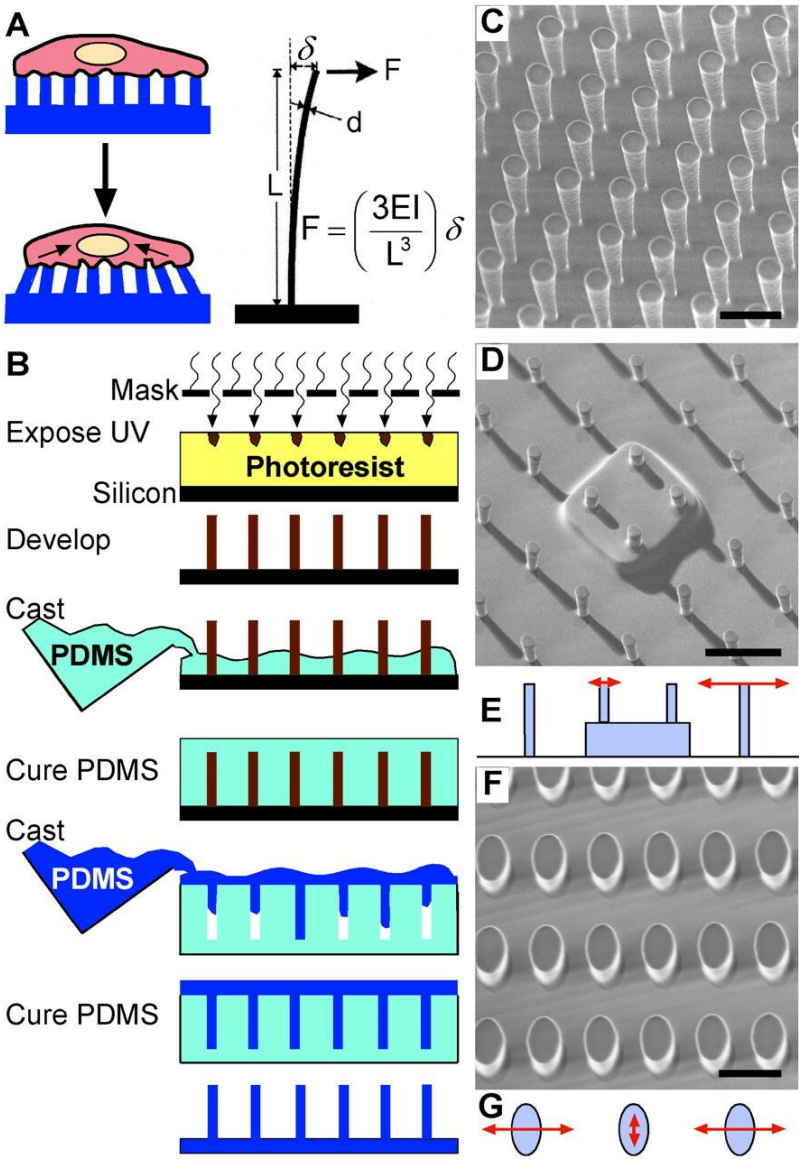

Figure 7 *Fabrication of arrays of posts. (A) With the appropriate surface density of the vertical post, a cell should spread across multiple posts. Under the proper geometric constraints of post height and width, cells exerting traction forces would deflect the elastomeric posts. (B) Scheme of the fabrication of the posts. (C-G) Scanning electron micrographs of fabricated arrays (C, D, and F), schematic drawing indicating the compliance of posts (E and G)*[52].

This micro post system can be used to detect force generated by cells and determine the mechanisms of cell-ECM interaction. Smooth muscle cells with inhibited myosin contractility generation with 2,3-butanedione monoxime are seeded on the substrate and a decrease in post-deflected is observed for several minutes **(Figure 8)**. The actin cytoskeleton contractility was also observed as decreased with cytochalasin D treatment. Force generated by cells is applied to the tip of single micro-posts when cells have strictly adhered to the top surface of the substrate. Quantifying and localizing the source of force is achieved by tracking the movement of the tips of multiple posts simultaneously through the use of immunofluorescence microscopy. The result of force tracking showed that the force vectors are summed to zero, which supported the reliability of force tracking with this substrate. The focal adhesion of a single cell is stained and imaged. Compared to the focal adhesion quantity resulting from the magnitude of force at a single post, the subcellular distribution of focal adhesion shows a correlation with the local traction forces.

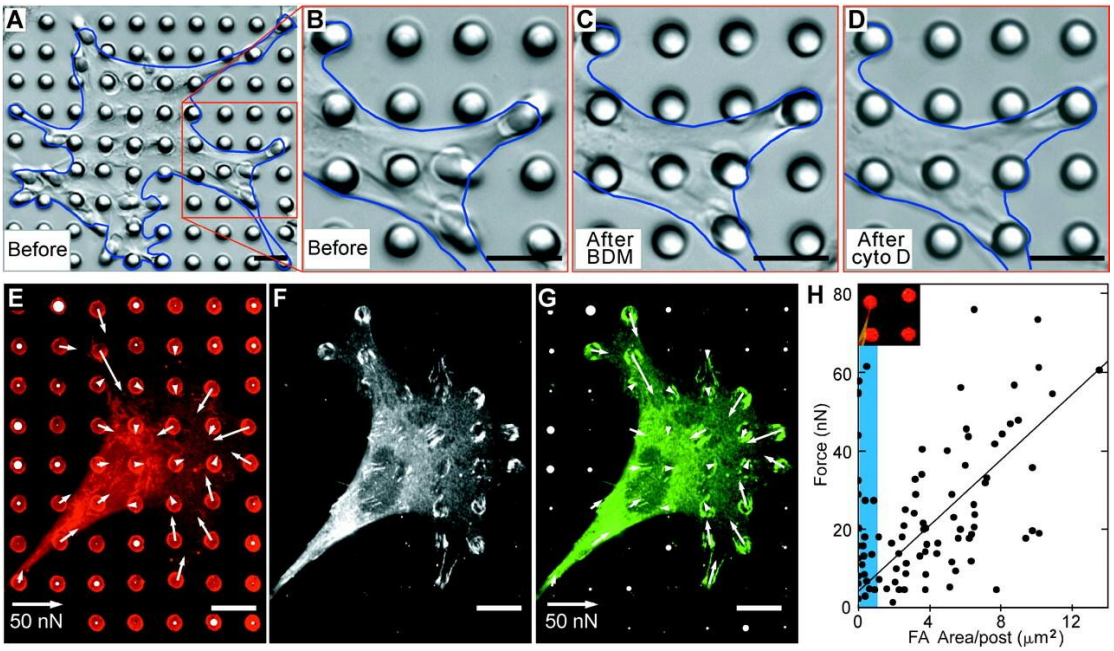

Figure 8 *Measurement of contractile forces in cells. (A–D) Differential interference contrast micrographs of a smooth muscle cell (outlined in blue) cultured for2 h on an array of posts in 10% serum (A and B), 20 min after 20 mM 2,3-butanedione monoxime (BDM) was added to the culture to inhibit myosin contractility (C), and after 2gml cytochalasin D (Cyto D) was added to the same culture for an additional 10 min to disrupt the actin cytoskeleton (D). (E–G) Confocal images of immunofluorescence staining of a smooth muscle cell on posts. The position of fibronectin (E, red) on the tips of the posts was used to calculate the force exerted by cells. The force map was spatially correlated to immunofluorescence localization of the focal adhesion protein vinculin (F, white; G, green). (H) A plot of the force generated on each post as a function of the total area of focal adhesion staining per post*[52].

Microtopographic substrates are substrates with various topographical features such as pores, wells, grooves, ridges, stops, and nodes in a nano or micro scale. Micro-topographical substrates can be used to understand cell-substratum interactions; the topography of substrates can dramatically influence the cell function and behaviors such as attachment, proliferation, differentiation, and gene expression. In recent years, nano-scale topographic substrates have received increasing attention due to their potential to mimic the in vivo environment. Nanoscale topography is fabricated using many approaches, including photolithography, reactive ion etching, and polymer fabrication[53-58]. Yim et al. reported the development of nano topographic substrate with nanoimprinting technology **(Figure 9)**. The mold for reproducing the imprinting molds is fabricated with microlithography. A poly (methyl methacrylate) (PMMA) mask mold is pressed via a pre-patterned SiO2 mold for 10 minutes at a pressure of 6 MPa and 180 °C, which is above the

glass transition temperature of PMMA, so that the PMMA substrate can be molded and flow. The PMMA substrate is then cooled down to a fixed pattern with gratings. The imprinting mold is prepared using soft lithography on PDMS, and the degassed PDMS solution with cross-linking reagent is poured onto the PMMA substrate in a weight boat and baked at 50°C overnight. The PDMS mold is separated from the PMMA mold after being cooled down for cell seeding. The prepared PMMA and replica PDMS substrates have 350nm wide gratings on the surface, the surface topography maintained its integrity with collagen coatings[57].

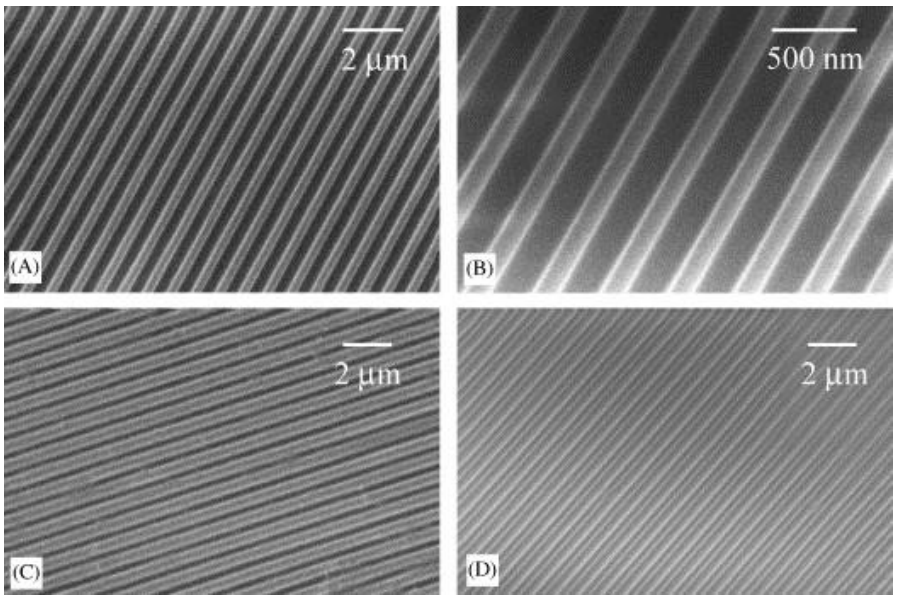

Figure 9 *Scanning electron micrographs of (A and B) nano-imprinted gratins on PMMA coating on SiO2 wafer, (C) PDMS nanopatterned by replica molding, and (D) collagen-coated PDMS with nanopattern. Bar=2µm for A, C, and D, bar=500 nm for B*[57].

Smooth muscle cells seeded on the surface of substrates with nanogratings showed an elongated morphology following the gratings **(Figure 10)**. The cells seeded on the

unpatterned substrates have not shown a clear orientation and are distributed randomly. The F-actin fiber and nuclei of cells are also to be elongated on the patterned substrates and align to the long axis of the cells. The percentage of aligned cells is also calculated, and the cells are considered aligned when the angle between the long axis of the cell and the grating is less than 15°. The percentage of the aligned cells on the PMMA and the PDMS substrates was 96.172.7% and 89.775.3%, respectively. The proliferation rate of SMCs is determined by adding BrdU into the culture media four hours before the fixation and staining of the samples with the anti-BrdU antibody. The incorporate rate is counted as the proliferation rate and the result shows that the proliferation rate is 56.67% and 47.77% for cells cultured on patterned PMMA and PDMS substrate surfaces, respectively. In contrast, the proliferation rate of cells seeded on the unpatterned surfaces is 35.57% and 30.97% on PMMA and PDMS, respectively. This result shows that the proliferation of SMCs is promoted on the nano-grating patterned substrates[57].

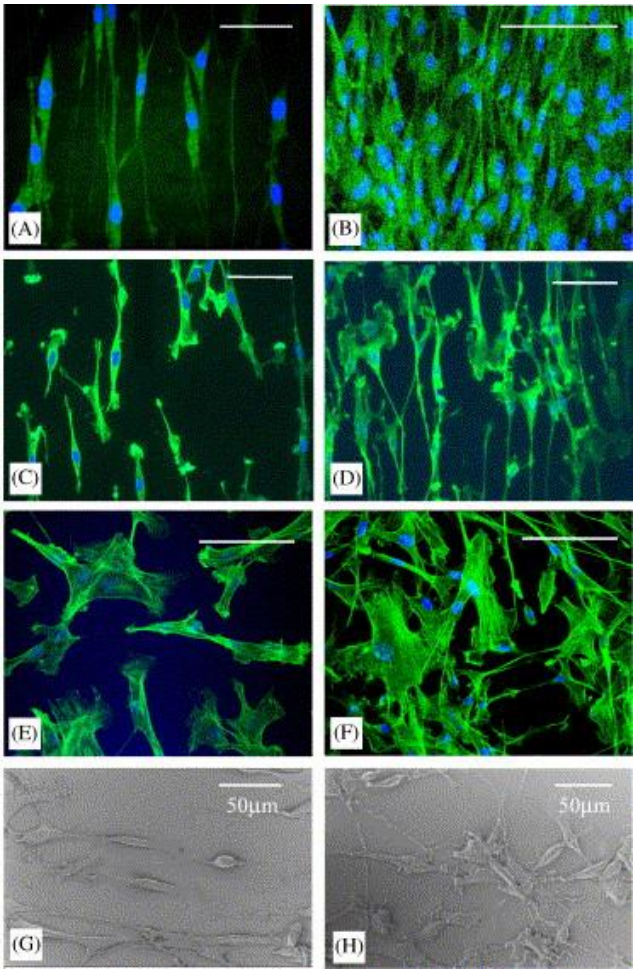

Figure 10 *Confocal micrographs of F-actin stained SMC on (A) nano-imprinted PMMA at low cell density, (B) nano-imprinted PMMA at high cell density, (C) nanopatterned PDMS at low cell density, (D) nano-patterned PDMS at high cell density, (E) non-patterned PMMA and (F) glass cover slip. Scanning electron micrographs of SMC cultured on (G) nano-imprinted gratings on PMMA coated on SiO2 wafer and (H) non-patterned PMMA coated on SiO2 wafer*[57].

1.3.2 Shape Memory Polymer

With recent developments in biomaterials fabrication, it is now possible to study cell behavior changes in dynamic extracellular environments on nano topographic substrates.

Shape memory polymer (SMP) is a type of smart polymer that can memorize a permanent shape, be programmed to a temporary shape by external stimuli, and recover to the permanent shape[59,60]. The implementation of SMPs enables cell-ECM studies to take multiple factors into the experiment design, including time, surface topography, and the stretch rate of SMPs. The dynamic topography of SMPs can be achieved with a stable surface coating. Henderson et al. developed the tBA-co-BA SMP that has a recovery temperature close to body temperature that enables SMP recovery triggered under intraoperative conditions[61]. Sun et al. used this SMP system with nano wrinkle topography on the surface to study changes in morphology and functions of hiPSC-derived cardiomyocytes **(Figure 11)**. The SMP is fabricated with 95 wt % tert-butyl acrylate (tBA) and 5 wt % butyl acrylate (BA) solution with 1 wt % 2,2- dimethoxy-2-phenyl acetophenone (DMPA) as photoinitiator and 5 wt % tetra- ethylene glycol dimethacrylate (TEGDMA) as crosslinker. The solution was mixed and injected onto two glass slides coated with Rain-X and separated with a 1 mm thick Teflon spacer and crosslinked in UV for 1 hour. The sample was then immersed overnight in a solution of 50% methanol and 50% water to remove excess monomers. The washed sample was then transferred to a vacuum oven at −15 psi at 40 °C for 24 hours for drying. The sample was then cut into 25 mm by 5 mm rectangles and then stretched to 140% strain. The stretched SMPs were then moved to the polyelectrolyte multilayer (PEM) coating in a spin coater. The sample is coated with polyethyleneimine, and 20 cycles of poly(styrene 4-sulfonate) (PSS) and poly(allylamine hydrochloride) (PAH) with two times Millipore water wash between PSS and PAH. The PEM-coated samples are then coated with Geltrex for cell seeding[62].

The results show that a nanoscale wrinkle topography is generated on the SMP surface after recovery. 75% of cells seeded on the SMPs are aligned with the wrinkles compared to

the alignment rate of 5% of cells seeded on the flat surface. The substrates have also been implemented in studying how disruption of myofibril remodeling impaired cells adapt to the dynamic environment. With the application of myosin kinase inhibitor, RhoA/ROCK kinase inhibitor, actin kinase inhibitor, and focal adhesion kinase inhibitor, all the inhibitors caused a decreased sarcomere index, indicating the disarray of sarcomere.

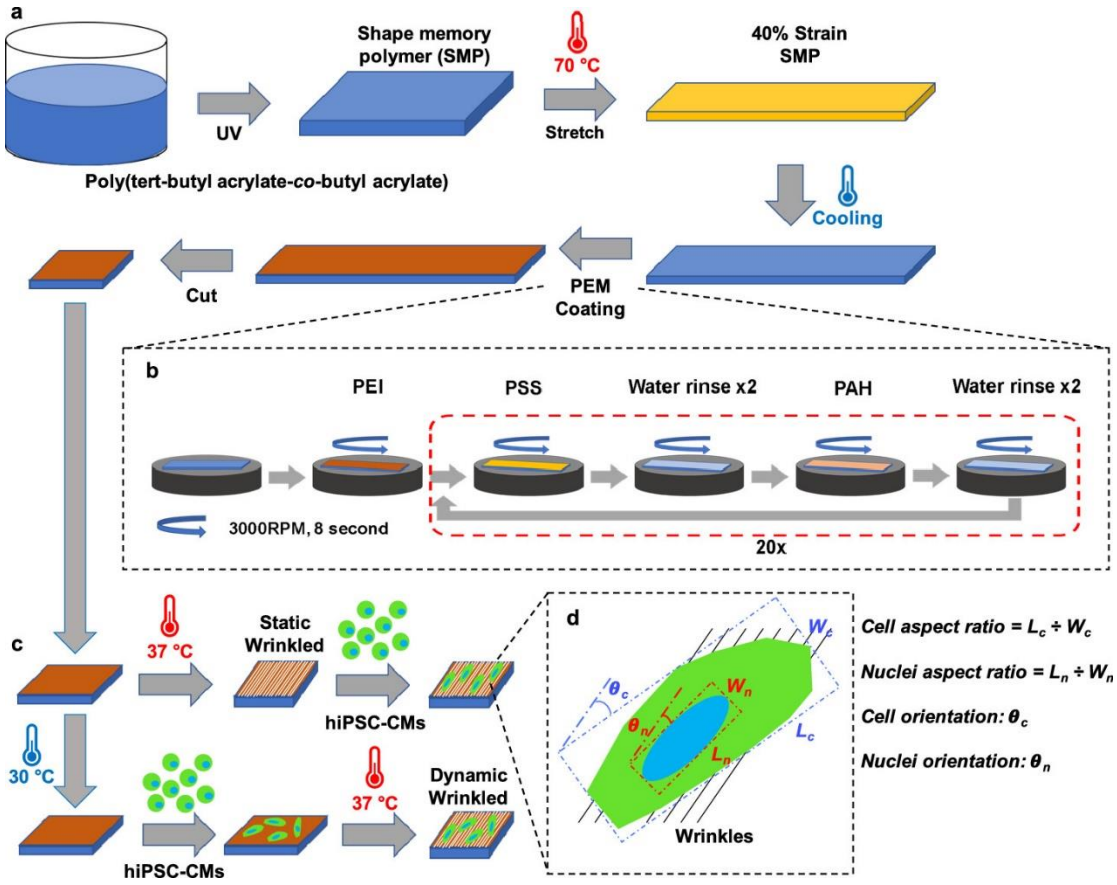

Figure 11 *Schematics of experimental procedures for SMP-PEM fabrication and dynamic cell culture. (a). tBA-co-BA polymer fabrication and stretched with 40% strain. (b). The stretched polymer is coated with PEM film with 20 cycles of coating process. (c) Human iPSCs are seeded on the sanitized SMPs for (d) cell alignment analysis*[61].

The applications of SMPs show a great potential for studying the dynamics of cells on nano-scale topography and mimicking the natural environment in the human body. The recovery of SMP makes it possible to observe the changes of cells in a dynamic environment, which is critical for understanding how cells respond to the changes of the external environment.

1.4 Research Goal

Following the previous studies of SMP, BAG3 gene mutation and myofibrillogenesis, the goal of this study is to understand how BAG3 gene mutation impairs the myofibril structure and function in a dynamic environment. Since the nano-wrinkled topography is required for the stretching of cardiomyocytes, the formation and the stability of the wrinkles during SMP recovery will be studied in this work with atomic force microscope. The localization of actinin to the sarcomere structure is disturbed in BAG3 mutant cells has been observed in previous studies but the impact of BAG3 gene mutation on the assembly of other sarcomere proteins remains unclear. The current studies have investigated BAG3 gene mutation in a static environment while the impact of BAG3 gene mutation on myofibrillogenesis in the dynamic environment is unclear. With the implementation of SMP, this work will study the BAG3 gene mutation in a dynamic environment to understand how the mutation disturbed myofibrillogenesis.

2 Materials and Methods

2.1 Overview

To study how BAG3 mutant cardiomyocytes' behaviors and functions are affected by external topography change, we used shape memory polymer to create the dynamic surface topography. The entire experiment process includes polymer fabrication, cell preparation, SMP recovery, and data collection.

Shape memory polymers are fabricated, stretched to an ideal strain, and coated with PEM coating. The polymers are then sanitized for cell seeding. BAG3 mutant cardiomyocytes are prepared by BAG3 mutant iPSC differentiation and purification. The cardiomyocytes are seeded on SMPs at low temperatures to avoid SMP recovery and allow cell attachment. The samples are recovered after cell seeding and the data is collected by microscope.

2.2 Polymer Preparation

2.2.1 Polymer Fabrication

The shape memory polymers have a major component of Tert-Butyl Acrylate (TBA). The monomer solution of SMP is composed of 95 percent weight TBA and 5 percent weight Butyl acrylate (BA), 1 percent weight 2-2- dimethoxy-2-phenyl acetophenone (DMPA) as initiator, and tetra ethylene glycol dimethacrylate (TEG DMA), as the crosslinker. The percentage of the components is calculated with the equation:

Volume in mL of TBA needed =

$$\frac{(\text{Mass of DMPA in grams}) * (\text{weight percent of TBA})}{(\text{Density of TBA})}$$

Volume in mL of TBA needed =

$$\frac{(\text{Mass of DMPA in grams}) * (\text{weight percent of BA})}{(\text{Density of BA})}$$

Since the standard DMPA volume is 25mg, the density of TBA is 0.875 g/ml, the density of BA is known as 0.894 g/ml and the volume of TEG DMA is the same volume of BA, the component volume needed for SMP fabrication is 2.714 ml TBA, 0.127 ml BA, 0.127 ml TEG DMA and 25mg DMPA.

The components are fully mixed in a glass flask which is washed with Millipore water and dried before the mixture. The solution was then injected into the polymer fabrication mold which has 2 glass slides, a Teflon spacer, and binder clips. The inner side of the slides is coated with Rain-X to avoid crosslinked polymer sticking on the slides. The Teflon spacer is cut to fit the size of the glass slides and fixed by the binder clips.

The mold with the mixture solution is moved into a UV box for photo-crosslink for 1 hour. After crosslinking, the polymer is immersed in a 50% methanol-DI water solution from the mold for washing away the rest monomers. The solution is placed onto a shaker overnight at room temperature. After washing, the polymer is placed into a hood for drying for 24 hours and then drying in a vacuum oven for 24 hours. The dried polymer is ready for use.

2.2.2 Polymer Stretching

The fabricated polymer is cut into pieces with a length of 2.3 cm and a width of 0.5 cm before stretching. Polymer samples can be stretched automatically or manually. The automatic stretching used Dynamic Mechanical Analysis (DMA) to stretch the polymer to a strain of 140%. The manual stretch used a manual stretcher, the polymer is fixed on the stretcher on the clips and the clips are screwed to be tightened at 5N force to avoid polymer sliding during the stretch. The stretcher with polymer is placed into a preheated oven at 70°C for 5 minutes. The polymer will become softened, and it is slowly stretched to the target strain by rotating the knob of the manual stretcher. After stretching, the stretcher is placed in the oven for 3 minutes and then the stretcher is taken out and cooled down to room temperature for PEM coating.

2.2.3 Polyelectrolyte Multilayers (PEM) Coating

The wrinkled topography on the SMP surface is formed by the folding of PEM film when the stretched SMP recovers to its permanent shape. The PEM coating includes a layer of PEI coating and 20 cycles of PSS coating, PAH coating, and Millipore water rinse between the coating process. The polymer is fixed on a round shape glass slide with double-sided tape and the glass slide is fixed on the spin coater with the vacuum. The coating solution is added to the polymer by dropper pipette to cover the entire surface of the polymer and spin-coated at 3000 RPM for 12 seconds.

2.2.4 Geltrex Coating

Polymers are coated with Geltrex for cell seeding. After the PEM coating, the polymer is cut into small pieces to fit the single well size of the 48-well cultural plate. The polymers are then sanitized and moved into 48-well cultural plate and incubated with Geltrex at room temperature overnight.

2.3 Cell Preparation

2.3.1 Cell Culture

The cardiomyocytes are derived from human-induced pluripotent stem cells (hiPSC-CMs). Cardiomyocytes are cultured in the well plates in a 37°C incubator with 5% CO2. The cells are maintained in RPMI media supplemented with B-27 complete.

2.3.2 Cell Seeding and Experiment Conduction

After the overnight Geltrex coating, the polymers are ready for cell seeding. hiPSC-CMs are washed with PBS solution and incubated with 0.025% trypsin at 37°C for 12 minutes to detach the cardiomyocytes from the culture plate. The warmed EB20 media is added into cell suspension to terminate the effect of trypsin. The cell suspension is then centrifuged for 5 minutes at 800 RPM, and the supernatant is aspirated after centrifuge. The RPMI-B27 media is added to re-suspend. The RPMI-B27 media is warmed to room temperature instead of warming to 37°C in a water bath to avoid the recovery of polymers.

The number of cells in the suspension is counted with the cell counter. 30,000 cells are seeded into each well of a 48-well plate. This number ensures the maximum number of cells attached to the polymer surface and also avoids tight junctions to keep the cells in a single-cell status. RPMI-B27 media at room temperature is added to each well to fill the well with 500µl media. Then, one piece of polymer is placed into each well with the PEM-coated side facing upwards. The culture plate is incubated at 30°C with 5% CO2 for cell recovery, and attachment and to avoid polymer recovery.

2.3.3 AFM Image Collection

To further investigate the formation and the stability of the wrinkled topography on the SMP surface, the SMPs coated with PEM are placed in a 48-well plate and covered with the RPMI media prewarmed to room temperature. The plate is incubated at 37°C and one piece of SMPs is taken out from the plate every 15 minutes for 1.5 hours, and every 2 hours for 6 hours. The recovered SMPs are then rinsed with Millipore water and dried for image collection with an atomic force microscope (AFM).

The surface topography image and the height of wrinkles are collected with AFM. The samples are fixed on the sample plate with double-sided tape. The data is collected with an AFM cantilever with a range of 20µm, 50µm, and 100µm. The data is analyzed automatically with the AFM controlling software.

2.3.4 Fluorescent Image Collection and Analysis

Cardiomyocytes are attached to the surface of polymers and well-spread after 2 days of incubation at 30°C. The culture plate is transferred to a 37°C incubator with 5% CO2 to trigger the polymer recovery. The initial transfer time is set as 0 hour. One piece of polymer is taken out every 1 hour for 6 hours. The sample is then fixed for immunostaining. The samples are washed by PBS 5 times immediately after being out from the plate, then the sample is fixed with 4% PFA solution for 15 minutes, 5 times PBS wash again. The sample is then immersed in 0.2% triton solution for 5 minutes and then immersed in 2% BSA solution for 30 minutes to wash away the triton solution.

After the fixation, the primary antibodies of α-actinin, actin, myomesin, and non-muscle-specific myosin are used to incubate the polymer for 1.5 hours at room temperature or overnight at 4°C, the samples are washed with PBS 5 times after the primary antibody staining. The secondary antibodies are then used to incubate the polymer for 1.5 hours to stain the proteins labeled by the primary antibodies. The samples are then washed with PBS 5 times before image collection.

Fluorescent images of cardiomyocytes are captured with a 40× oil objective on a Nikon microscope. The direction of wrinkles is examined with the brightfield channel. The immunostaining labeled proteins are detected with the fluorescent channels. The fluorescent images are processed with Fiji Image J, and a plugin called Adaptive Threshold is used to conduct the original images to threshold masks. The masks showed the distribution of the specific protein. The masks are then analyzed with a MATLAB software called Z-line

Detection Master. The software automatically detects the protein distribution and produce a mask as output, then it analyzed the different parameters of sarcomere proteins with the output masks **(Figure 12)**.

The statistical analysis is processed with one-way ANOVA test and tukey multiple comparison. Data from different cell types and dynamic/static groups are analyzed within the same time point to see if there is a significant difference between the cell groups at that time point.

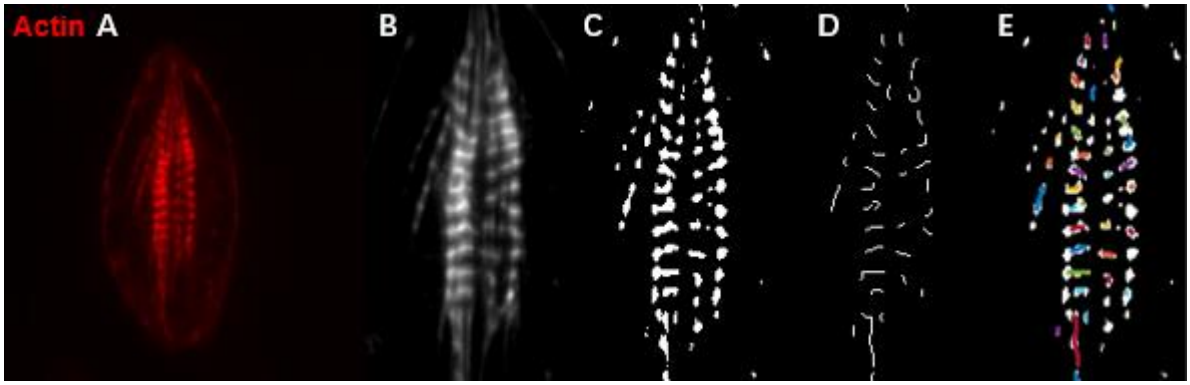

Figure 12 *The processing of immunofluorescent images. (A) the original image that cell stained with actin. (B) The sarcomere structure of cell. (C) The threshold mask of the sarcomere structure. (D) The sarcomere bands mask produced by MATLAB. (E) The detection of sarcomere bands to produce the sarcomere bands mask.*

3 Results

3.1 The Formation and Stability of Nano Wrinkles on SMP

3.1.1 The Formation of Nano Wrinkles

To investigate the process of wrinkle formation on the SMPs, the SMPs with PEM coating are incubated at 37℃ for recovery, and the topography is detected with an atomic force microscope (AFM). The surface topography of non-recovered SMPs is detected. The surface of unrecovered SMPs showed a flat topography with no significant pattern existed. The height of the unrecovered SMP also suggested that the surface is flat **(Figure 13)**. The formation of wrinkles can be observed from 15 minutes after the samples were moved to the incubator. The density of wrinkles increased over time and became stable after 45 minutes of incubation **(Figure 14)**.

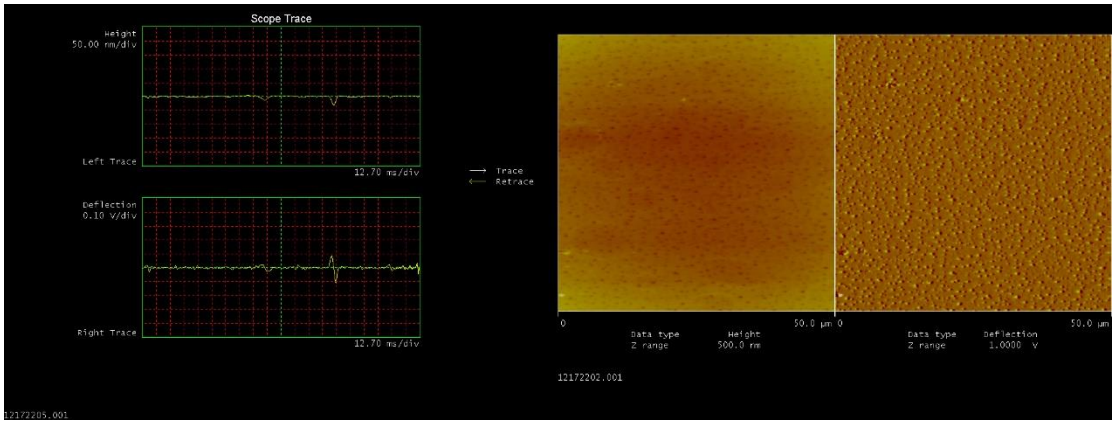

Figure 13 *The AFM image of SMP surface topography without the recovery process. No significant topography feature has been shown.*

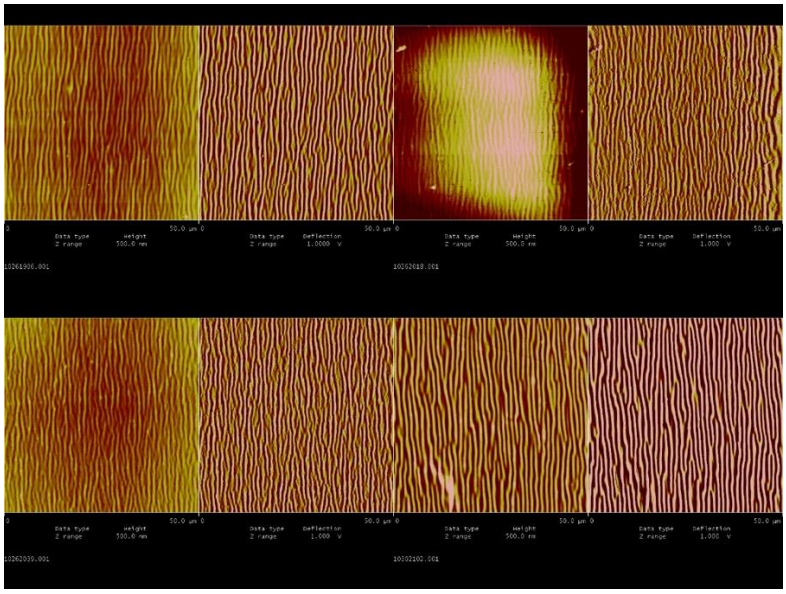

Figure 14 *The AFM images of SMP surface topography after recovery at 37°C. Wrinkles are formed on the SMPs after 15 minutes of incubation and the wrinkle density increased over the incubation time.*

The detected height of the wrinkles also suggested the same result that the height and density of nano wrinkles increased over the incubation time. The height of wrinkles is detected by capturing the movement of the AFM cantilever **(Figure 14)**. The result shows that the formation of wrinkles can be observed on the SMPs from 15 minutes of incubation, the average height of wrinkles is about 50nm and average wavelength of 1.7857μm. The height of the wrinkles is increased to 100 and 150 nm after 30 and 45 minutes of incubation and the average wavelength are 1.9231μm and 2.0000μm, respectively **(Figure 15)**. After 60 minutes of incubation, the SMP is fully recovered, and the height of wrinkles is increased to 200nm while the density of wrinkles also increased that the average wavelength is 1.3514μm. The result suggested that the recovery of SMPs is completed within 60 minutes of incubation at

37℃. The height and density of the wrinkles are increased by the increase in the PEM film folding rate on the SMP.

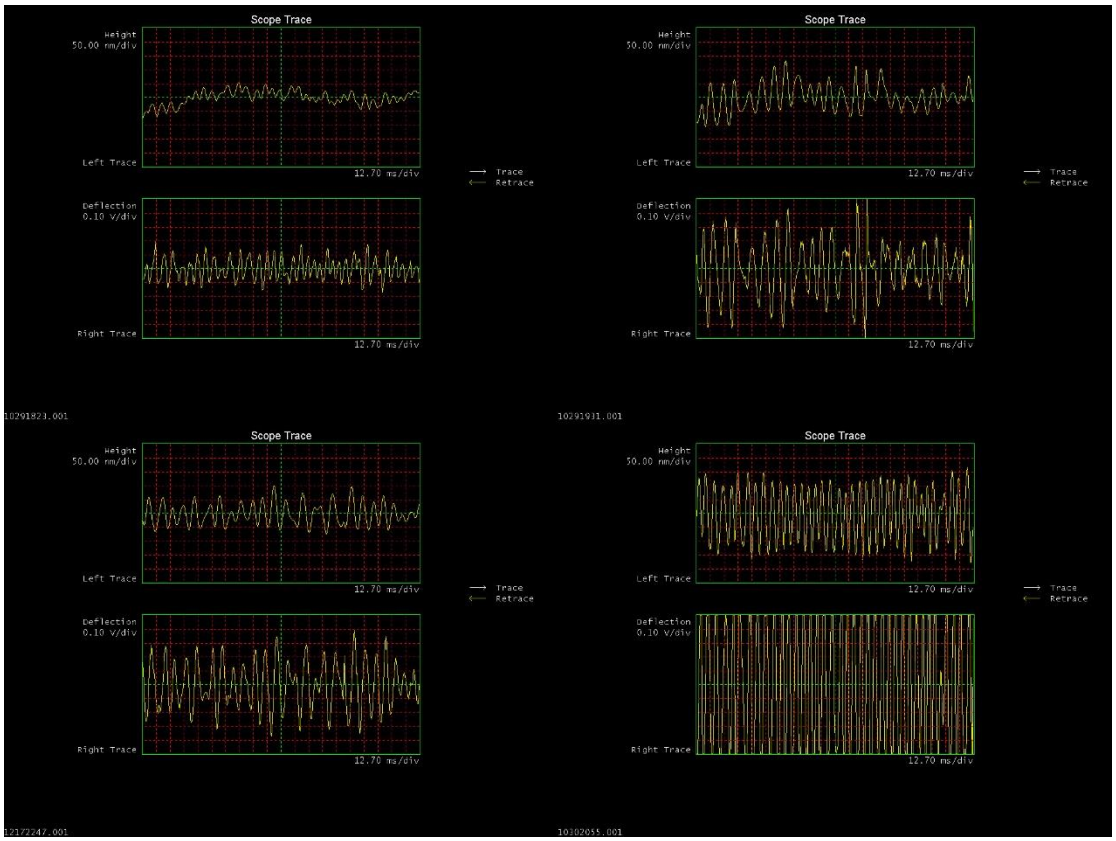

Figure 15 *The height result of SMPs. Wrinkles can be observed from 15 minutes of incubation with an average of 50nm. The average height of wrinkles increased over the incubation time and stabilized at 200nm after 45 minutes of incubation.*

3.1.2 The Stability of Nano Wrinkles

After detecting the surface topography of SMPs during the recovery phase, we also tested the stability of nano wrinkles during the entire experiment **(Figure 16)**. The surface topography of SMPs is detected by AFM after 2, 4, and 6 hours of incubation at 37℃. The result of AFM indicated that the surface topography of SMPs remains stable after the recovery. The average height of nano wrinkles remains at the level of 150nm and the average wavelength is 1.1364μm, 1.1628μm and 1.1628μm, which is consistent with the result of 60 minutes of incubation. This result suggested that the surface topography of SMPs is stable during the incubation and the external impact on cells seeded on the SMP is consistent.

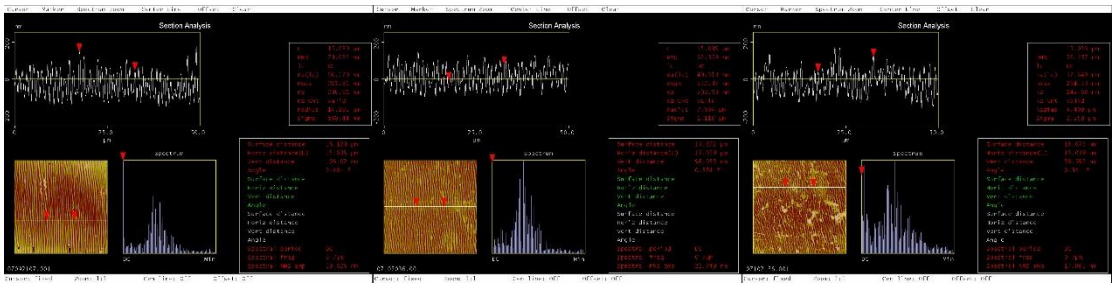

Figure 16 *The section analysis of wrinkles on the SMPs. After 6 hours of incubation, wrinkles on the SMP surface are still stable and have the same average height of 200nm as they were formed.*

3.2 BAG3 induced sarcomere changes

3.2.1 Immunofluorescent images

The wild-type and BAG3 mutant cells are stained with α-actinin, non-muscle specific myosin **(Figure 17, 18)**, myomesin and actin **(Figure 19, 20)**. In the wild type cells, the non-muscle

specific myosin is localized near the cytomembrane of cells to form the structure of the premyofibril. α-actinin is distributed in the entire cell, the filaments of α-actinin are localized near the cytomembrane that join the non-muscle specific myosin to form the premyofibrils. The bands of α-actinin are localized at the center of the cell to form the mature myofibril/ sarcomere structure. During the SMP recovery, non-muscle specific myosin is produced at the nuclei **(Figure 17)**.

In the BAG3 mutant cells, the amount of the mature myofibril is less than the amount of the wild-type cells. α-actinin is less localized at the sarcomere and existed in the cell as filaments. The amount of α-actinin bands is significantly reduced in the BAG3 mutant cells compared to the wild-type cells **(Figure 18)**. The localization of actin and myomesin is also impaired in BAG3 mutant cells. In the wild-type cells, myomesin and actin bands are localized at the myofibril to form the repeating bands pattern of sarcomere. Compared to the wild-type cells, the amount of myofibril is reduced in the BAG3 mutant cells, which indicates the localization of myomesin and actin is impaired in BAG3 mutant cells **(Figure 19, 20)**.

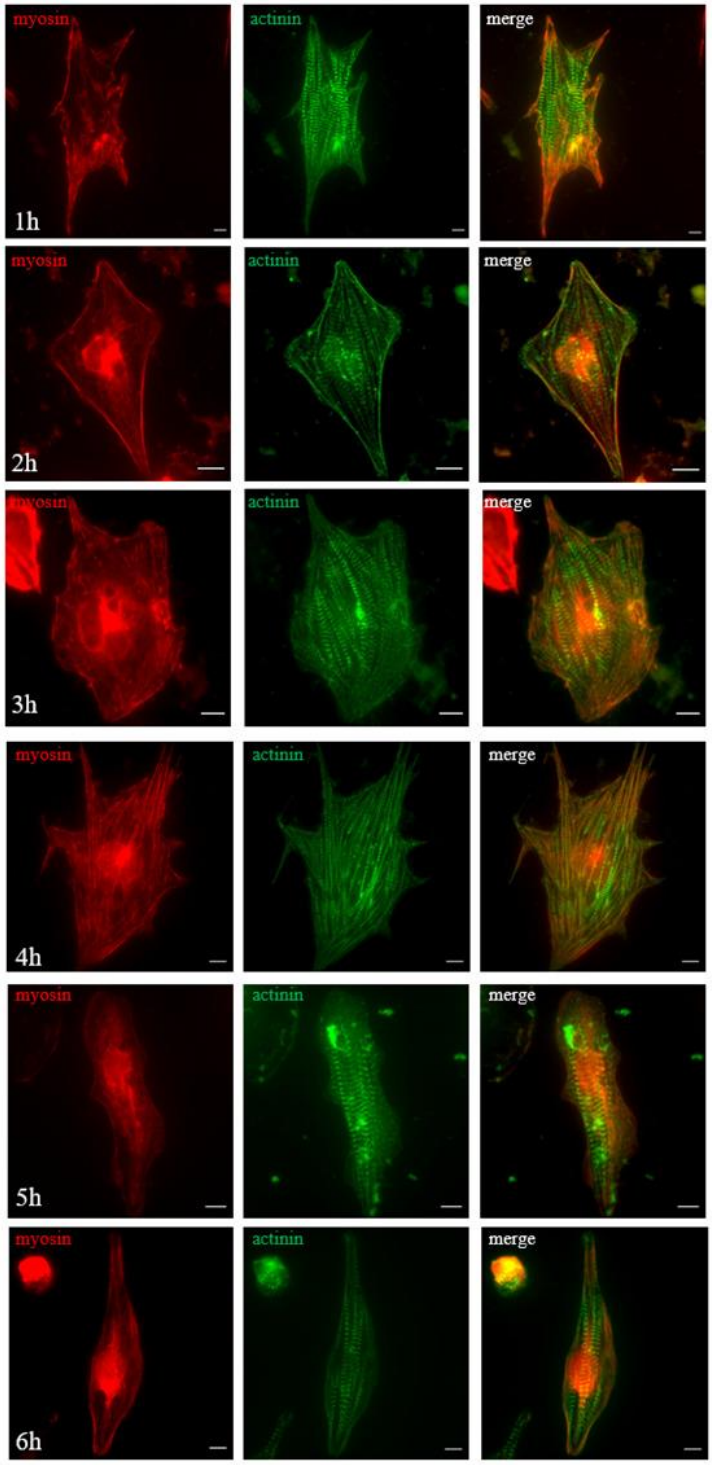

Figure 17 *The immunofluorescent images of the wild-type cells. Non-muscle specific myosin is located near the cytomembrane. α-actinin joins the premyofibril as filaments and construct*

the sarcomere as bands. Non-muscle specific myosin is produced during the SMP recovery (Scale bar:10μm).

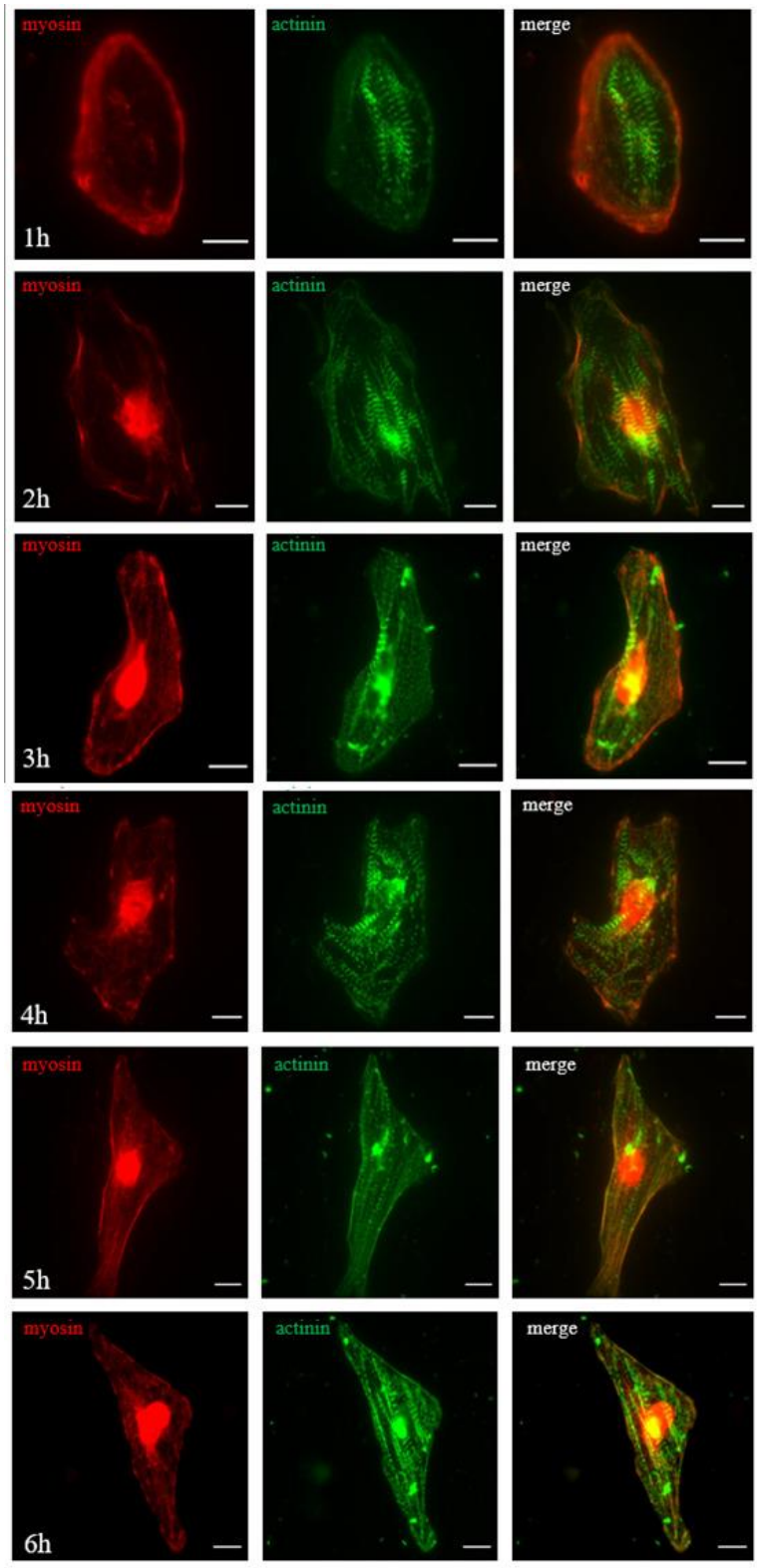
myosin
actinin
merge
1h
myosin
actinin
merge
2h
myosin
actinin
merge
3h
myosin
actinin
merge
4h
myosin
actinin
merge
5h
myosin
actinin
merge
6h

Figure 18 *The immunofluorescent images of the BAG3 mutant cells. Non-muscle specific myosin is located near the cytomembrane. α-actinin joins the premyofibril as filaments and construct the sarcomere as bands (Scale bar:10μm).*

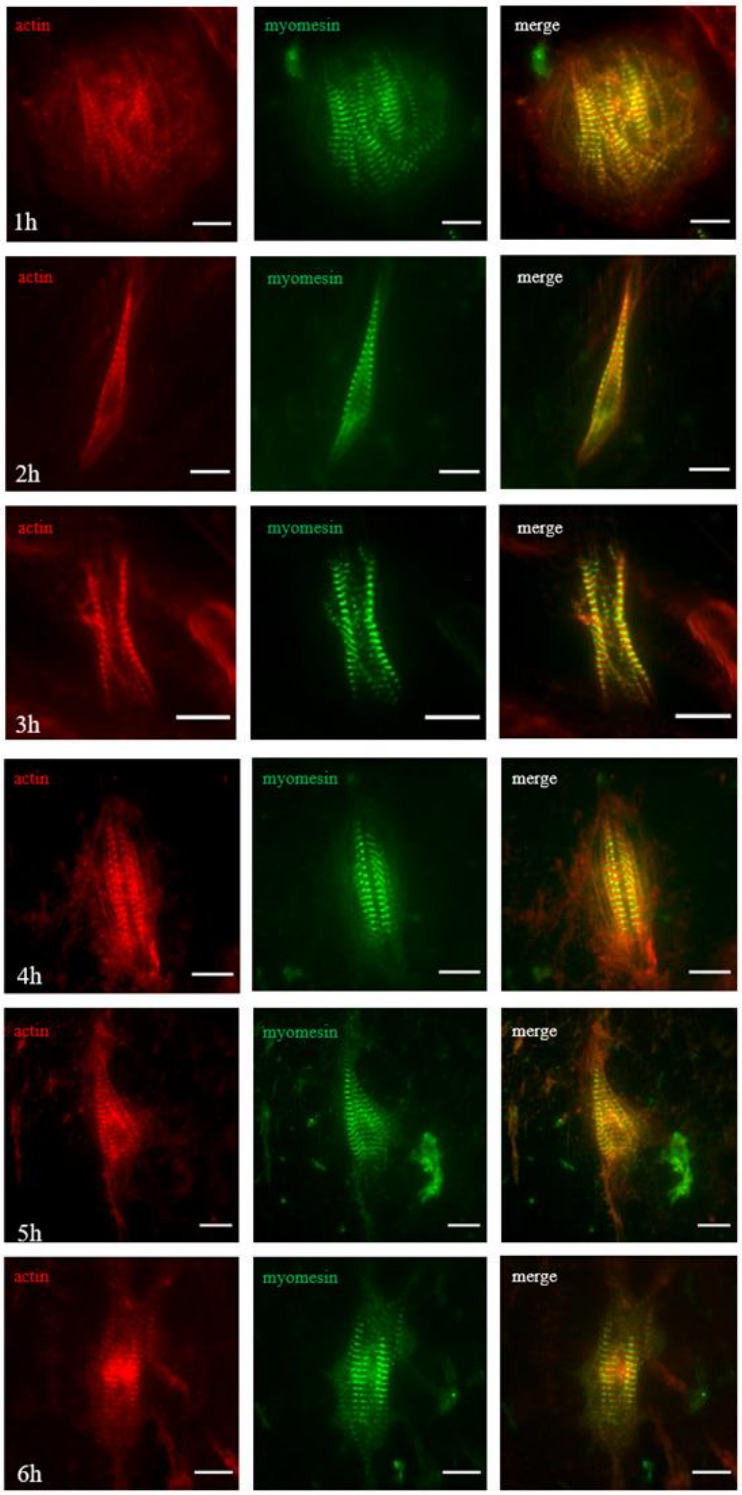

Figure 19 *The immunofluorescent images of the wild-type cells. Myomesin and actin bands are localized at the myofibril to form the repeating bands pattern of sarcomere. Cells are filled with myofibrils (Scale bar:10μm).*

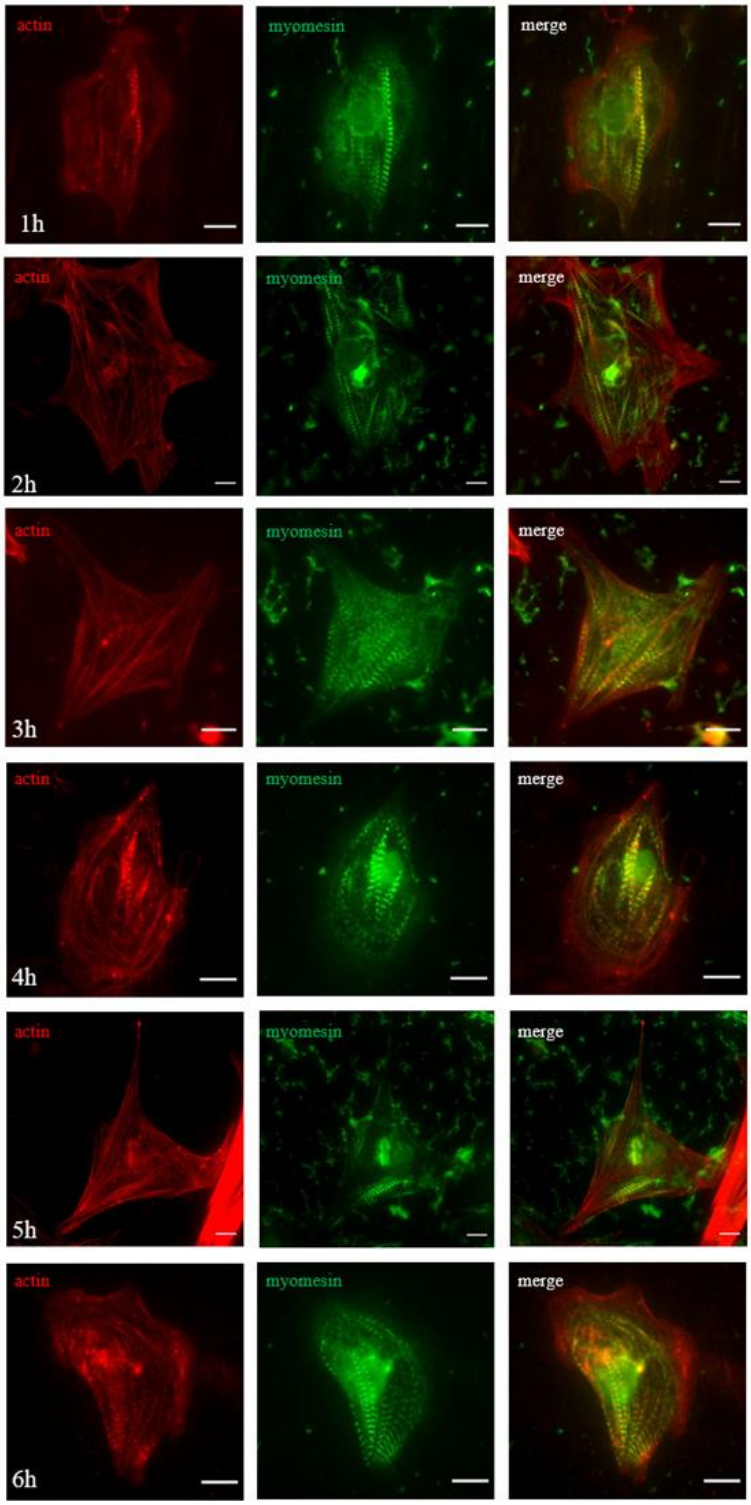

Figure 20 *The immunofluorescent images of the BAG3 mutant cells. The amount of myofibril is reduced in the BAG3 mutant cells. The assembly of myomesin and actin to the sarcomere is impaired, which indicated the impair of sarcomere integrity (Scale bar:10μm).*

3.3 Sarcomere Protein Length

3.3.1 Median Z-line length

Sarcomere protein length is a parameter to indicate the sarcomere integrity and the cell function of sarcomere protein assembly. The median Z-line length is obtained by detecting the length of α-actinin and calculating the median α-actinin length in a single cell **(Figure 21)**. The median Z-line length of the BAG3 mutant cell is shorter than the median Z-line length of the wild-type cells. In the dynamic group, the mean median Z-line length of BAG3 cells in the dynamic group is 1.029μm while the mean median Z-line length of wild-type cells is 1.104μm. In the static group, the mean median Z-line length of BAG3 cells in the dynamic group is 1.015μm while the mean median Z-line length of wild-type cells is 1.047μm. The median Z-line length of wild-type cells in the dynamic group showed a slight increase in the first 3 hours of incubation, decreased for 2 hours, and recovered to the original level while no significant change in median z-line length is observed in BAG3 mutant cells.

The p-value of the unpaired t-test is 0.007 and 0.0310 in the dynamic and static groups, suggesting a significant difference between the 2 cell groups. The grouped t-test result shows that the difference between the BAG3 mutant cells and the wild-type cells is significant in the first 3 hours of SMP recovery **(Figure 22)**. The one-way ANOVA test shows the significant

difference between BAG3 dynamic group and WT dynamic group at the first 3 hours of incubation **(Figure 23)**.

The result of the median Z-line length indicated that the integrity of the Z-line is impaired in the BAG3 mutant cells that the median Z-line length is reduced in the BAG3 mutant cells. In the first 3 hours of SMP recovery, the median Z-line length increased in the wild-type cells as the response to the stretching while there is no significant change in the BAG3 mutant cells. The median Z-line length decreased after 3 hours of incubation, which may indicate the formation of premyofibril that shorter α-actinin filaments are produced.

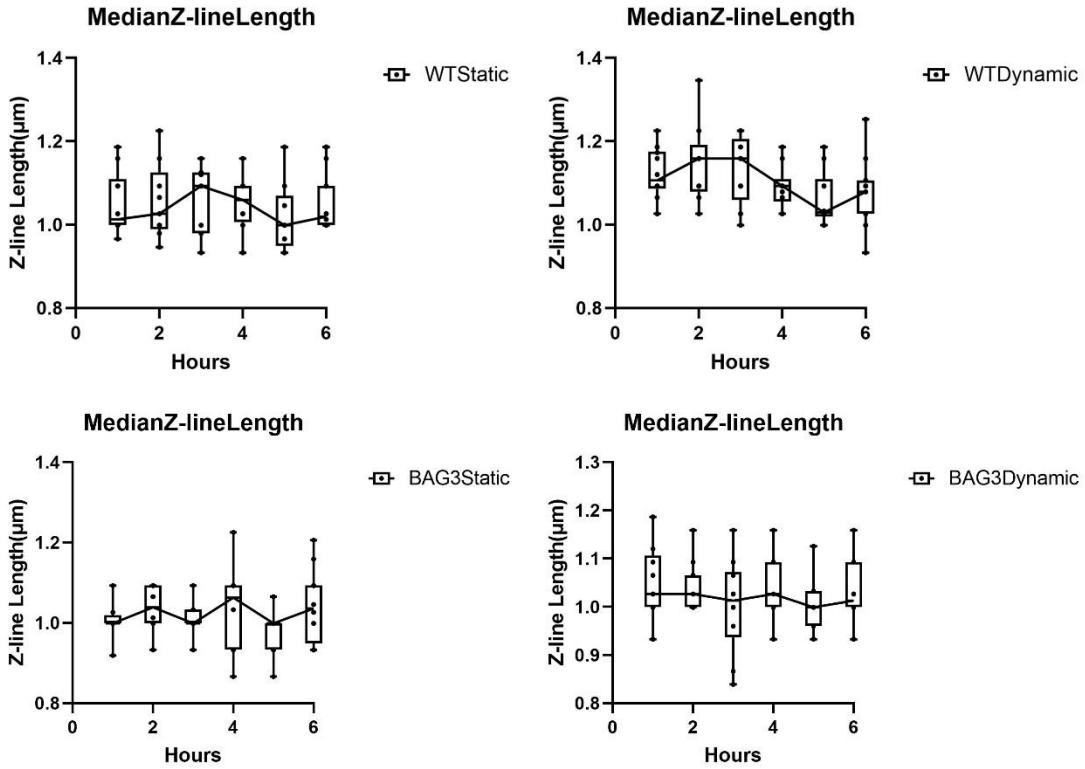

Figure 21 *The median Z-line length. BAG3 mutant cells have shown a short median Z-line length compared to the wild-type cells. BAG3 mutant cells have not shown a significant level change in the incubation over time.*

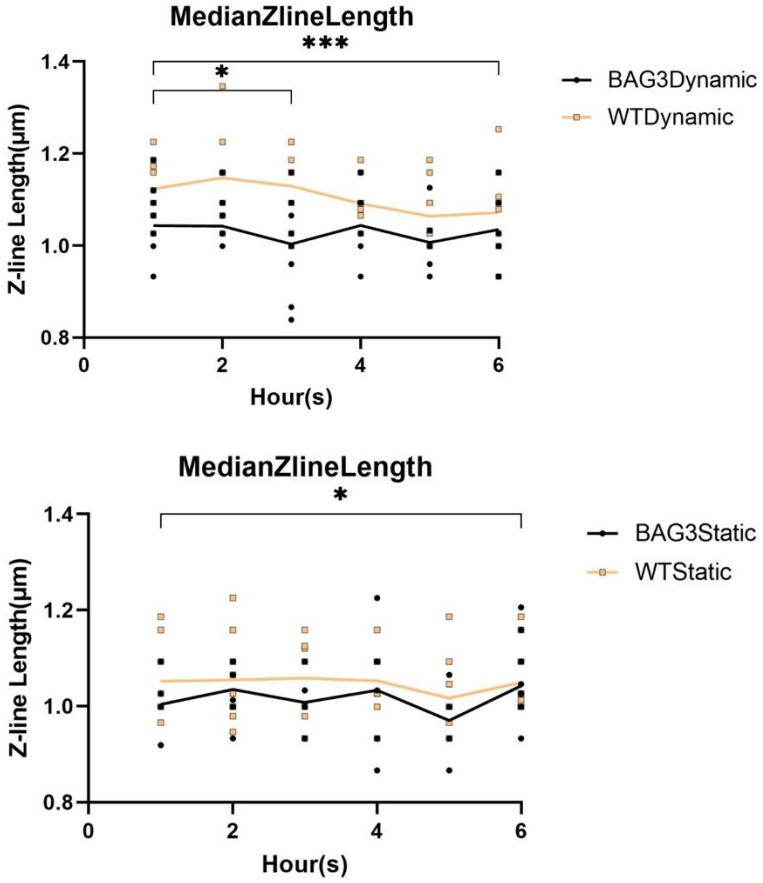

Figure 22 *The comparison between the BAG3 mutant cells and the wild-type cells of the median Z-line length. The p-value of the unpaired t-test is 0.007 and 0.0310 in the dynamic and static groups, suggests the significant different between the 2 cell groups. In the multiple unpaired t-test, the samples of the first 3 hours of SMP recovery have shown a q-value below 0.05, which suggests the significant different between these samples.*

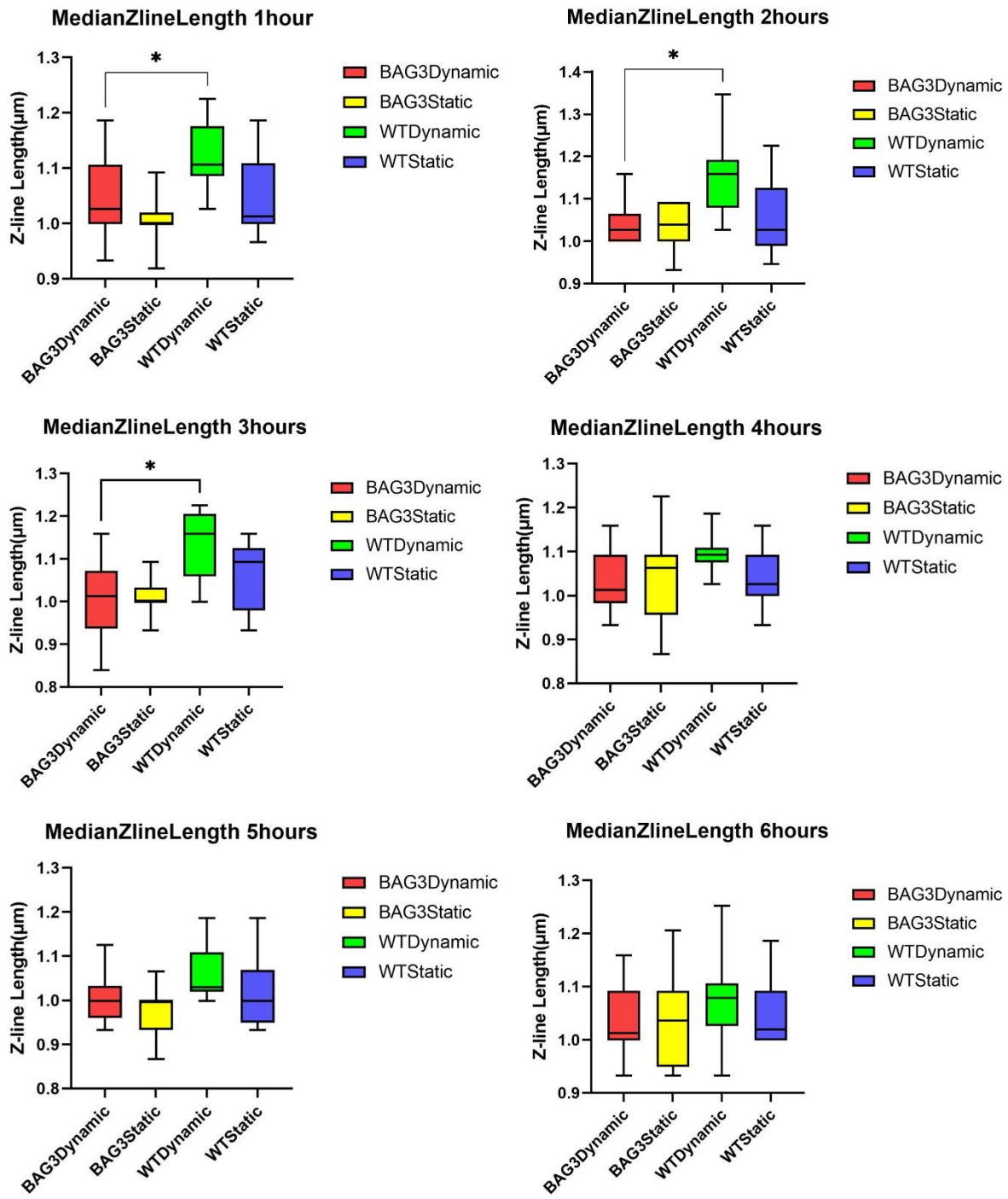

Figure 23 *The statistical analysis of median Z-line length. The significant difference is shown at the first 3 hours of incubation between BAG3 dynamic and WT dynamic group.*

3.3.2 Median M-band Length

The median M-band length is obtained by detecting the length of myomesin and calculating the median myomesin length in a single cell **(Figure 24)**. The mean median M-band length of BAG3 cells is shorter than the mean median M-band length of the wild-type cells. In the dynamic group, the mean median M-band length of BAG3 cells in the dynamic group is 0.9156μm while the mean median M-band length of wild-type cells is 0.9966μm. In the static group, the mean median M-band length of BAG3 cells in the dynamic group is 0.9138μm while the mean median Z-line length of wild-type cells is 1.042μm. In the dynamic group, there is no significant change in the median M-band length in both wild-type cells and BAG3 mutant cells over time.

The unpaired t-test of the median M-band length has a p-value of 0.0673, which suggests no significant difference between the 2 groups. The p-value of the unpaired t-test is 0.0013 in the static group, which suggests a significant difference between the 2 cell groups. The only significant difference in the dynamic group is shown at 6 hours after SMP recovery **(Figure 25).** The ANOVA test shows that the significant difference is shown 2 hours of incubation between BAG3 static and WT static group. A significant difference is also shown at 6 hours between BAG3 dynamic and WT dynamic group **(Figure 26)**. The significant difference of the median M-band length in the static group indicates that the integrity of the M-band is impaired in the BAG3 mutant cells. The no significant difference in the dynamic group may be explained by the stretching of the M-band by the SMP recovery. In the dynamic group, the M-band length increased slightly over the incubation time in the wild-type cells, which may indicate the repair of the M-band in response to the external force. This phenomenon is not

observed in the BAG3 mutant cells, which indicates that the assembly of M-band is impaired in the BAG3 mutant cells.

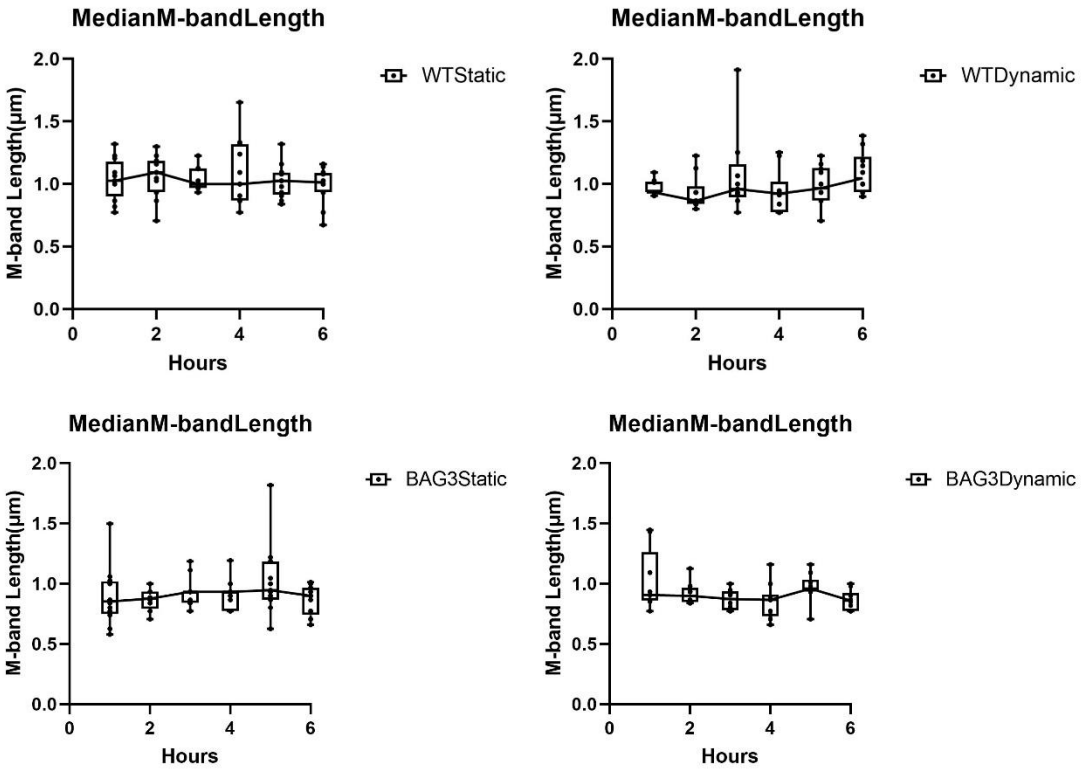

Figure 24 *The median M-band length. The median M-band length of BAG3 mutant cells is slightly shorter than the median M-band length of the wild-type cells. No significant is shown in the median M-band length of the BAG3 mutant cells.*

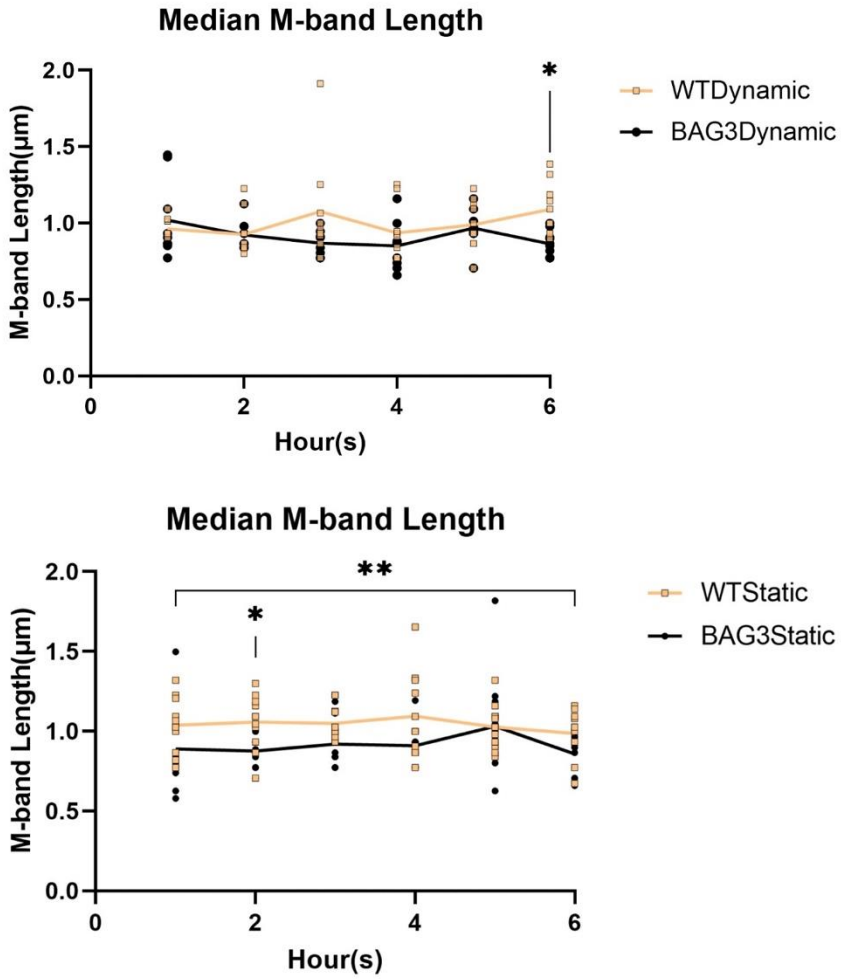

Figure 25 *The comparison between the BAG3 mutant cells and the wild-type cells in median M-band length. The p-value of the unpaired t-test is 0.0673 in the dynamic group, suggests no significant difference between the 2 cell groups. In the multiple unpaired t-test, only the samples at 6 hours incubation shown a q-value below 0.05, which shows significant difference. The p-value of the unpaired t-test is 0.0013 in the static group, suggests a significant difference between the 2 cell groups.*

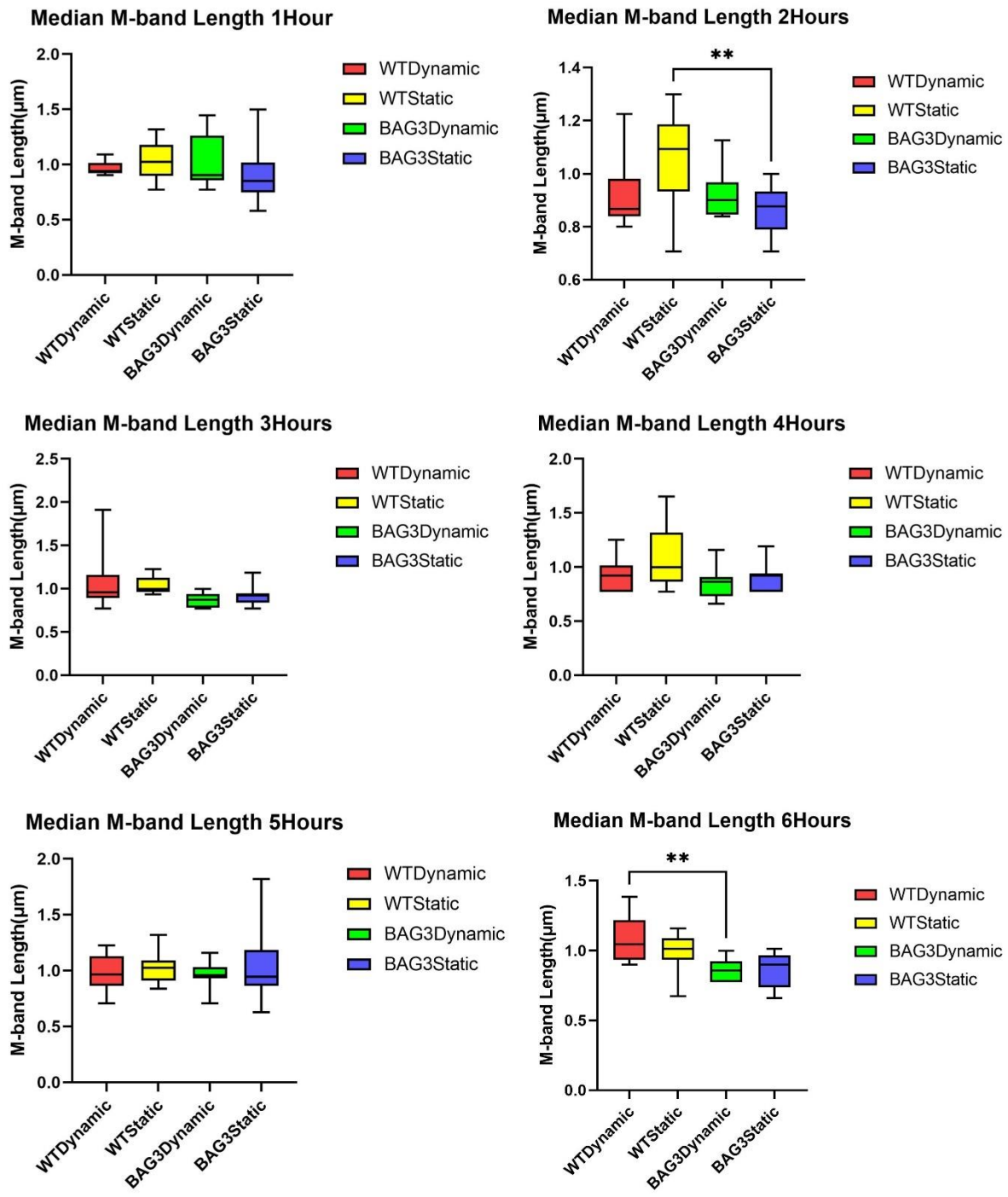

Figure 26 *The statistical analysis of median M-band length. The significant difference is shown 2 hours of incubation between BAG3 static and WT static group. A significant difference is also shown at 6 hours between BAG3 dynamic and WT dynamic group.*

3.3.3 Median Actin Length

The mean median actin length of the BAG3 mutant cells is short than the mean median actin length of wild-type cells **(Figure 27)**. In the dynamic group, the mean median actin length of BAG3 cells in the dynamic group is 0.8746μm while the mean median actin length of wild-type cells is 0.9480μm. In the static group, the mean median actin length of BAG3 cells is 0.8650μm while the mean median actin length of wild-type cells is 1.030μm. No significant change in median actin length in the dynamic group is observed in both BAG3 mutant and the wild-type cells over time. The t-test result of the median actin length shows a p-value of 0.0675, which indicates no significant different between the wild-type and BAG3 mutant cells in the dynamic group. The p-value of the static group is 0.0043, which indicates a significant difference. The q-value of all time points shows a result of no significant difference in the dynamic group **(Figure 28).** The ANOVA test shows that the significant difference is shown at 4 hours of incubation between BAG3 static, WT static groups and WT dynamic, WT static groups **(Figure 29)**. The stable median actin length in the dynamic group is consistent with the sliding filament theory that the contraction of myofibril is functionalized by the sliding of the thin filaments. The t-test of the static group shows that the integrity of the thin filament is impaired in the BAG3 mutant cells. The no significant result of the dynamic group may be explained by the premyofirbil genesis in the stretched cells that shorter actin filaments are produced in the wild-type cells.

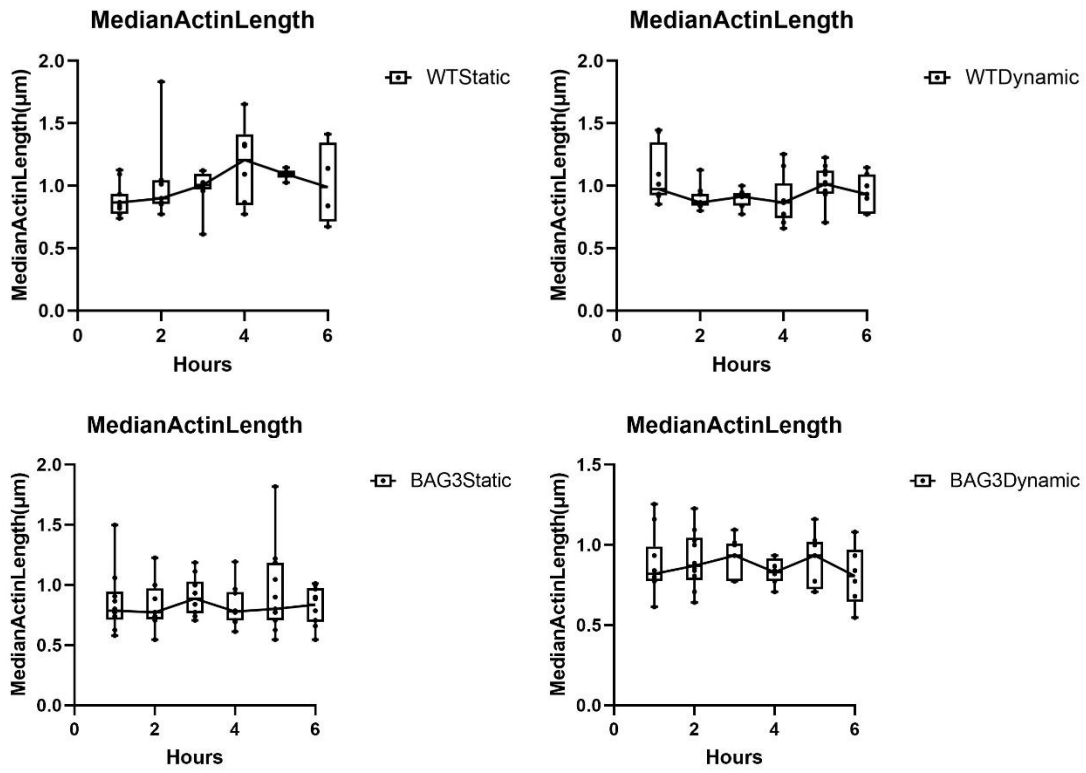

Figure 27 *The median actin length. The median actin length of BAG3 mutant cell is shorter than the wild-type cells. No significant change in median actin length in the dynamic group is observed in both BAG3 mutant and the wild-type cells over time.*

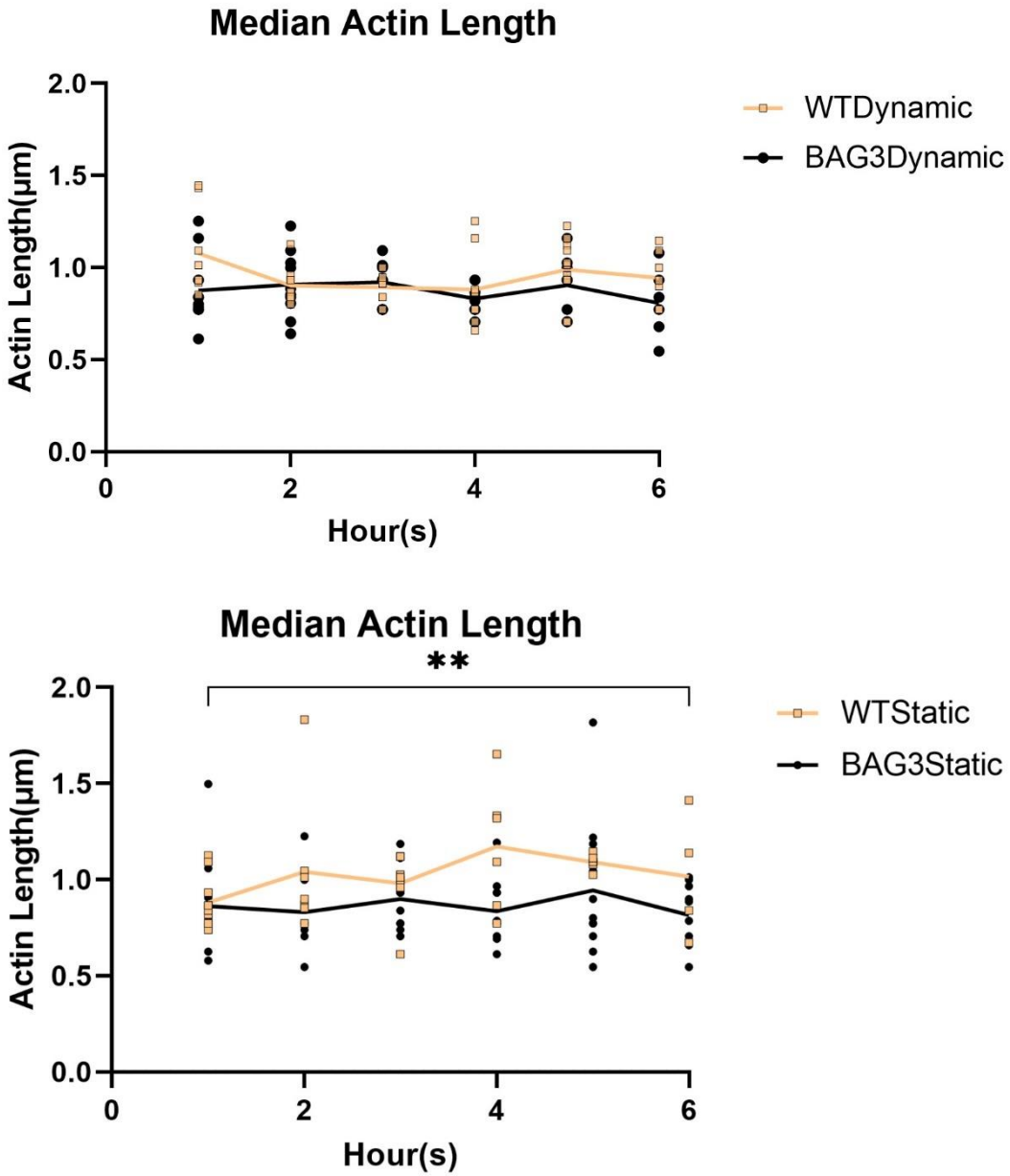

Figure 28 *The result comparing the BAG3 mutant cells and the wild-type cells in median actin length. The p-value of the unpaired t-test is 0.0675 of the dynamic group, suggests no significant different between the 2 cell groups. No significant difference is observed between the dynamic groups. The p-value of the unpaired t-test is 0.0043 of the static group, suggests a significant difference between the 2 cell groups.*

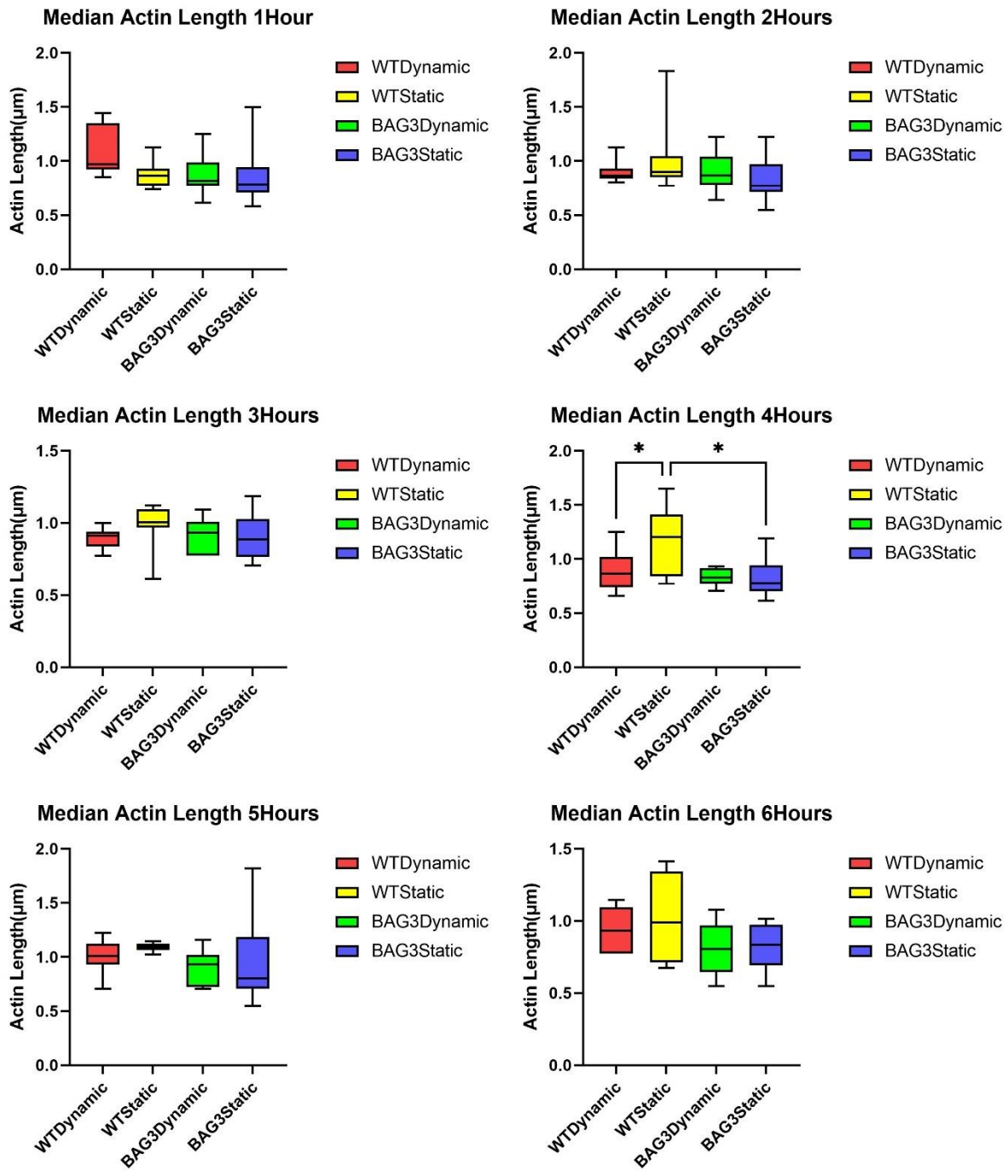

Figure 29 *The statistical analysis of median actin length. The significant difference is shown at 4 hours of incubation between BAG3 static, WT static groups and WT dynamic, WT static groups.*

3.4 Sarcomere Protein Orientational Order Parameter (OOP)

3.4.1 Z-line OOP

The orientational order parameter (OOP) is a parameter to describe the alignment rate of a structure. In our study, OOP is used to measure the rate of cell stretching and the sarcomere integrity of cells. The Z-line OOP is to measure the alignment rate of the entire Z-line. The mean Z-line OOP of BAG3 mutant cells and the wild-type cells in the dynamic and static groups are 0.1912, 0.2975, 0.1039, and 0.0910, respectively **(Figure 30)**. The higher mean OOP of the dynamic group shows that the cell morphology is changed during the SMP recovery, and the sarcomere Z-line is more aligned. In the dynamic group, the OOP increased at the beginning of SMP recovery. The increase rate in BAG3 mutant cells is lower than the increase rate in the wild-type cells.

The t-test result of the Z-line OOP has a p-value of 0.0158, which means a significant difference between the wild-type and BAG3 mutant cells. The p-value of the static group is 0.3856, which shows no significant difference. The q-value of multiple t-tests shows that the samples of 1 and 4 hours of SMP recovery are significantly different **(Figure 31)**. The one-way ANOVA test shows that the significant difference between WT dynamic and WT static groups has shown at the first 5 hours of incubation. The significant difference between BAG3 dynamic and WT static group is shown at 1, 3 and 4 hours of incubation **(Figure 32)**.

The result indicates that the ability to rebuild the Z-line structure in the BAG3 mutant cells is impaired. Since the increase in the Z-line OOP is resulted from the cell stretching during

SMP recovery, the lower Z-line OOP in the BAG3 mutant cells indicates the impaired assembly ability of α-actinin to the sarcomere structure that the filaments are not stretched by the external force. The multiple t-test result also indicates that the wild-type cells take about 4 to 5 hours to repair the Z-line structure while the assembly of Z-line is disturbed in the BAG3 mutant cells. In the dynamic group, the Z-line OOP of the wild-type cells increased in the first 3 hours of incubation and decreased after 3 hours. This result suggests that the Z-line structure is being stretched for the first 3 hours and then the cells may start to repair the stretched Z-line. This change is delayed in the BAG3 mutant cells, which may indicate that the force distribution capacity in the BAG3 cells is impaired.

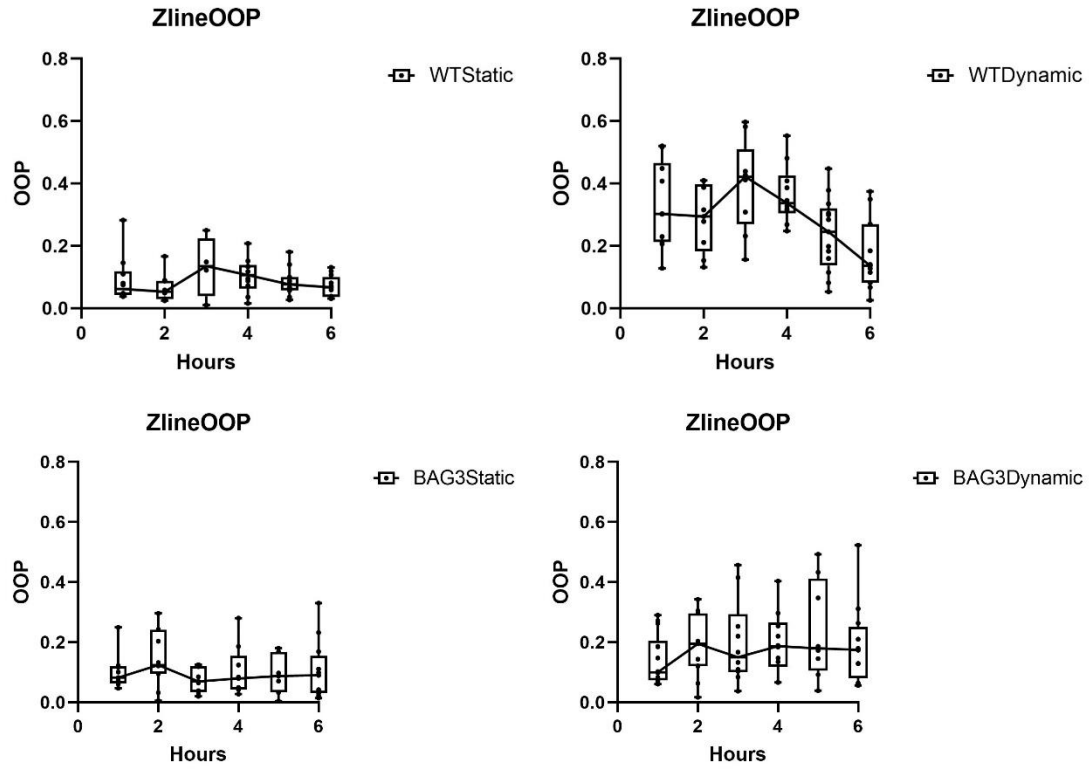

Figure 30 *The Z-line OOP. BAG3 mutant cells have lower Z-line OOP in the dynamic group compared to the wild-type cells. During the recovery, the Z-line OOP of WT cells increased in the first 3 hours, and then decrease. This process is delayed in the BAG3 mutant cells.*

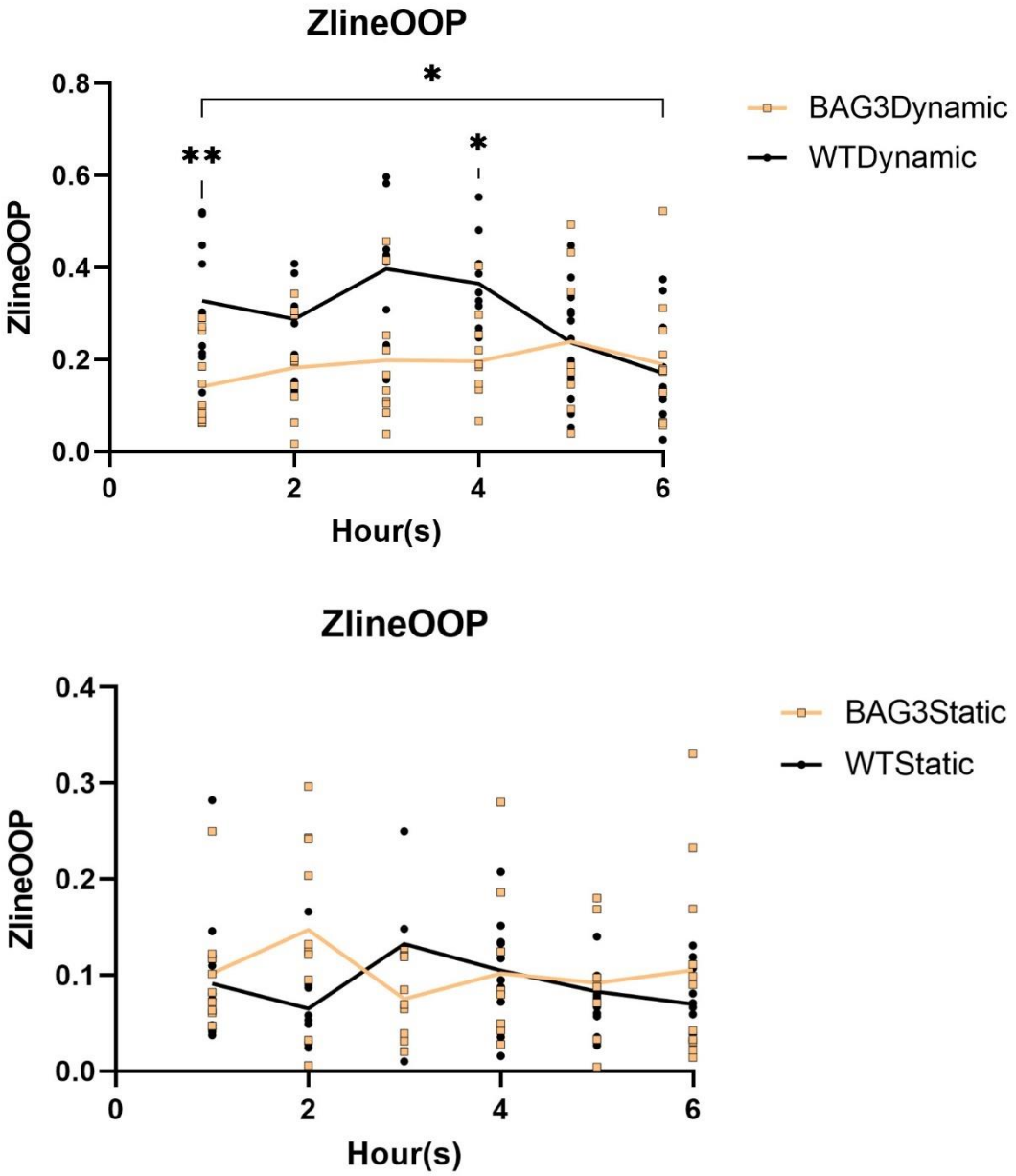

Figure 31 *The result comparing the BAG3 mutant cells and the wild-type cells in the Z-line OOP. The p-value of the unpaired t-test is 0.0158 and 0.3856 of the dynamic and the static groups, suggests no significant difference between the 2 cell groups. The q-value of the samples of 1 and 4 hours for SMP recovery shows significant difference in the dynamic group.*

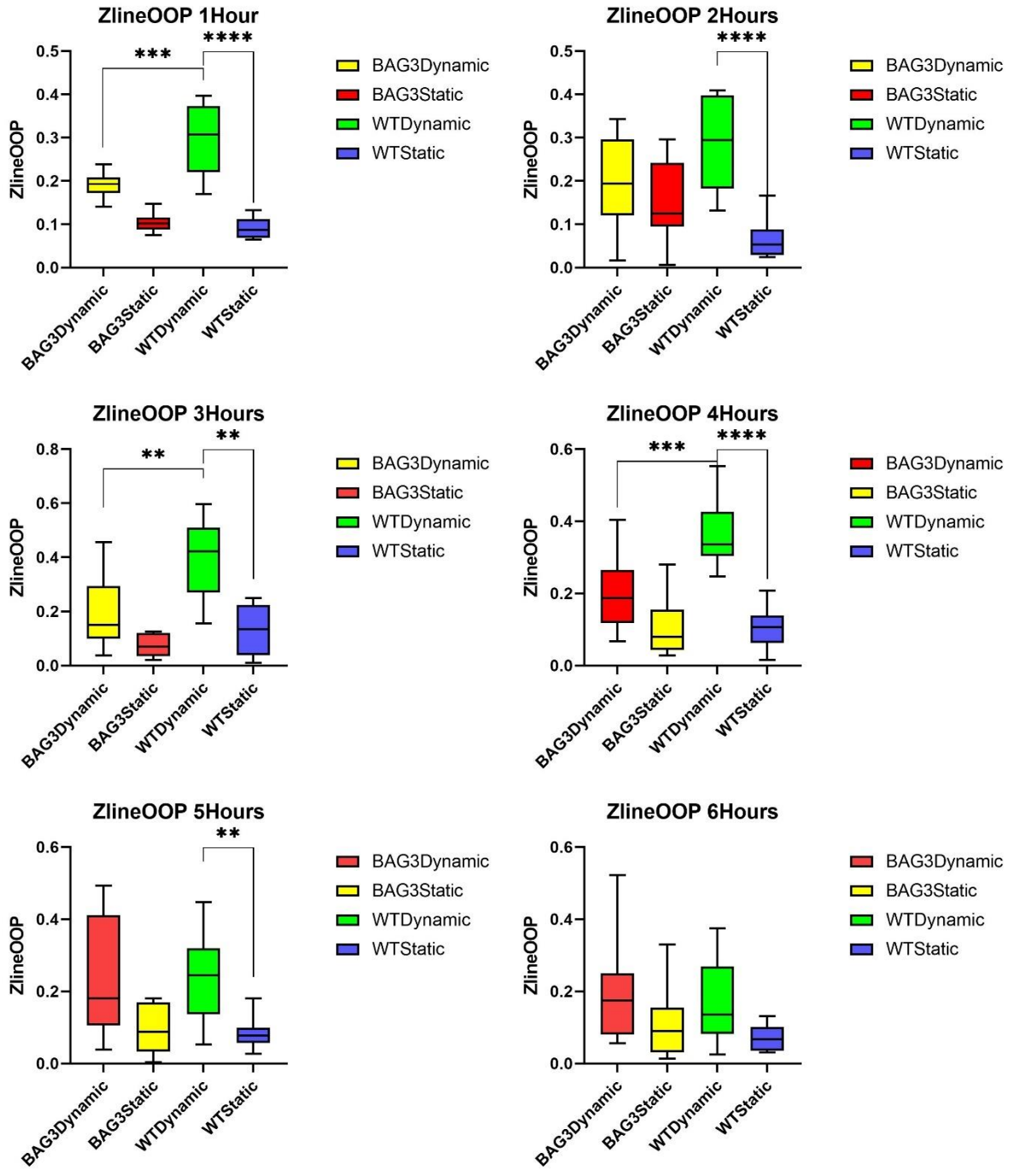

Figure 32 *The statistical analysis of Z-line OOP. The significant difference between WT dynamic and WT static groups has shown at the first 5 hours of incubation. The significant*

difference between BAG3 dynamic and WT static group is shown at 1, 3 and 4 hours of incubation.

3.4.2 M-band OOP

The mean M-band OOP of BAG3 mutant cells and the wild-type cells in the dynamic and static groups are 0.1038, 0.2202, 0.07762, and 0.1358, respectively **(Figure 33)**. This result also indicates that the cells are stretched in the dynamic group during the SMP recovery. The M-band OOP of wild-type cells increased in the first 2 hours and then decreased while the OOP of BAG3 mutant cells has no significant change, this result indicates that the cell's ability to adapt to external change in BAG3 mutant cells is impaired.

The t-test result of M-band OOP has a p-value of 0.0449, which shows a significant difference between the cell groups. The p-value of the unpaired t-test is 0.9298 for the static group, which suggests no significant difference between the 2 cell groups. The q-value of the multiple t-tests has only shown a significant difference in the 2 hours samples **(Figure 34)**. The one-way ANOVA test shows that the significant difference between WT dynamic and WT static groups has shown 2 and 4 hours of incubation. The significant difference between BAG3 dynamic and WT static group is shown at 2 hours of incubation **(Figure 35)**.

The result of M-band OOP is consistent with the Z-line OOP that the M-band OOP increased at the first 4 hours of incubation in the wild-type cells while there is no significant difference

in the BAG3 mutant cells. The result also suggests that the integrity of sarcomere is impaired in the BAG3 mutant cell that the sarcomere structure could not respond to the external force.

The sharp increase of the M-band OOP in the first 2 hours of incubation of the wild-type cell in the dynamic group may indicate that the M-band structure is the structure that the external force applied to. After 2 hours of increase, the M-band OOP decreased to the same value of the BAG3 mutant cells, which may indicate that the cells are repairing the stretched M-band structure.

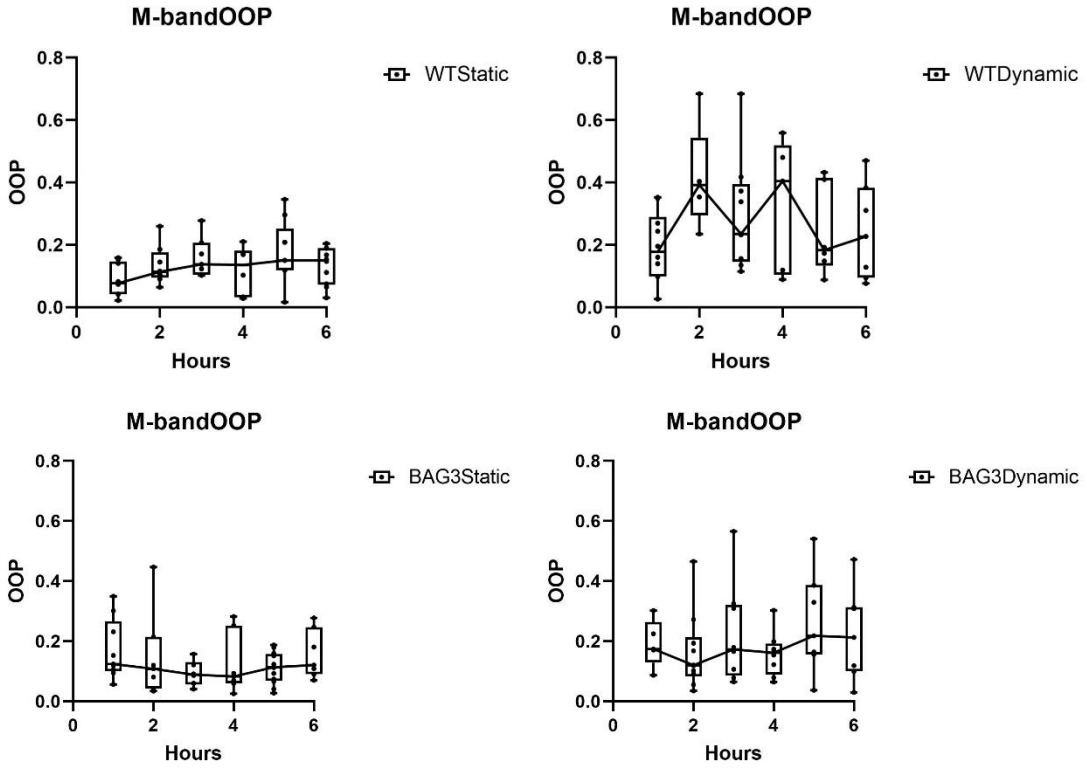

Figure 33 *M-band OOP. The M-band OOP of BAG3 mutated CMs is lower than the M-band OOP of WT CMs. The M-band OOP of WT CMs increased during the first 2 hours of SMP recovery and then decreased while no significant change shown in BAG3 mutant cells.*

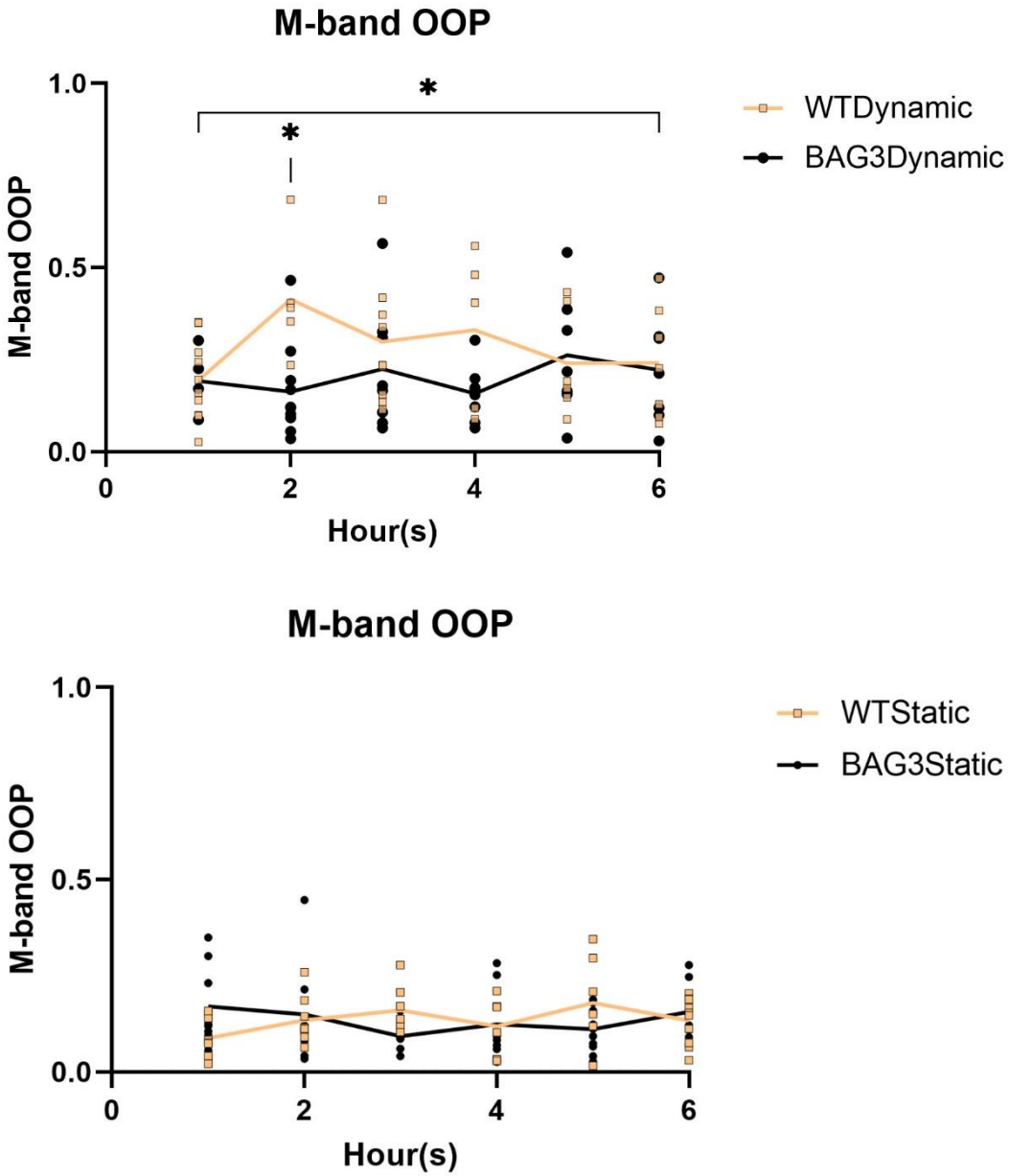

Figure 34 *The result comparing the BAG3 mutant cells and the wild-type cells in the M-band OOP. The p-value of the unpaired t-test is 0.0449 of the dynamic group, suggests a significant difference between the 2 cell groups. Only the sample of 2 hours incubation has shown a q-value of significant different. The p-value of the unpaired t-test is 0.9298 of the static group, suggests no significant difference between the 2 cell groups.*

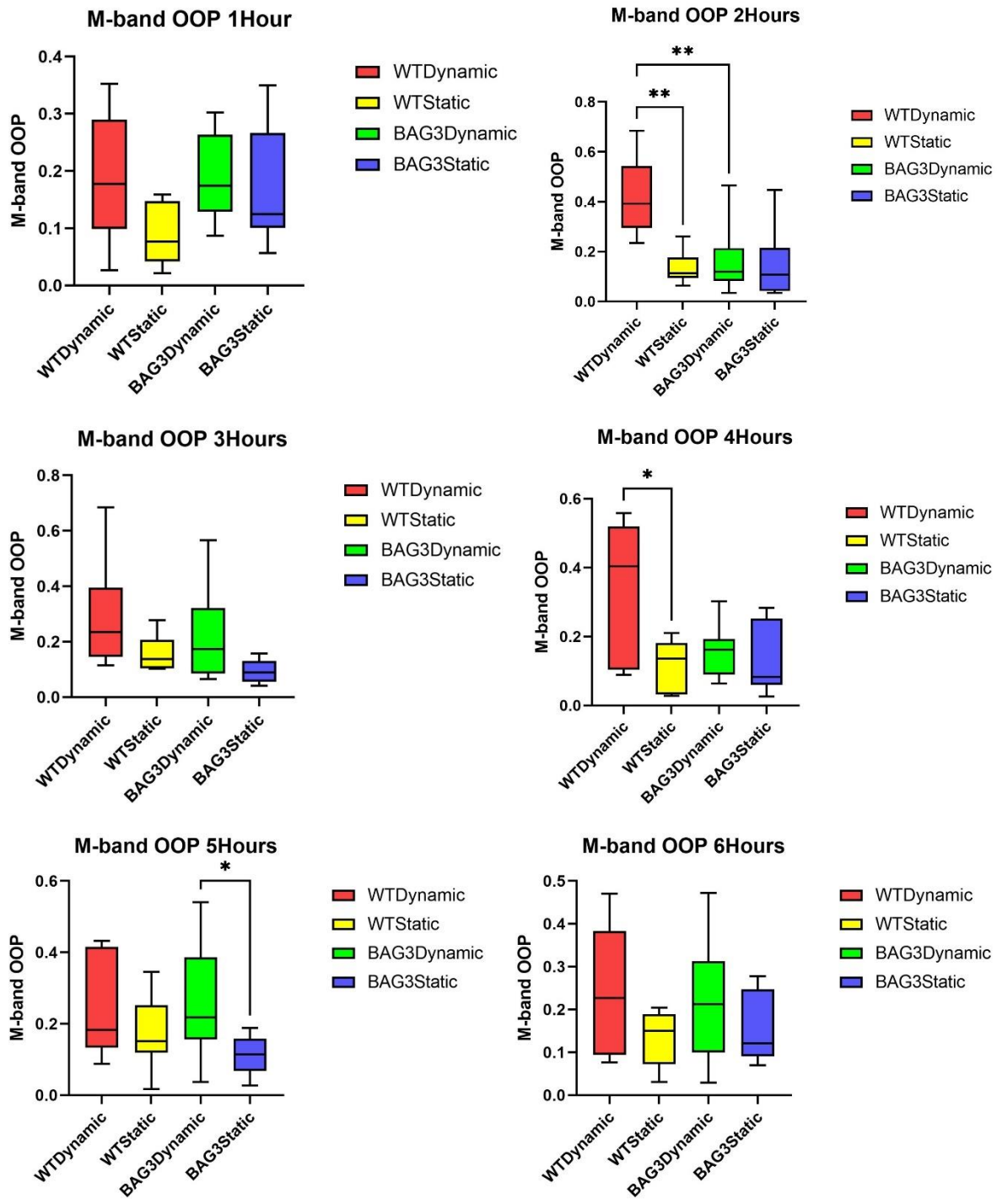

Figure 35 *The statistical analysis of M-band OOP. The significant difference between WT dynamic and WT static groups has shown 2 and 4 hours of incubation. The significant difference between BAG3 dynamic and WT static group is shown at 2 hours of incubation.*

3.4.3 Actin OOP

The mean actin OOP of the wild-type cells is lower than the mean actin OOP of the BAG3 mutant cells in the dynamic group, which are 0.3138 and 0.4392 respectively **(Figure 36)**. The t-test result has a p-value of 0.0050, which indicates a significant different between the groups. The p-value of the unpaired t-test is 0.3640 for the static group, suggests no significant difference between the 2 cell groups. Consistent with the M-band OOP, the only significant difference is the 2-hour incubation sample **(Figure 37)**.

Since the contraction of myofibrils is functioned by the sliding of the thin filaments, the increased actin OOP in the BAG3 mutant cells might happen because of the impaired Z-line and M-band integrity damaged the connection between thin filaments and these structures.

No significant change in the actin OOP in the dynamic group over the SMP recovery time is observed. The one-way ANOVA also suggests no significant difference between the cell groups **(Figure 38)**.

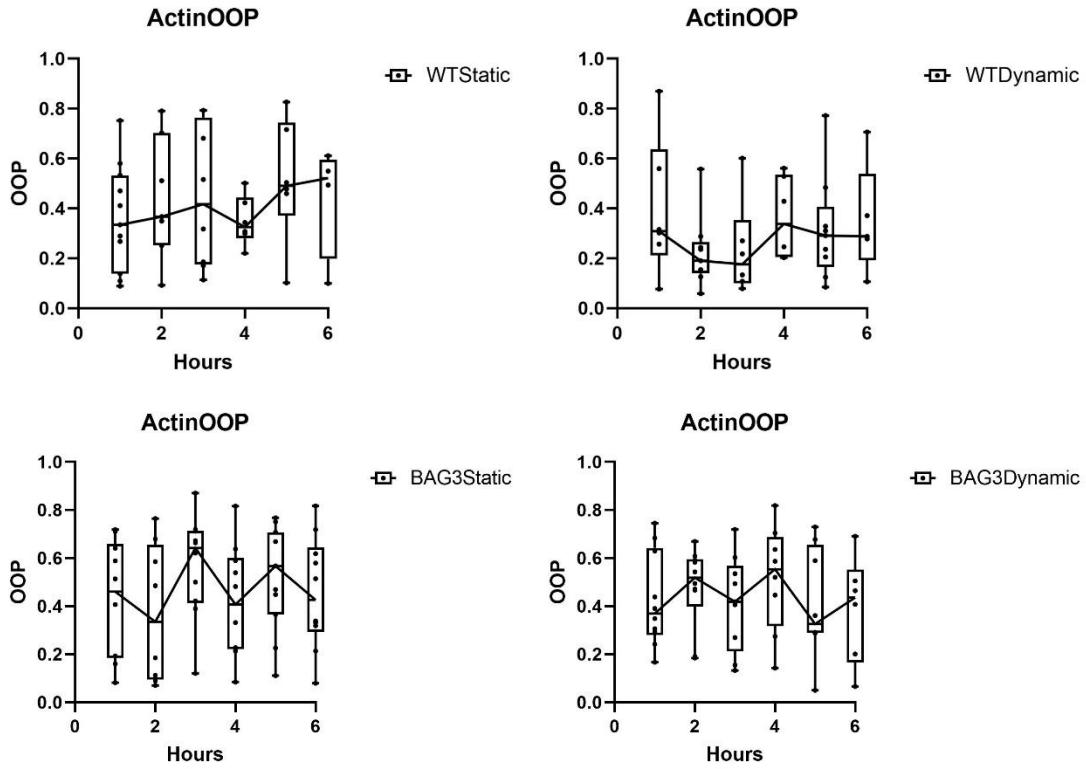

Figure 36 *The actin OOP. The mean actin OOP of the wild-type cells is lower than the mean actin OOP of the BAG3 mutant cells in the dynamic group.*

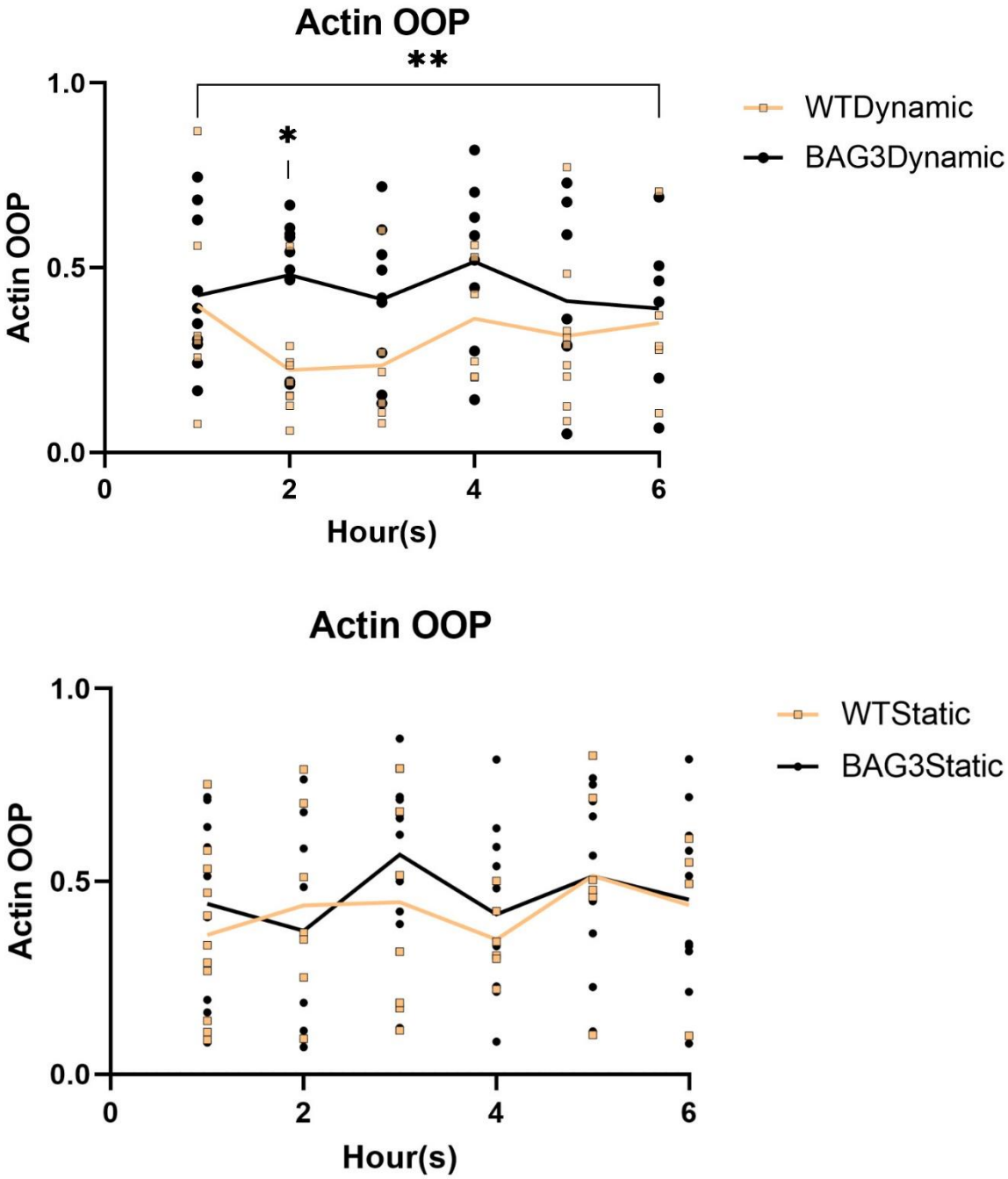

Figure 37 *The result comparing the BAG3 mutant cells and the wild-type cells in the actin OOP. The p-value of the unpaired t-test is 0.0050 for the dynamic group, suggests a significant difference between the 2 cell groups. Only the sample of 2 hours incubation has shown a q-value of significant different. The p-value of the unpaired t-test is 0.3640 for the static group, suggests no significant difference between the 2 cell groups.*

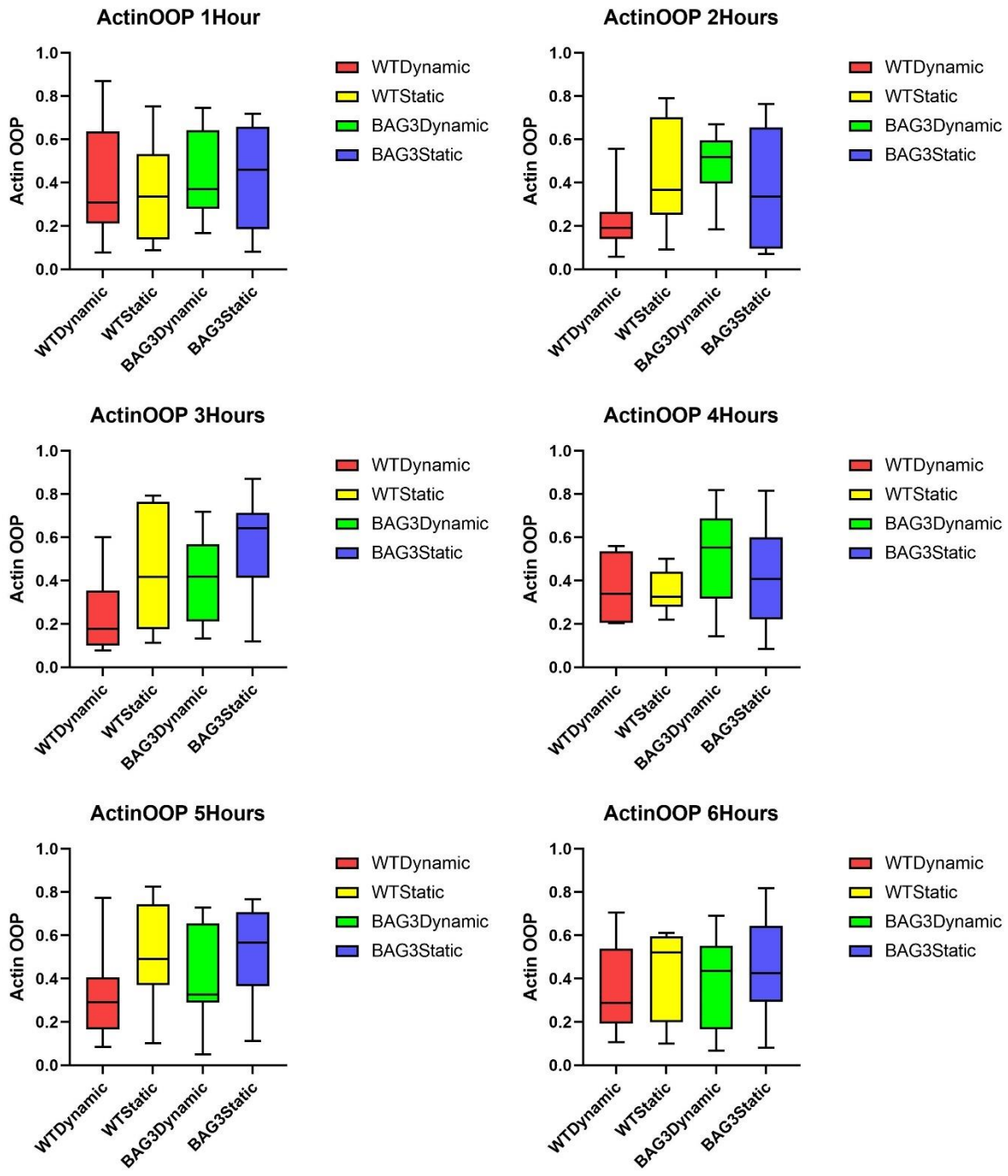

Figure 38 *The statistical analysis of actin OOP. No significant difference is shown between cell groups.*

3.5 Sarcomere Protein Distance

3.5.1 Mean Z-line Distance

The Z-line distance is the distance between α-actinin bands in cells. In the dynamic group, the mean Z-line distance of BAG3 mutant cells and the wild-type cells are 1.762μm and 1.455μm, respectively **(Figure 39)**. In the static group, the mean Z-line distance of BAG3 mutant cells and the wild-type cells are 1.552μm and 1.453μm, respectively. The difference in mean Z-line distance between the static and dynamic group of the wild-type cells again proved that cells are stretched during the SMP recovery, the sarcomere is also stretched and the distance between α-actinin bands increased. However, there is no significant difference between the static group and the dynamic group in the BAG3 mutant cells. The t-test result of the mean Z-line distance has a p-value of 0.0001 for the dynamic group, which suggests that there is a significant difference between the groups. The p-value of the unpaired t-test is 0.5252 in the static group, which suggests no significant difference between the 2 cell groups. The multiple t-tests show that the samples of 1-, 2-, 3-, 4- and 6-hours incubation has a significant difference **(Figure 40)**. The one-way ANOVA test shows that the significant difference has shown at 1,2,3,4,6 hours of incubation between the BAG3 dynamic group and the WT dynamic group. The significant difference has shown at 1,2,4 hours of incubation between the BAG3 static group and the WT static group. The significant difference has shown at 2,5,6 hours of incubation between the WT static group and the WT dynamic group **(Figure 41)**.

The mean Z-line distance of the wild-type cells is longer than the mean Z-line distance of the BAG3 mutant cells. Since the M-band is an elastic hinged structure that binding thin filament and thick filament that facilitate sarcomere contraction, the impairment of the M-band in the

BAG3 mutant cells may result in a lower elasticity of the sarcomere structure when responding to the force generated by SMP recovery. The Z-line distance in the dynamic group is longer than in the static group, which suggests the cells are stretched by the SMP recovery. The Z-line distance of the wild-type cells in the dynamic group is decreasing over the incubation time, which may indicate the cells are repairing the stretched sarcomere when this process is not observed in the BAG3 mutant cells.

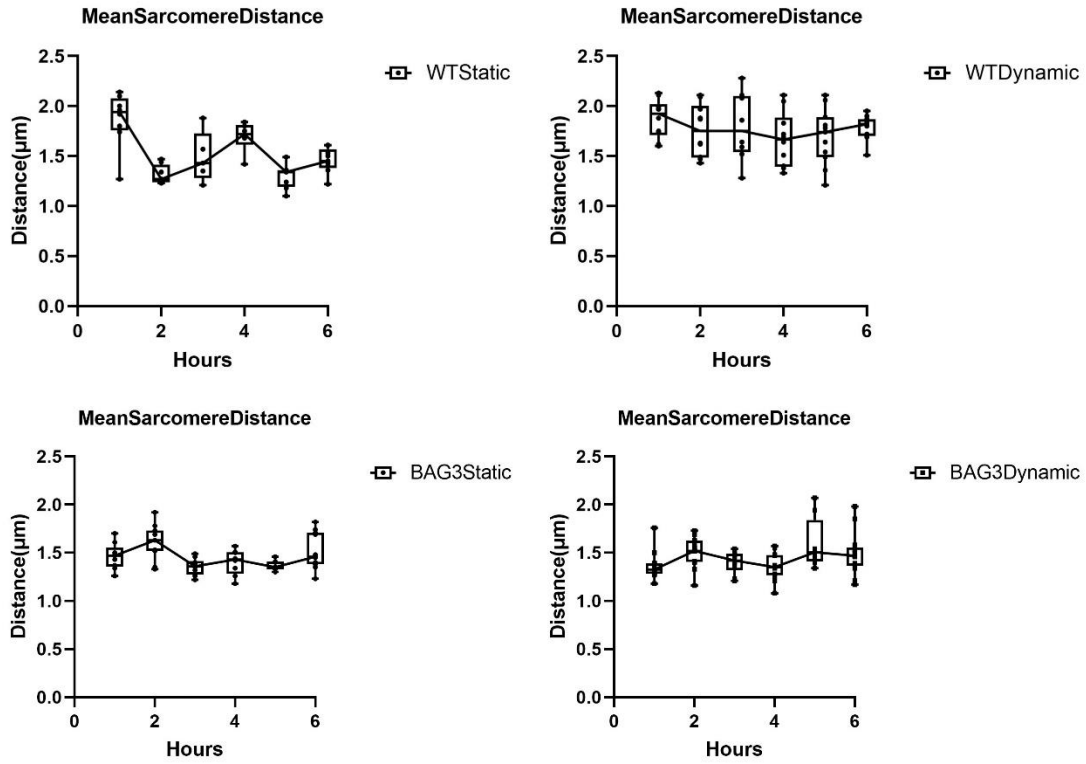

Figure 39 *The mean Z-line distance. The mean Z-line distance of the wild-type cells is shorter than the BAG3 mutant cells. The mean Z-line distance in the dynamic group is longer than in the static group.*

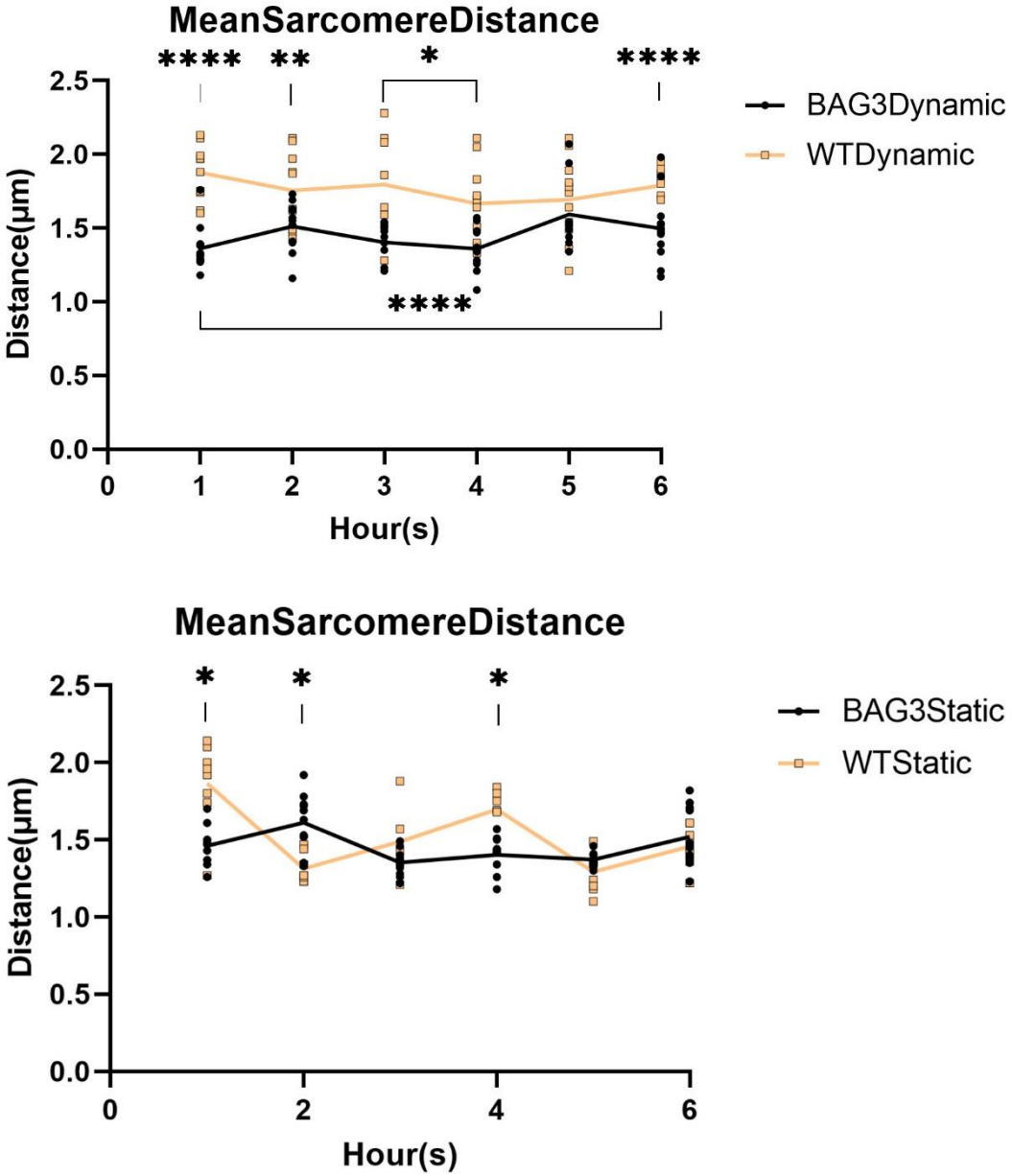

Figure 40 *The result comparing the BAG3 mutant cells and the wild-type cells in the mean Z-line distance. The p-value of the unpaired t-test is 0.0001 in the dynamic group, suggests a significant difference between the two cell groups. The p-value of the unpaired t-test is 0.5252 in the static group, suggests no significant difference between the 2 cell groups. The multiple t-test shows significant differences in the 1, 2 and 4 hours of the static group.*

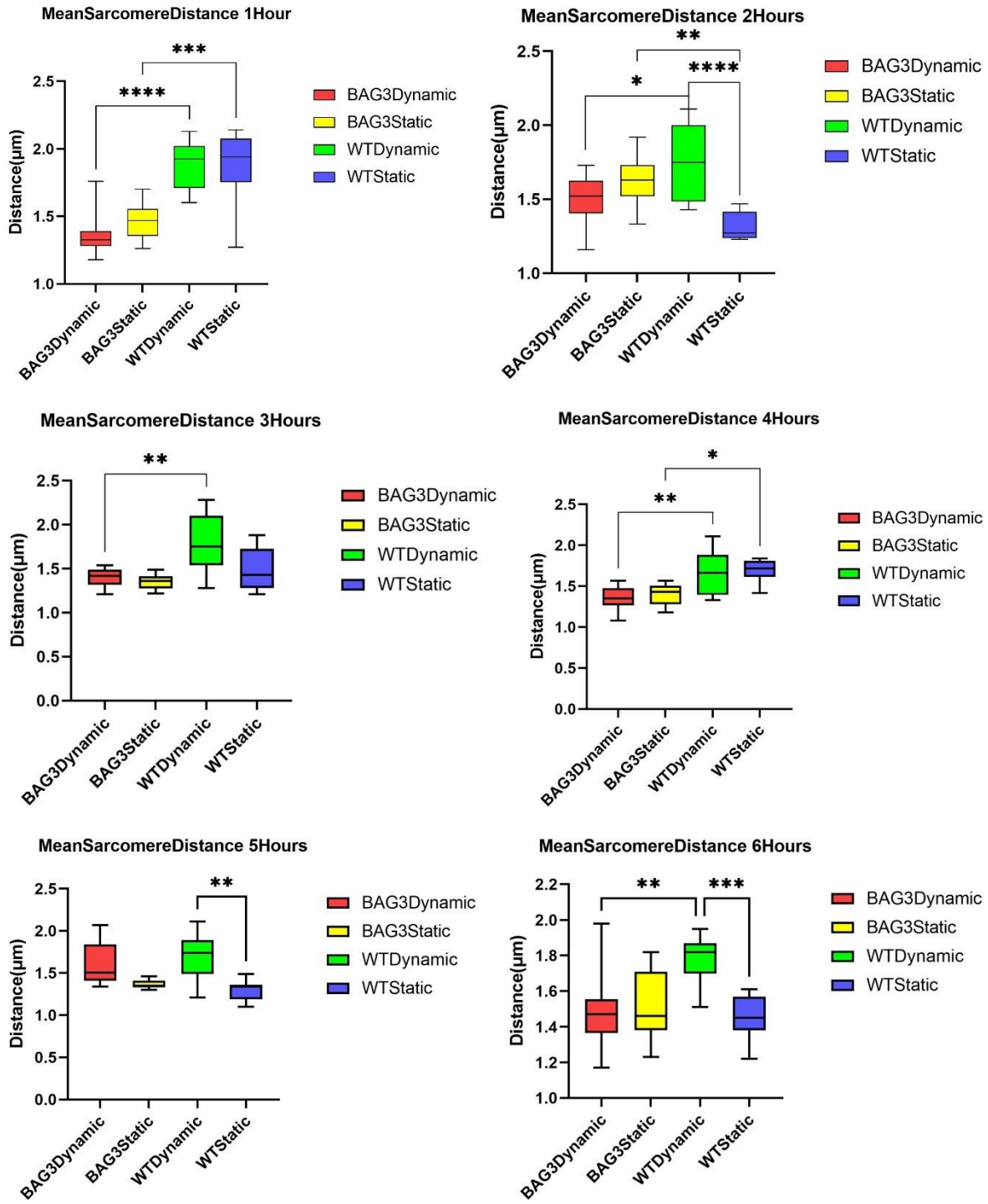

Figure 41 *The statistical analysis of mean Z-line distance. The significant difference has shown at 1,2,3,4,6 hours of incubation between the BAG3 dynamic group and the WT dynamic group. The significant difference has shown at 1,2,4 hours of incubation between the*

BAG3 static group and the WT static group. The significant difference has shown at 2,5,6 hours of incubation between the WT static group and the WT dynamic group.

3.5.2 Mean M-band Distance

The mean M-band distance of the wild-type cells and the BAG3 mutant cells in the dynamic and static group is 1.828μm, 1.653μm, 1.767μm and 1.538μm, respectively. The t-test of the dynamic and static groups have a p-value of 0.5054 and 0.1367, which indicated no significant difference in the 2 groups. No significant difference is showed in comparison of individual sample groups. The one-way ANOVA test shows no significant difference between cell groups **(Figure 42, 43, 44)**.

The comparison between the dynamic and static group has shown that the M-band structure is stretched during the SMP recovery. However, there is no significant change in the M-band distance with the incubation time. The wild-type cells have a longer M-band distance compared to the BAG3 mutant cells. Since M-band is an elastic structure in the sarcomere to maintain the stability of the sarcomere structure, the impaired M-band integrity may result in a decreased M-band elasticity that the M-band distance in the BAG3 mutant cells is reduced.

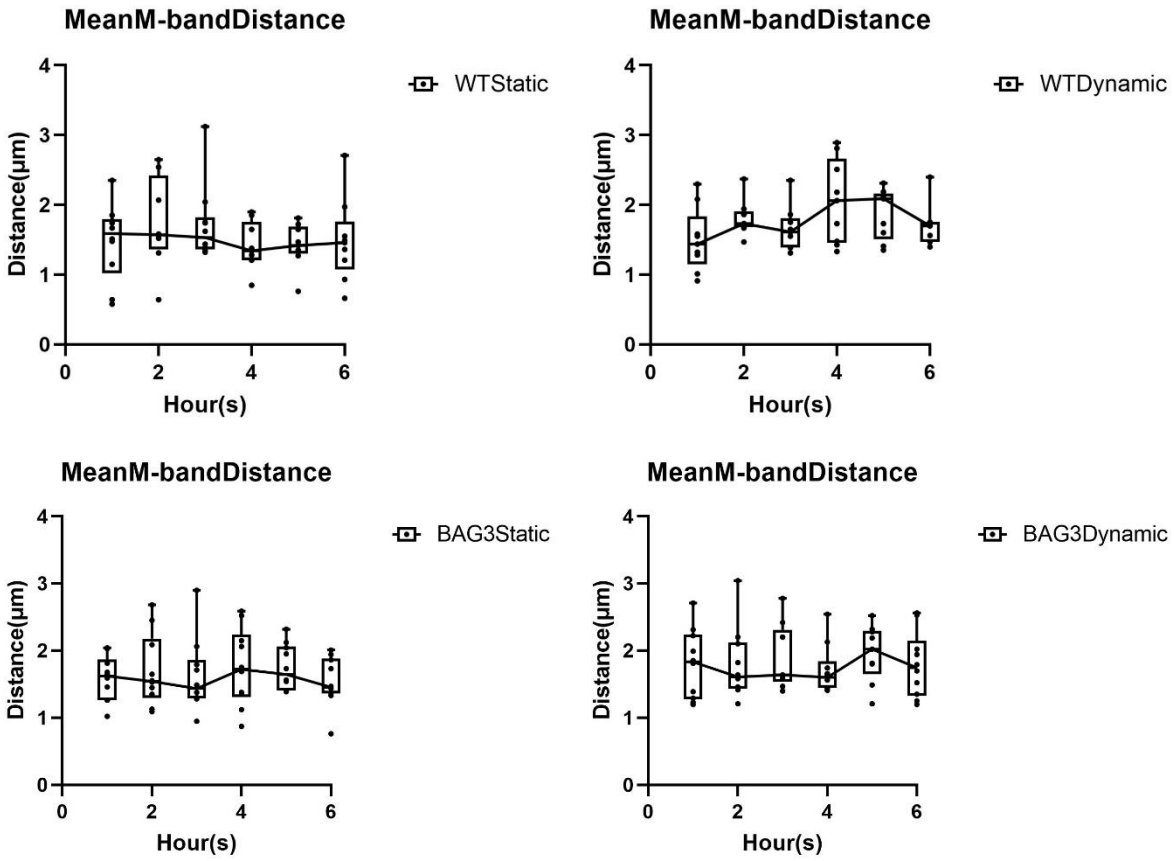

Figure 42 *The mean M-band distance of the wild-type and the BAG3 mutant cells. The mean value of the M-band distance of the wild-type and BAG3 mutant cells are in the dynamic and static groups are 1.828µm, 1.653µm, 1.767µm and 1.538µm, respectively.*

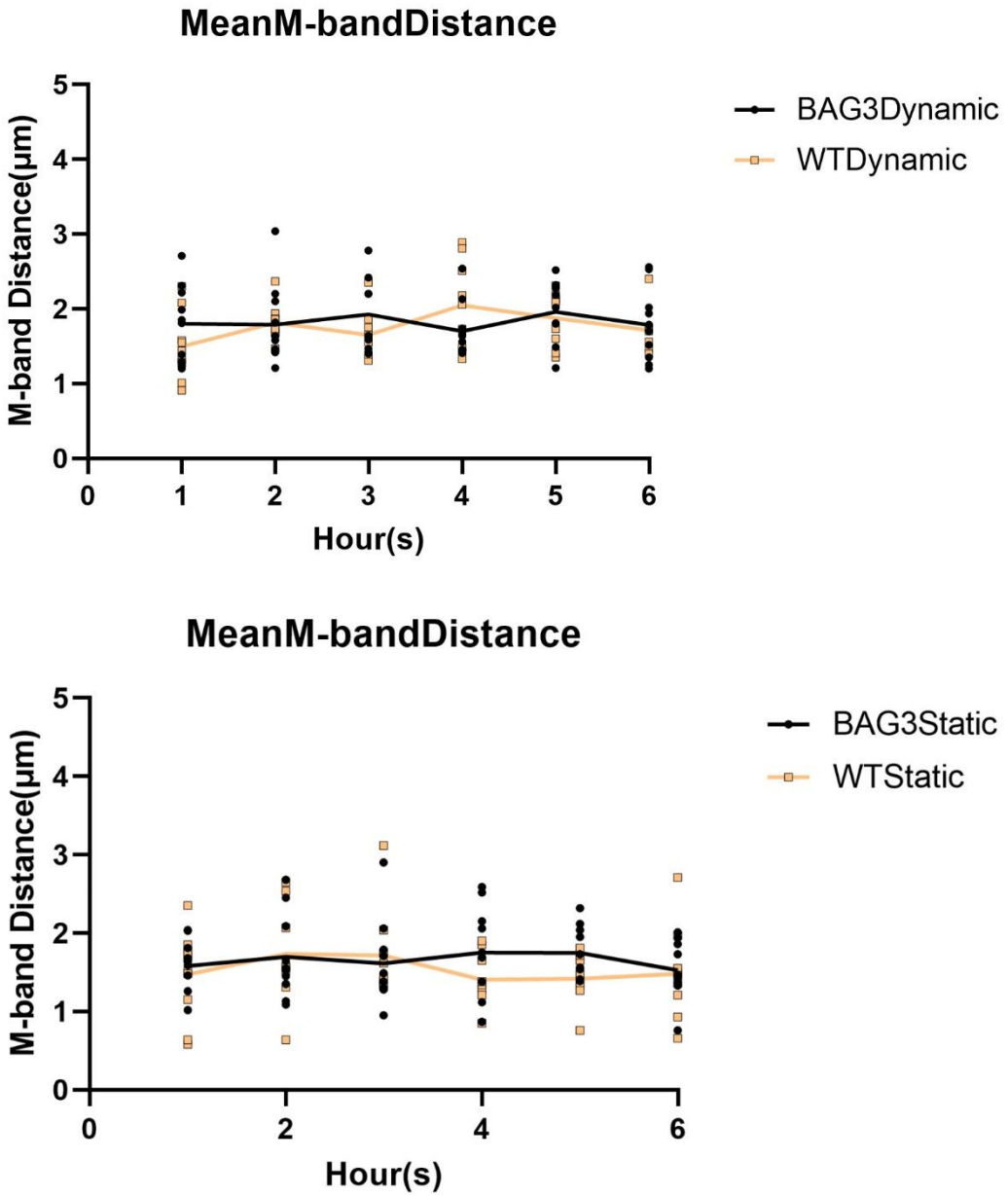

Figure 43 *The comparison of the mean M-band distance between the wild-type cells and the BAG3 mutant cells in the dynamic group and the static group. The p-value of the dynamic group and the static group are 0.5054 and 0.1367, which shows no significant difference in both groups.*

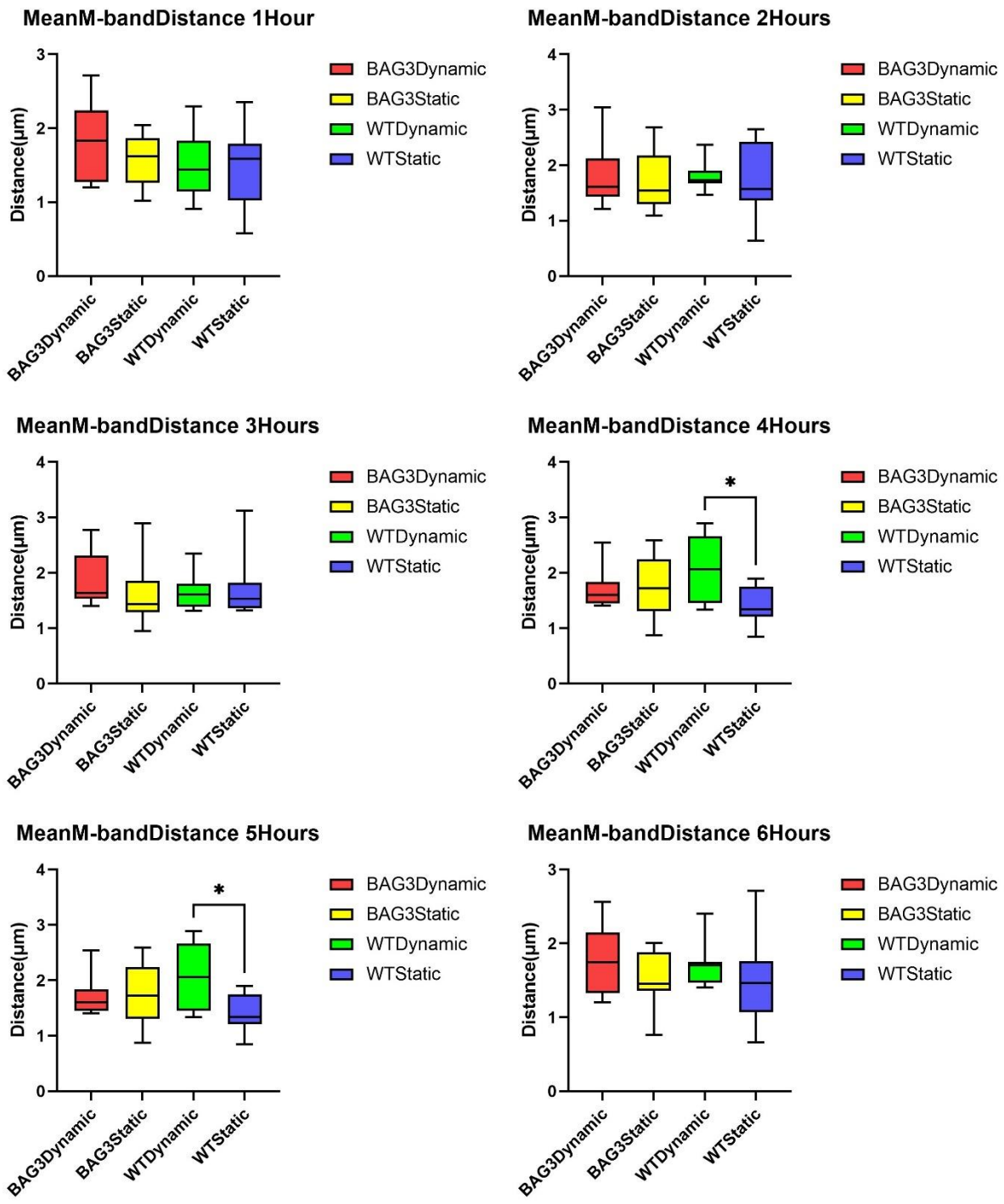

Figure 44 *The statistical analysis of mean M-band distance. No significant difference is shown between cell groups.*

3.5.3 Mean Actin Distance

The mean actin distance of the wild-type cells and the BAG3 mutant cells in the dynamic and static group is 1.770μm, 1.780μm, 1.863μm and 1.683μm, respectively. The t-test of the dynamic and static groups have a p-value of 0.4997 and 0.6028, which indicated no significant difference in the 2 groups. No significant difference is shown in the comparison of individual sample groups **(Figure 45, 46)**. No significant change of the mean actin distance is showed in the dynamic group by the incubation time. The one-way ANOVA test shows that the significant difference has shown at 3 hours between the BAG3 static and WT static groups. The significant difference is shown at 4 hours between the WT dynamic and WT static groups **(Figure 47).**

The test result shows that the mean actin distance of the wild-type cells and the BAG3 mutant cells have no significant difference in both the dynamic and the static groups. Since actin is the sliding filament that functionalizes the sarcomere contraction, the result indicates that the thin filaments are not stretched by the SMP recovery. Since the contraction of the sarcomere is facilitated by hinging the M-band, the force generated by the SMP recovery may be only applied to the hinged M-band structure.

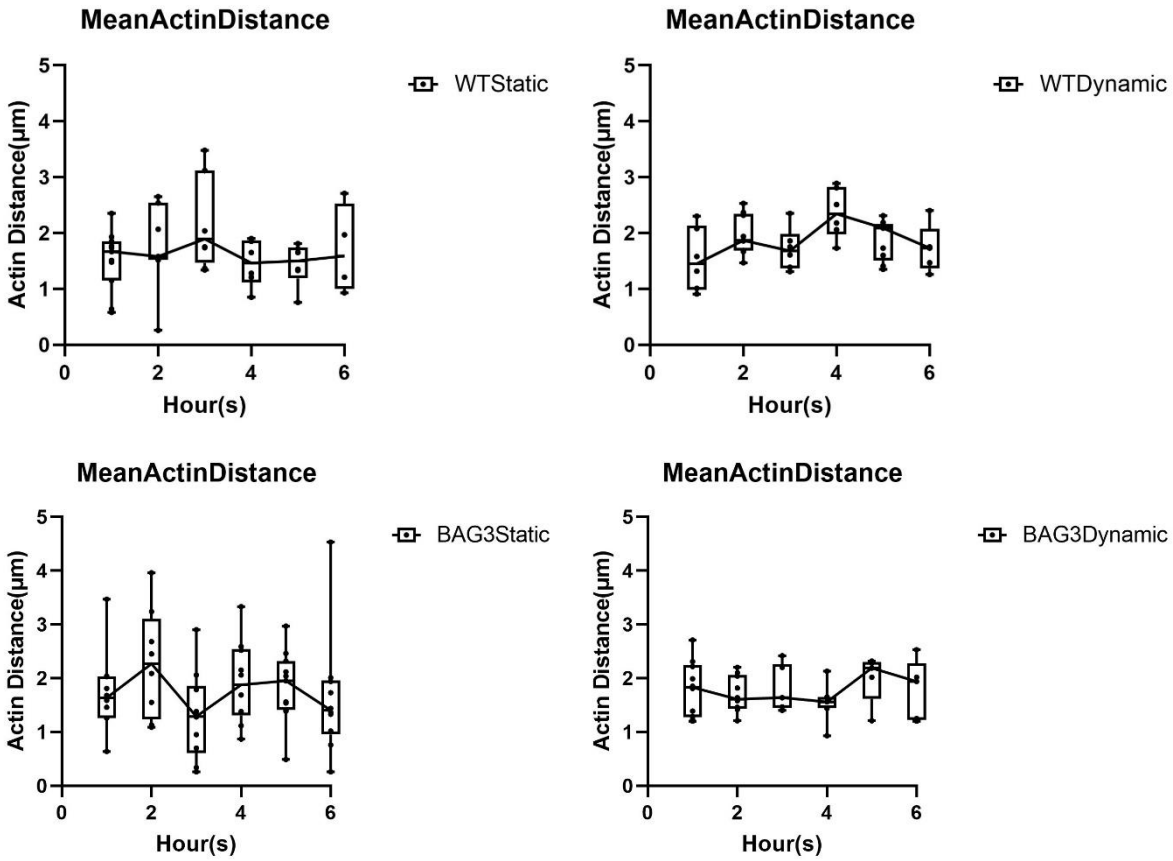

Figure 45 *The mean actin distance of the wild-type and the BAG3 mutant cells. The mean value of the actin distance of the wild-type and BAG3 mutant cells are in the dynamic and static groups are 1.770μm, 1.780μm, 1.863μm and 1.683μm, respectively.*

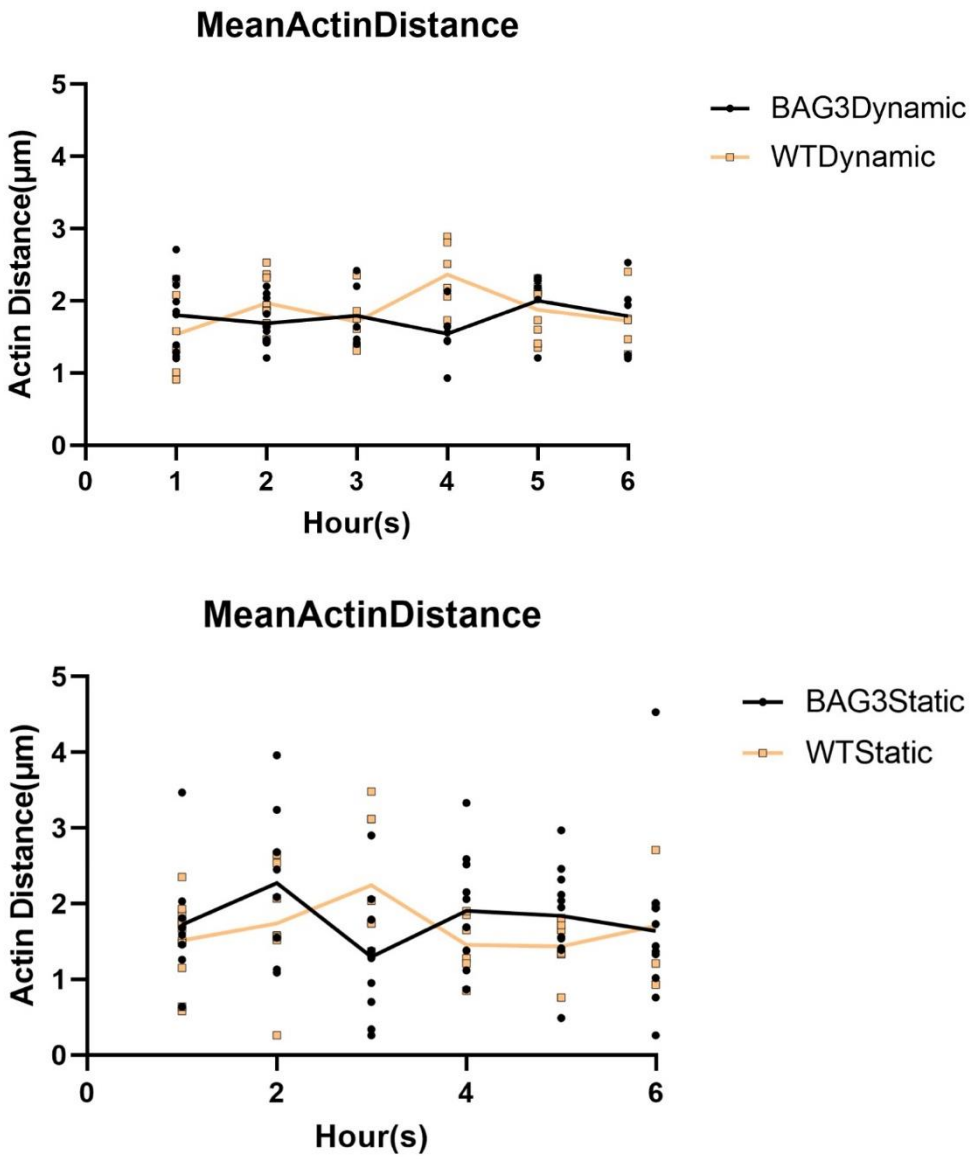

Figure 46 *The comparison of the mean actin distance between the wild-type cells and the BAG3 mutant cells in the dynamic group and the static group. The p-value of the dynamic group and the static group are 0.4997 and 0.6028, which shows no significant difference in both groups.*

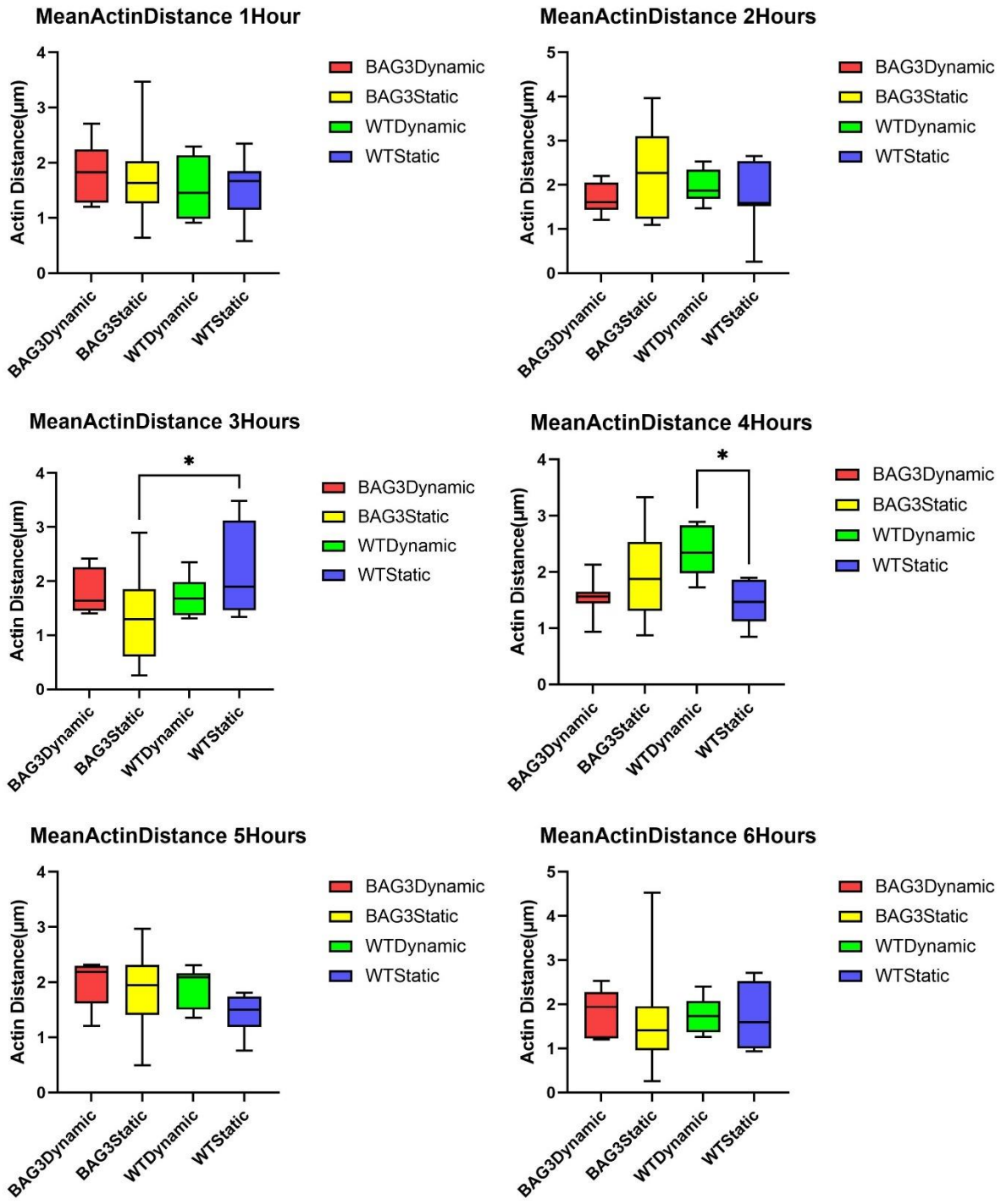

Figure 47 *The statistical analysis of mean actin distance. The significant difference has shown at 3 hours between the BAG3 static and WT static groups. The significant difference is shown at 4 hours between the WT dynamic and WT static groups.*

4 Discussion

In this study, the formation and the stability of nano wrinkles on the SMPs have been investigated. The nano wrinkles are formed within 1 hour of incubation at 37°C which triggers the recovery of SMPs. After formation, nano wrinkles can be stable in the culture media at 37°C incubation for 6 hours. This result shows that SMPs with PEM coating can be an ideal biomaterial to study cell-ECM interactions with a straightforward topography generation process. Since the generation of the surface topography happens during the incubation, it can provide a dynamic environment to study cell- ECM interactions. The wrinkles can also mimic the natural environment surrounding cardiomyocytes that squeeze the cells.

With the analysis of the 3 sarcomere parameters, this work investigated how BAG3 gene mutation, as a major reason for DCM, impaired the sarcomere structure. Previous studies have revealed that the BAG3 gene mutation could disturb the assembly and formation of the Z-line and impair the force generation capacity of the cells. In this work, we have revealed that the integrity of the M-band and the thin filament is also impaired in the BAG3 mutant cells. Since the M-band is the functional unit that facilitates the sarcomere contraction by controlling the sliding of the thin filaments, the impairment of M-band integrity could be the reason for the reduced force generation capacity.

During the SMP recovery, the sarcomere structure is stretched, and the Z-line distance is increased as a result of stretching. The thin filament and the M-band structure have not been stretched significantly by the SMP recovery. This result may indicate that the functional elastic unit of the M-band and the thin filament are hinged and have the capacity to adapt to the external force. The result also shows the repairment of the sarcomere structure in the wild-type cells that was triggered by the SMP recovery after several hours of incubation. This capacity to repair the sarcomere structure is impaired in the BAG3 mutant cells.

5 Future Work

The current work has investigated how BAG3 disturbed sarcomere integrity with observing the assembly and the integrity of the Z-line, M-band and thin-filaments in a dynamic environment. Besides these proteins, myosin and titin are the other important component of the sarcomere structure. Myosin has played an important role in myofibrillogenesis that the non-muscle-specific myosin is the major component of premyofibril, and the muscle-specific myosin is the component of the thick filament in the mature myofibril. Since the non-muscle-specific myosin exists in the cell in a beaded pattern, it is unable to quantify the volume of the non-muscle-specific myosin in the cells. However, understanding the production of the non-muscle-specific myosin and the substitution of the muscle-specific myosin is critical for us to understand the mechanism that how BAG3 gene mutation disturbed myofibrillogenesis.

Muscle-specific myosin is the component of sarcomere thick filaments. The head of myosin is connected to actin to form a cross-bridge during muscle activation or contraction. If the disturbance on the integrity of actin filaments will also disturb the integrity of the thick filament is not studied in this work. Since the length of thick filament does not change during muscle contraction, the stretching of cells may damage the structure of thick filament and how BAG3 gene mutation disturb the response to the damage is worthy to investigate.

Titin is the connecting protein that binding Z-line and the thick filament. The assembly of titin to the myofibril is also a symbol of the nascent myofibril. The disturbance of titin

integrity could impair the sarcomere integrity significantly. How BAG3 gene mutation impairs the nascent myofibril stage, and the production of titin is worthy to study.

This work has investigated the impact of BAG3 gene mutation on sarcomere structure and the formation of myofibril in a dynamic environment with a 6-hour incubation of the SMPs and the cells. However, the recovery of the sarcomere structure from the damage caused by stretching and the cell spreading on the wrinkles may require a longer time in incubation. To investigate the long-term impact of BAG3 gene mutation on cells, a 24-hour incubation can be used for observing the change in sarcomere structure. This study can help us further understand the impact of BAG3 gene mutation on cell integrity in a dynamic environment.

6 Reference

1. Takahashi, K., & Yamanaka, S. (2006). Induction of Pluripotent Stem Cells from Mouse Embryonic and Adult Fibroblast Cultures by Defined Factors. *Cell*, *126*(4), 663–676. https://doi.org/https://doi.org/10.1016/j.cell.2006.07.024
2. Stem cell 101. Institute for Stem Cell & Regenerative Medicine. (2020, July 16). Retrieved April 11, 2022, from https://iscrm.uw.edu/stem-cell-101/
3. Klimanskaya, I., Chung, Y., Becker, S., Lu, S.-J., & Lanza, R. (2006). Human embryonic stem cell lines derived from single blastomeres. *Nature*, *444*(7118), 481–485. https://doi.org/10.1038/nature05142
4. Sharma A, Burridge PW, McKeithan WL, et al. High-throughput screening of tyrosine kinase inhibitor cardiotoxicity with human induced pluripotent stem cells. *Sci Transl Med*. 2017;9(377):eaaf2584. doi:10.1126/scitranslmed.aaf2584
5. Sanger, J.W., Ayoob, J.C., Chowrashi, P., Zurawski, D., Sanger, J.M. (2000). Assembly of Myofibrils in Cardiac Muscle Cells. In: Granzier, H.L., Pollack, G.H. (eds) Elastic Filaments of the Cell. Advances in Experimental Medicine and Biology, vol 481. Springer, Boston, MA. https://doi.org/10.1007/978-1-4615-4267-4_6
6. Au, Y. The muscle ultrastructure: a structural perspective of the sarcomere. Cell. Mol. Life Sci. C. 61, 3016–3033 (2004).
7. Johnson, L. R. Gastrointestinal Physiology E-Book: Mosby Physiology Monograph Series. (Elsevier Health Sciences, 2013).
8. Dabiri, G. A., Turnacioglu, K. K., Sanger, J. M. & Sanger, J. W. Myofibrillogenesis visualized in living embryonic cardiomyocytes. Proc. Natl. Acad. Sci. 94, 9493–9498 (1997).

9. Morimoto, S. (2008). Sarcomeric proteins and inherited cardiomyopathies. *Cardiovascular Research*, *77*(4), 659–666. https://doi.org/10.1093/cvr/cvm084

10. Sanger, J. W., Wang, J., Fan, Y., White, J., & Sanger, J. M. (2010). Assembly and dynamics of myofibrils. *Journal of Biomedicine and Biotechnology*, *2010*(Figure 2). https://doi.org/10.1155/2010/858606

11. J. R. Fallon and V. T. Nachmias, "Localization of cytoplasmic and skeletal myosins in developing muscle cells by double-label immunofluorescence," Journal of cell Biology, vol. 87, no. 1, pp. 237–247, 1980.

12. A. A. Dlugosz, P. B. Antin, V. T. Nachmias, and H. Holtzer, "The relationship between stress fiber-like structures and nascent myofibrils in cultured cardiac myocytes," Journal of Cell Biology, vol. 99, no. 6, pp. 2268–2278, 1984.

13. J. M. Sanger, B. Mittal, M. B. Pochapin, and J. W. Sanger, "Myofibrillogenesis in living cells microinjected with fluorescently labeled alpha-actinin," Journal of Cell Biology, vol. 102, no. 6, pp. 2053–2066, 1986

14. J. W. Sanger, S. Kang, C. C. Siebrands, et al., "How to build a myofibril," Journal ofMuscle Research and Cell Motility, vol. 26, no. 6–8, pp. 343–354, 2005.

15. J. W. Sanger, J. M. Sanger, and C. Franzini-Armstrong, "Assembly of the skeletal muscle cell," in Myology, A.G.Engel and C. Franzini-Armstrong, Eds., pp. 45–65, McGraw-Hill, New York, NY, USA, 3rd edition, 2004.

16. G. A. Dabiri, K.K. Turnacioglu, J.M. Sanger, and J.W. Sanger, "Myofibrillogenesis visualized in living embryonic cardiomyocytes," Proceedings of the National Academy of Sciences of the United States of America, vol. 94, no. 17, pp. 9493–9498, 1997.

17. D. Rhee, J.M.Sanger, and J.W.Sanger, “The premyofibril: evidence for its role in myofibrillogenesis,” Cell Motility and the Cytoskeleton, vol. 28, no. 1, pp. 1–24, 1994.

18. Geisterfer-Lowrance, A. A., Kass, S., Tanigawa, G., Vosberg, H. P., McKenna, W., Seidman, C. E., & Seidman, J. G. (1990). A molecular basis for familial hypertrophic cardiomyopathy: a beta cardiac myosin heavy chain gene missense mutation. Cell, 62(5), 999–1006.

19. Functional Consequences of a Mutation in an Expressed Human α-Cardiac Actin at a Site Implicated in Familial Hypertrophic Cardiomyopathy * Bookwalter, Carol S. et al. Journal of Biological Chemistry, Volume 281, Issue 24, 16777 - 16784

20. Vang, S., Corydon, T.J., Børglum, A.D., Scott, M.D., Frydman, J., Mogensen, J., Gregersen, N. and Bross, P. (2005), Actin mutations in hypertrophic and dilated cardiomyopathy cause inefficient protein folding and perturbed filament formation. The FEBS Journal, 272: 2037-2049. https://doi.org/10.1111/j.1742-4658.2005.04630.x

21. Wong, W.W., Doyle, T.C., Cheung, P. et al. Functional studies of yeast actin mutants corresponding to human cardiomyopathy mutations. J Muscle Res Cell Motil 22, 665–674 (2001). https://doi.org/10.1023/A:1016354308436

22. Epstein, N. D., Cohn, G. M., Cyran, F., & Fananapazir, L. (1992). Differences in clinical expression of hypertrophic cardiomyopathy associated with two distinct mutations in the beta-myosin heavy chain gene. A 908Leu----Val mutation and a 403Arg----Gln mutation. Circulation, 86(2), 345–352. https://doi.org/10.1161/01.CIR.86.2.345

23. Watkins, H., Rosenzweig, A., Hwang, D.-S., Levi, T., McKenna, W., Seidman, C. E., & Seidman, J. G. (1992). Characteristics and Prognostic Implications of Myosin Missense

Mutations in Familial Hypertrophic Cardiomyopathy. New England Journal of Medicine, 326(17), 1108–1114. https://doi.org/10.1056/NEJM199204233261703

24. T., G.-L. A. A., Michael, C., A., C. D., S., I. J., J., S. F., E., S. C., & G., S. J. (1996). A Mouse Model of Familial Hypertrophic Cardiomyopathy. Science, 272(5262), 731–734. https://doi.org/10.1126/science.272.5262.731
25. Tyska, M. J., Hayes, E., Giewat, M., Seidman, C. E., Seidman, J. G., & Warshaw, D. M. (2000). Single-Molecule Mechanics of R403Q Cardiac Myosin Isolated From the Mouse Model of Familial Hypertrophic Cardiomyopathy. Circulation Research, 86(7), 737–744. https://doi.org/10.1161/01.RES.86.7.737
26. P., S. J., P., D. E., Ferhaan, A., Amy, A., Andrea, F., A., C. D., Ulrike, M., J., L. M., David, W., E., S. C., & G., S. J. (2006). Cardiac myosin missense mutations cause dilated cardiomyopathy in mouse models and depress molecular motor function. Proceedings of the National Academy of Sciences, 103(39), 14525–14530. https://doi.org/10.1073/pnas.0606383103
27. Itoh-Satoh, M., Hayashi, T., Nishi, H., Koga, Y., Arimura, T., Koyanagi, T., Takahashi, M., Hohda, S., Ueda, K., Nouchi, T., Hiroe, M., Marumo, F., Imaizumi, T., Yasunami, M., & Kimura, A. (2002). Titin Mutations as the Molecular Basis for Dilated Cardiomyopathy. Biochemical and Biophysical Research Communications, 291(2), 385–393. https://doi.org/https://doi.org/10.1006/bbrc.2002.6448
28. Hayashi T, Arimura T, Itoh-Satoh M, et al. Tcap gene mutations in hypertrophic cardiomyopathy and dilated cardiomyopathy. J Am Coll Cardiol. 2004 Dec, 44 (11) 2192–2201.https://doi.org/10.1016/j.jacc.2004.08.058
29. Morimoto, S. (2008). Sarcomeric proteins and inherited cardiomyopathies. *Cardiovascular Research, 77*(4), 659–666. https://doi.org/10.1093/cvr/cvm084

30. Japp, A. G., Gulati, A., Cook, S. A., Cowie, M. R., & Prasad, S. K. (2016). The Diagnosis and Evaluation of Dilated Cardiomyopathy. *Journal of the American College of Cardiology*, *67*(25), 2996–3010. https://doi.org/https://doi.org/10.1016/j.jacc.2016.03.590

31. Mahmaljy H, Singhal M (2018) Dilated cardiomyopathy. In: StatPearls. StatPearls Publishing StatPearls Publishing LLC., Treasure Island (FL)

32. Haas J, Frese KS, Peil B, Kloos W, Keller A, Nietsch R, Feng Z, Muller S, Kayvanpour E, Vogel B, Sedaghat-Hamedani F, Lim WK,ZhaoX,Fradkin D, Kohler D, Fischer S, Franke J, Marquart S, Barb I, Li DT, Amr A, Ehlermann P, Mereles D, Weis T, Hassel S,KremerA,KingV,Wirsz E, Isnard R, Komajda M, Serio A, Grasso M, Syrris P, Wicks E, Plagnol V, Lopes L, Gadgaard T, Eiskjaer H, Jorgensen M, Garcia- Giustiniani D, Ortiz-Genga M, Crespo-Leiro MG, Deprez RH, Christiaans I, van Rijsingen IA, Wilde AA, Waldenstrom A, Bolognesi M, Bellazzi R, Morner S, Bermejo JL, Monserrat L, Villard E, Mogensen J, Pinto YM, Charron P, Elliott P, Arbustini E, Katus HA, Meder B (2015) Atlas of the clinical genetics of human dilated cardiomyopathy. Eur Heart J 36(18):1123–1135a. https://doi.org/10.1093/eurheartj/ehu301

33. Kimura A. (2010). Molecular basis of hereditary cardiomyopathy: abnormalities in calcium sensitivity, stretch response, stress response and beyond. *Journal of human genetics*, *55*(2), 81–90. https://doi.org/10.1038/jhg.2009.138

34. Martin, T. G., Myers, V. D., Dubey, P., Dubey, S., Perez, E., Moravec, C. S., Willis, M. S., Feldman, A. M., & Kirk, J. A. (2021). Cardiomyocyte contractile impairment in heart failure results from reduced BAG3-mediated sarcomeric protein turnover. *Nature Communications*, *12*(1). https://doi.org/10.1038/s41467-021-23272-z

35. Arimura, T., Ishikawa, T., Nunoda, S., Kawai, S., & Kimura, A. (2011). Dilated cardiomyopathy-associated BAG3 mutations impair Z-disc assembly and enhance

sensitivity to apoptosis in cardiomyocytes. Human Mutation, 32(12), 1481–1491. https://doi.org/10.1002/humu.21603

36. Lange, S., Pinotsis, N., Agarkova, I., & Ehler, E. (2020). The M-band: The underestimated part of the sarcomere. Biochimica et Biophysica Acta (BBA) - Molecular Cell Research, 1867(3), 118440. https://doi.org/https://doi.org/10.1016/j.bbamcr.2019.02.003
37. Takayama, S., Xie, Z., & Reed, J. C. (1999). An Evolutionarily Conserved Family of Hsp70/Hsc70 Molecular Chaperone Regulators*. Journal of Biological Chemistry, 274(2), 781–786. https://doi.org/https://doi.org/10.1074/jbc.274.2.781
38. Homma, S., Iwasaki, M., Shelton, G. D., Engvall, E., Reed, J. C., & Takayama, S. (2006). BAG3 Deficiency Results in Fulminant Myopathy and Early Lethality. The American Journal of Pathology, 169(3), 761–773. https://doi.org/https://doi.org/10.2353/ajpath.2006.060250
39. Fang, X., Bogomolovas, J., Wu, T., Zhang, W., Liu, C., Veevers, J., Stroud, M. J., Zhang, Z., Ma, X., Mu, Y., Lao, D.-H., Dalton, N. D., Gu, Y., Wang, C., Wang, M., Liang, Y., Lange, S., Ouyang, K., Peterson, K. L., … Chen, J. (2017). Loss-of-function mutations in co-chaperone BAG3 destabilize small HSPs and cause cardiomyopathy. *The Journal of Clinical Investigation*, *127*(8), 3189–3200. https://doi.org/10.1172/JCI94310
40. Feldman, A. M., Gordon, J., Wang, J., Song, J., Zhang, X.-Q., Myers, V. D., Tilley, D. G., Gao, E., Hoffman, N. E., Tomar, D., Madesh, M., Rabinowitz, J., Koch, W. J., Su, F., Khalili, K., & Cheung, J. Y. (2016). BAG3 regulates contractility and Ca2+ homeostasis in adult mouse ventricular myocytes. *Journal of Molecular and Cellular Cardiology*, *92*, 10–20. https://doi.org/https://doi.org/10.1016/j.yjmcc.2016.01.015
41. Franaszczyk M, Bilinska ZT, Sobieszczańska-Małek M, Michalak E, Sleszycka J, Sioma A, Małek ŁA, Kaczmarska D, Walczak E, Włodarski P, Hutnik Ł, Milanowska

B, Dzielinska Z, Religa G, Grzybowski J, Zieliński T, Ploski R. The BAG3 gene variants in Polish patients with dilated cardiomyopathy: four novel mutations and a genotype-phenotype correlation. J Transl Med. 2014 Jul 9;12:192. doi: 10.1186/1479-5876-12-192. PMID: 25008357; PMCID: PMC4105391.

42. Domínguez, F., Cuenca, S., Bilińska, Z., Toro, R., Villard, E., Barriales-Villa, R., Ochoa, J. P., Asselbergs, F., Sammani, A., Franaszczyk, M., Akhtar, M., Coronado-Albi, M. J., Rangel-Sousa, D., Rodriguez-Palomares, J. F., Jiménez-Jáimez, J., Garcia-Pinilla, J. M., Ripoll-Vera, T., Mogollón-Jiménez, M. V., Fontalba-Romero, A., … Sammani, A. (2018). Dilated Cardiomyopathy Due to BLC2-Associated Athanogene 3 (BAG3) Mutations. *Journal of the American College of Cardiology*, *72*(20), 2471–2481. https://doi.org/10.1016/j.jacc.2018.08.2181
43. Weiss, P. Shape and Movement of Mesenchyme Cells as Functions of the Physical Structure of the Medium: Contributions to a Quantitative Morphology. Proc. Natl. Acad. Sci. - PNAS 38, 264–280 (3AD).
44. Kim, D.-H., Wong, P. K., Park, J., Levchenko, A., & Sun, Y. (2009). Microengineered Platforms for Cell Mechanobiology. *Annual Review of Biomedical Engineering*, *11*(1), 203–233. https://doi.org/10.1146/annurev-bioeng-061008-124915
45. Olivetti, G., Ricci, R., Lagrasta, C., Maniga, E., Sonnenblick, E. H., & Anversa, P. (1988). Cellular basis of wall remodeling in long-term pressure overload-induced right ventricular hypertrophy in rats. *Circulation Research*, *63*(3), 648–657. https://doi.org/10.1161/01.RES.63.3.648
46. Bishop, S. P., Anderson, P. G., & Tucker, D. C. (1990). Morphological development of the rat heart growing in oculo in the absence of hemodynamic work load. *Circulation Research*, *66*(1), 84–102. https://doi.org/10.1161/01.RES.66.1.84

47. Simpson, D. G., Terracio, L., Terracio, M., Price, R. L., Turner, D. C., & Borg, T. K. (1994). Modulation of cardiac myocyte phenotype in vitro by the composition and orientation of the extracellular matrix. *Journal of Cellular Physiology*, *161*(1), 89–105. https://doi.org/https://doi.org/10.1002/jcp.1041610112

48. Kim, D.-H., Wong, P. K., Park, J., Levchenko, A., & Sun, Y. (2009). Microengineered Platforms for Cell Mechanobiology. *Annual Review of Biomedical Engineering*, *11*(1), 203–233. https://doi.org/10.1146/annurev-bioeng-061008-124915

49. Hochmuth RM. 2000. Micropipette aspiration of living cells. J. Biomech. 33:15–22

50. Hogan, B., Babataheri, A., Hwang, Y., Barakat, A. I., & Husson, J. (2015). Characterizing Cell Adhesion by Using Micropipette Aspiration. *Biophysical Journal*, *109*(2), 209–219. https://doi.org/https://doi.org/10.1016/j.bpj.2015.06.015

51. Dembo M,Wang YL. 1999. Stresses at the cell-to-substrate interface during locomotion of fibroblasts. Biophys. J. 76:2307–16

52. Tan JL,Tien J, Pirone DM, Gray DS, Bhadriraju K, Chen CS. 2003. Cells lying on a bed ofmicroneedles: an approach to isolate mechanical force. Proc. Natl. Acad. Sci. USA 100:1484–89

53. Wood MA. 2007. Colloidal lithography and current fabrication techniques producing in-plane nanoto- pography for biological applications. J. R. Soc. Interface 4:1–17

54. DalbyMJ, RiehleMO,Johnstone HJ, Affrossman S, Curtis AS. 2002. Polymer-demixed nanotopography: control of fibroblast spreading and proliferation. Tissue Eng. 8:1099–108

55. Liang D, Hsiao BS, Chu B. 2007. Functional electrospun nanofibrous scaffolds for biomedical applica- tions. Adv. Drug. Deliv. Rev. 59:1392–412

56. Sill TJ, von Recum HA. 2008. Electrospinning: applications in drug delivery and tissue engineering. Biomaterials 29:1989–2006

57. Yim EK, Reano RM, Pang SW, Yee AF, Chen CS, Leong KW. 2005. Nanopattern-induced changes in morphology and motility of smooth muscle cells. Biomaterials 26:5405–13

58. Kim DH, Kim P, Song I, Cha JM, Lee SH, et al. 2006. Guided three-dimensional growth of functional cardiomyocytes on polyethylene glycol nanostructures. Langmuir 22:5419–26

59. Yang, P.; Baker, R. M.; Henderson, J. H.; Mather, P. T. In Vitro Wrinkle Formation via Shape Memory Dynamically Aligns Adherent Cells. Soft Matter 2013, 9, 4705−4714.

60. Hardy, J. G.; Palma, M.; Wind, S. J.; Biggs, M. J. Responsive Biomaterials: Advances in Materials Based on Shape-Memory Polymers. Adv. Mater. 2016, 28, 5717−5724.

61. Baker, R. M., Tseng, L.-F., Iannolo, M. T., Oest, M. E., & Henderson, J. H. (2016). Self-deploying shape memory polymer scaffolds for grafting and stabilizing complex bone defects: A mouse femoral segmental defect study. Biomaterials, 76, 388–398. https://doi.org/https://doi.org/10.1016/j.biomaterials.2015.10.064

62. Sun, S., Shi, H., Moore, S., Wang, C., Ash-Shakoor, A., Mather, P. T., Henderson, J. H., & Ma, Z. (2020). Progressive Myofibril Reorganization of Human Cardiomyocytes on a Dynamic Nanotopographic Substrate. ACS Applied Materials and Interfaces, 12(19), 21450–21462. https://doi.org/10.1021/acsami.0c03464

Vita

Xiangjun Wu xwu164@syr.edu

Education

Syracuse University M.S August 2019 to August 2022

Thesis: "BAG3 Mutation Interferes Myofibril Integrity of hiPSC-derived Cardiomyocytes on a Dynamic Substrate"

South China University of Technology B.S. August 2015 to July 2019

PUBLICATIONS

Xiangjun Wu, Huaiyu Shi, Chenyan Wang, James H. Henderson, Zhen Ma." BAG3 mutation interferes myofibril maturation of hiPSC-derived cardiomyocytes on a dynamic substrate." Stevenson Biomaterials Lecture Series and Research Poster Session, Syracuse, NY, 2021, Poster

Huaiyu Shi, Xiangjun Wu, Shiyang Sun, Chenyan Wang, Zacharias Vangelatos, Ariel Ash-Shakoor, Costas P. Grigoropoulos, Patrick T. Mather, James H. Henderson, Zhen Ma, "Profiling the responsiveness of focal adhesions of human cardiomyocytes to extracellular dynamic nano-topography", Bioactive Materials, Volume 10, 2022, Pages 367-377, ISSN 2452-199X, https://doi.org/10.1016/j.bioactmat.2021.08.028.